CONTROL OF CHEMICAL REACTIONS USING SHAPED FEMTOSECOND PULSES

By

Xin Zhu

A DISSERTATION

Submitted to
Michigan State University
in partial fulfillment of the requirements
for the degree of

DOCTOR OF PHILOSOPHY

Chemistry

2011

ABSTRACT

CONTROL OF CHEMICAL REACTIONS USING SHAPED FEMTOSECOND PULSES

By

Xin Zhu

The possibility that chemical reactions may be controlled by tailored femtosecond laser pulses has inspired recent studies that take advantage of their short pulse duration, comparable to intramolecular dynamics, and high peak intensity to fragment and ionize molecules. Among them are dreams, breakthroughs and disappointments. In this dissertation, the results from a comprehensive study are presented for isolated molecules interact with shaped near-IR laser pulses with peak intensities ranging from 10^{13} to 10^{16} W/cm^2. Important lessons were learned for laser control chemistry under such conditions from exhaustive evaluation of hundreds of thousands of experiments from 16 compounds. Its potential applications in analytical chemistry are also discussed.

Results studying the dynamics occurring soon after isolated molecules interact with an intense non-resonant laser field are also presented in this dissertation. This study reveals dynamics that take place over a range that extends through four orders of magnitude in time, which provide information about how molecules interact with intense laser fields and how pulse shaping influences the yield of different fragment ions.

ACKNOWLEDGEMENT

I would like to express my deepest gratitude to my advisor, Prof. Marcos Dantus, for his excellent guidance, caring, patience, and providing me with an excellent atmosphere for doing research.

I would also like to thank my parents who were always supporting me and encouraging me with their best wishes.

Finally, I would like to thank my wife, Ying Huang. She was always there cheering me up and stood by me through the good times and the bad.

Table of Contents

List of Tables

List of Figures

Chapter 1 Introduction

Many chemical reactions can follow more than one reaction pathways, each leading to a different product. Normally only one of these pathways is desired and the side reactions decrease the yield of the desired product. Chemists has been strived to devise methods for controlling chemical reactions and decreasing the yield of undesired products. Traditionally, macroscopic parameters such as temperature and pressure were manipulated as well as using different catalysts. In 1960s, the invention of the laser inspired a broad range of scientists with the prospect of controlling the outcome of laser matter interactions. Selective chemical bond cleavage was expected to be possible by delivering coherent photons with the right frequency (Letokhov *et al.*, 1978; Ronn, 1979). However, it was soon realized that energy deposited in one bond quickly redistributed along the various degrees of freedom available to the system.

In 1980, Nobel Prize Laureate Ahmed Zewail proposed using femtosecond laser pulses to control chemical reactions, taking advantage of its ultrashort time duration to overcome the fast intramolecular vibrational energy redistribution (IVR) (Zewail, 1980). A series of experiments were then carried out on iodine molecules by Warren and Zewail to demonstrate the photon echo response using femtosecond pulses shaped in time domain (Warren *et al.*, 1981, 1983a, 1983b, 1983c). The first direct measurement of the timescales for chemical bond dissociation was achieved for ICN (Dantus *et al.*, 1987; Rose *et al.*, 1988) using femtosecond colliding pulse modelocked dye laser (Fork *et al.*, 1981) in early 1980s. The limitations due to the laser sources made these experiments extremely difficult to perform until the invention of self-modelocked Ti:sapphire laser in early 1990s providing long-term stability (Spence *et al.*, 1991). The research presented in this dissertation was performed using this type of solid-state femtosecond laser systems.

Unlike a conventional monochromatic laser, ultrafast pulses consist of a broad range of phase-locked frequency components. The relative phases of different frequency components can be altered which play a crucial role in the control of physicochemical processes using femtosecond pulses. Pulse shaping techniques which manipulate the amplitude and phase of the pulses have been developed complimentary to the femtosecond laser sources since 1980s. The most widely used method for pulse shaping, sometimes called Fourier synthetics, was developed by Weiner and Heritage in 1987 (Weiner *et al.*, 1987; 1988; 1990).

In the early days, the development of controlling physicochemical processes especially chemical reactions with lasers mainly remained in theory. Tanner and Rice first discussed to control the observed fragments of molecules by optimizing laser fields (Tannor *et al.*, 1985). Brumer and Shapiro realized that coherent photons from the laser would cause interference between particular photochemical pathways, opening an attractive means of laser control of chemistry using nanosecond lasers (Brumer *et al.*, 1986). Pump-probe scheme was also outlined to use two or more carefully timed pulses to create a molecular wave packet that could be followed in time to cause selective chemistry (Tannor *et al.*, 1986).

In 1992, Judson and Rabitz proposed a powerful strategy in which they suggested using computer algorithms that would learn from the feedback and guide the system to generate the shaped pulse that optimized the desired outcome (Judson *et al.*, 1992). The field of laser control of chemical reactions was fueled by this new scheme to a great extent. Despite the high hopes, a limited number of experiments were actually conducted. The first experimental realization was published by Assion et al on the control of fragmentation on $CpFe(CO)_2X$ (X=Cl,Br,I) (Assion *et al.*, 1998). Phase and amplitude shaped femtosecond pulses clearly resulted in a significant change on the relative yield of different fragment ions, although no information was available about what aspects of the laser field caused the observed control. A series of subsequent experiments on $Fe(CO)_5$ (Bergt *et al.*, 1999) and CH_2BrCl (Damrauer *et al.*, 2002) were carried out from the same group, showing that transform limited pulses produced more molecular ions while shaped pulses produced more fragment ions. The ratio between CH_2Br^+/CH_2Cl^+ generated from the fragmentation of CH_2BrCl could be controlled from 1.0 to 1.7, indicating that the stronger bond (C-Cl) could be cleaved preferably rather than the weaker bond (C-Br) by shaping the pulses. Since then, the combination of shaped femtosecond pulses with mass spectrometry (MS) has been considered as the ideal technology for studying laser control of chemical reactions.

Following the observations by Gerber, Levis studied the effects of phase and amplitude shaping on the photofragmentation of acetone, trifluoroacetone, and acetophenone in the gas phase (Levis *et al.*, 2001; Levis *et al.*, 2002). The most significant result was the observation of the toluene formation (m/z=92) from the fragmentation of gas phase acetophenone molecules. Two chemical bonds have to be cleaved at the same time as well as the formation of a new chemical bond, which is very unlikely to happen in conventional chemistry. It was explained as a complex pathway directed by the shaped laser field, and it was considered only possible to find such pulses by using feedback based learning algorithm. A number of studies were stimulated by this exciting result in which the dream of selective bond cleavage seemed to be realized. However, a revisit of the experiment discussed later in this dissertation shows a different conclusion.

More experiments on acetone and halogen substituted acetone molecules including CH_3COCF_3 (2005a; Cardoza *et al.*, 2004; 2005c; Langhojer *et al.*, 2005), CH3COD3 (Cardoza *et al.*, 2005b), CH3COCCl3 (Cardoza *et al.*, 2005b), and the di-halogen CH2BrI (Cardoza *et al.*, 2005c; Langhojer *et al.*, 2005) were also studied by the Weinacht research group. In these experiments, a number of different pulse shaping strategies including unconstrained phase amplitude to differential, polynomial and periodical functions were evaluated for better understanding of the laser induced ionization and fragmentation, as well as the fundamentals of learning algorithm approach. The main message delivered is that the ionization of gas phase molecules takes place within a very short time after the interaction with the laser field and is followed by enhanced autodissociation (Cardoza *et al.*, 2005a).

Despite the success demonstrated in vast theoretical and experimental results implementing feedback based learning algorithm, this so called “closed-loop” approach suffers from several drawbacks. First of all, learning algorithms usually reach a consistent fitness value, but each optimization run will give rise to different phase and amplitude functions. The poor reproducibility poses serious problem for a wide range of applications using shaped femtosecond pulses. In addition, since most physicochemical processes is more complex than needle-in-the-haystack type, the optimization is highly possible to be trapped in a local minimum rather than a global minimum, and the result depends largely on the initial guess. More importantly, by running learning algorithms, very limited knowledge is learned about the light matter interaction and the molecular system. Being aware of these problems, the Dantus research group has adopted a different approach, often called “open-loop”, in which sets of different shaped pulses is evaluated for their ability to control chemistry (Lozovoy, V. V. *et al.*, 2005a, 2006b; 2006c; Pastirk *et al.*, 2005; Shane *et al.*, 2006). In these experiments, it was determined that as long as the excitation pulse was not resonant with the molecular system, control of amplitude of the pulses was not necessary. A simple set of binary phase functions were found to provide controllability over different fragments comparable to those obtained in closed-loop experiments (Pastirk *et al.*, 2005). Under the experimental conditions applied in these experiments, laser intensity was found to have no effect on the fragment ion relative yields. Near transform limited (TL) pulses preferably produced heavier ions while shaped pulses produced smaller fragments. These results revealed pieces of valuable information. However, a comprehensive study is needed for a thorough understanding of laser control chemistry in gas phase using shaped femtosecond pulses, which is the motivation for my PhD research.

In this dissertation, chapter 2 discusses the experimental tools and underline fundamentals related to the projects presented later. Chapter 3 presents the results of an exhaustive evaluation of laser control chemistry with tens of thousands of systematically designed phase and amplitude pulse shaping functions over 16 different compounds including isomers. Chapter 4 presents a follow up study of chapter 3, in which the photo-dissociation dynamics is discussed. The results shown in this dissertation should be able to shed some light on better understanding of control of chemical reactions using shaped femtosecond pulses.

Chapter 2 Experimental and the Principles

2.1 The Laser System and the Pulse Shapers

A schematic of the laser system used is presented in Figure 2.1. The Ti:Sapphire oscillator (K&M Labs) is pumped by the second harmonic of a Nd:YVO$_4$ laser (Spectra-Physics, Millennia) resulting in femtosecond pulses with a center wavelength of 800 nm and a spectral bandwidth of 40 nm FWHM at 80 MHz and average power of 300 mW (Figure 2.1a). The output from the oscillator is collimated with a telescope and is directed to the first pulse shaper (Pulse Shaper I), located between the oscillator and the amplifier (Figure 2.1b). Pulse Shaper I has an 830 groves/mm dispersive grating, a 15 cm focal length spherical mirror and a 128 pixel liquid crystal spatial light modulator (SLM-128, CRI), in a reflective mode. The spectral phase modulation applied by Pulse Shaper I is preserved during amplification, a fact that has been experimentally verified (Pastirk *et al.*, 2006b), and was used for phase shaping experiments to systematically apply predetermined pulse shaping strategies.

When conducting pulse shaping experiments, pulse profile distortion at the focus when changing the phases of the pulses is always a concern. As discussed by Sussman et al (2008), this arrangement (Oscillator-Shaper-Amplifier) adopted in this research reduces the spatio-temporal coupling, a process that distorts the pulses, because the amplifier modes themselves are usually much smaller than the seed laser mode and therefore acts as a spatial filter. Moreover, the spot size at the SLM is ~20 μm, which is much smaller than the pixel size (100 μm). This also reduces spatio-temporal coupling. Figure 2.2 shows the beam profiles at the focus of 50mm and 300mm focal length lenses for pulses with different spectral phases. The pulse profiles at the focus when applying different phases will be different if there is any spatial temporal coupling, which is apparently not observed here.

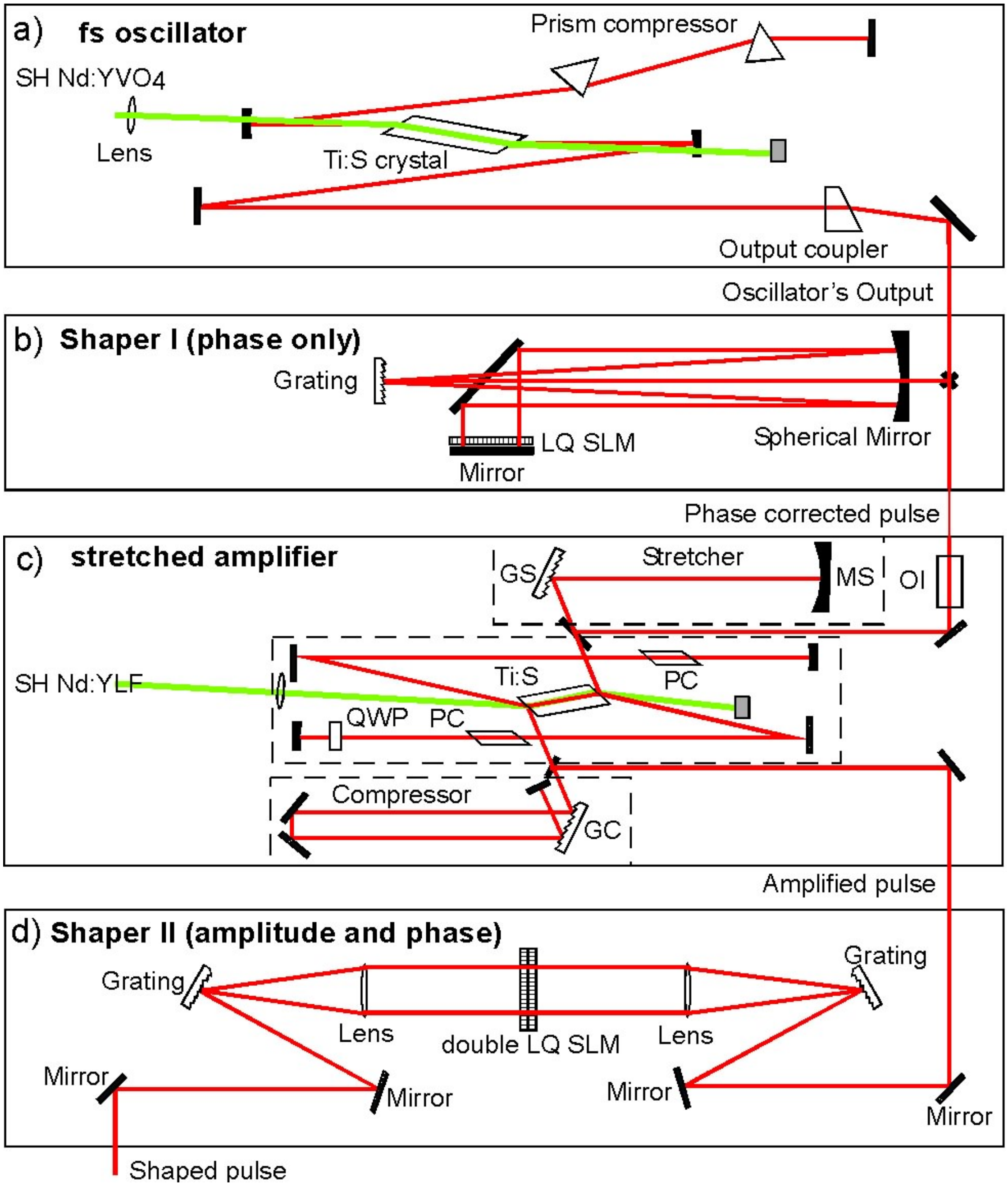

Figure 2.1 Schematic of the laser system including; a) fs laser oscillator, b) folded phase only pulse shaper, c) regenerative laser amplifier, d) phase and amplitude pulse shaper. For interpretation of the references to color in this and all other figures, the reader is referred to the electronic version of this dissertation.

a) 50mm lens

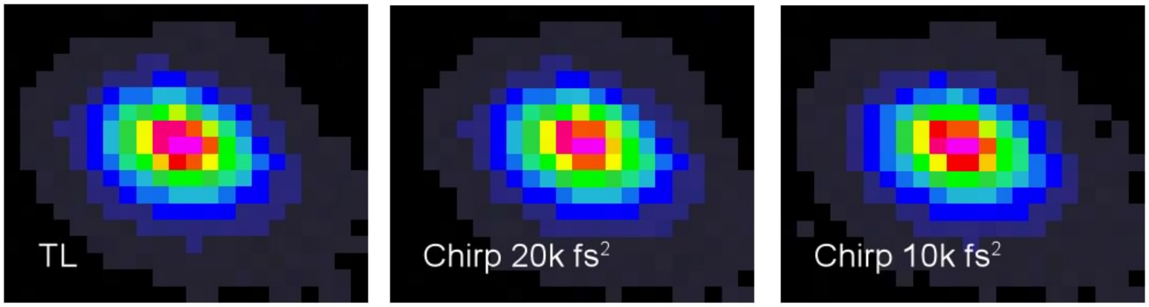

b) 300mm lens

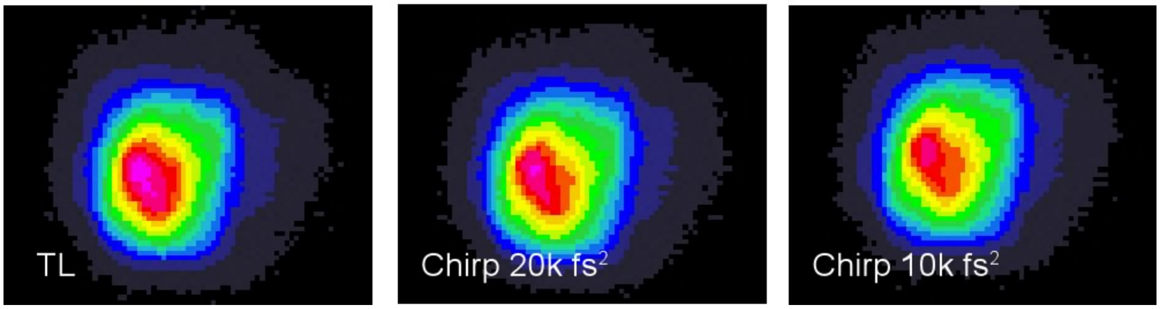

Figure 2.2 Beam profiles for pulses with TL phase, 20,000 fs^2 positive chirp, 10,000 fs^2 positive chirp at the focus of both 50 mm and 300 mm lens. For interpretation of the references to color in this and all other figures, the reader is referred to the electronic version of this dissertation.

The amplifier used in this system is a Ti:Sapphire regenerative amplifier (Spectra-Physics, Spitfire) pumped by the second harmonic of the Nd:YLF laser (Spectra-Physics, Evolution X, 1 kHz) which gives 800 nm pulses at 1 kHz with energy about 800 μJ (Figure 2.1c). The bandwidth of the output pulses is ~ 30 nm FWHM, which results in 35 fs (FWHM) transform limited pulses. The polarization of the laser is horizontal as it enters the mass spectrometer, perpendicular to the ion collection optics.

The shaped output of the amplifier is used for experiments that require phase-only pulse shaping. Pulse Shaper II is used for experiments that required both amplitude and phase pulse shaping. Pulse Shaper II consists of two identical dispersive gratings (830 groves/mm), two identical cylindrical lenses (F=225 mm) and a dual mask 128 pixel liquid crystal SLM (SLM-256, CRI) programmed for applying both amplitude and phase shaping. The setup is arranged in unfolded 4*f* geometry (see Figure 2.1d). The spectral resolution of the two pulse shapers is ~1 nm/pixel. Pulse-to-pulse variation in the energy of the pulses for the amplified system was determined to be less than 2%. The spectrum of the second harmonic generation (SHG) of the shaped laser pulses is measured after frequency doubling in a 50 μm Type I β-BBO crystal using a miniature spectrometer (USB2000 Ocean Optics) and is used to establish pulse shaping reproducibility. The pulse-to-pulse variations in the measured SHG signal were less than 4%.

2.2 Pulse characterization and compensation with MIIPS technology

One of the most critical steps in reproducible laser control experiments with shaped pulses is accurate phase characterization and then the compensation of the unwanted spectral phase distortions introduced by the surfaces of mirrors or dispersive media, since femtosecond lasers are prone to phase distortions which cause temporal broadening. The highly nonlinear interaction between the intense laser pulses and the molecules is very sensitive to phase variations in the laser pulses. Previous methods on characterization and compensation involved a two-beam technique of autocorrelation or interferometry (Iaconis *et al.*, 1998; Trebino *et al.*, 1993). These methods require rather complicated optical setup and depend a lot on the beam quality so that very sensitive to air flows and changes in temperature. Unlike them, multiphoton intrapulse interference phase scan (MIIPS) (Coello *et al.*, 2008; Lozovoy, V. V. *et al.*, 2003; Walowicz *et al.*, 2002; Xu *et al.*, 2006), developed in our group, takes advantage of the influence that phase modulation has on the probability of nonlinear optical processes at specific frequencies. Multiphoton intrapulse interference (Lozovoy, V. V. *et al.*, 2003; Walowicz *et al.*, 2002) refers to the process that multiple frequencies in a broad femtosecond laser pulse interfere with each other to achieve multiphoton excitation controlled by phase. MIIPS is a single-beam method that not only characterizes the spectral phase but also compensates for unwanted phase distortions and can deliver accurate user-specified phase functions at the location of a sample (Abbott *et al.*, 2002; Dantus *et al.*, 2007; Lozovoy, V. V. *et al.*, 2004; Xu *et al.*, 2006).

In MIIPS, a well know phase function, $f(\omega)$ is added to the unknown spectral phase $\phi(\omega)$ of the pulse by spatial light modulator so that the actual spectral phase of the pulses would be:

$$\varphi(\omega) = \phi(\omega) + f(\omega) \qquad (1)$$

The second harmonic generation (SHG) is then used to measure $\phi(\omega)$ accurately. For a pulse with spectral phase $\varphi(\omega)$ the spectral power of the second harmonic field is given by

$$I_{SHG}(2\omega) \propto \left| \int \left| E_0(\omega+\Omega) \right| \left| E_0(\omega-\Omega) \right| \exp\left[i(\varphi(\omega+\Omega)+\varphi(\omega-\Omega)) \right] d\Omega \right|^2 \quad (2)$$

Since phase function is usually a continuous function, we can write a Taylor expansion for the sum $\varphi(\omega+\Omega)+\varphi(\omega-\Omega)$ near point ω

$$\varphi(\omega+\Omega)+\varphi(\omega-\Omega) = 2\varphi(\omega)+\varphi''(\omega)\Omega^2 + \ldots + 2/(2n)!\times d^n\varphi(\omega)/d\varphi^n\Omega^{2n} \quad (3)$$

To first approximation, the spectral maximum appears at 2ω when the second derivative $\varphi''(\omega)$ of the phase equals zero, i.e. when the spectrum of SHG has a local maximum.

$$\varphi''(\omega) = \phi''(\omega) + f''(\omega) \to 0 \quad (4)$$

At this frequency, $f''(\omega)$ compensates $\phi''(\omega)$. By scanning $f(\omega)$ across the whole spectrum, $\phi''(\omega)$ for all the frequencies in the spectrum can be measured and $\phi(\omega)$ can be obtained through double integration. Phase distortion can then be compensated by applying $-\phi(\omega)$ on the pulses via SLM. The process is repeated and the sum $-(\phi'(\omega)+\phi''(\omega))$ is used as the correction function for the next iteration. The convergence toward an accurate result is exponentially fast and the phase distortion is close to zero after 3 to 5 iterations.

In practical, $f(\omega)$ used is cosine function and the result of a MIIPS scan is a 2-D contour plot of SHG. A typical MIIPS setup and a MIIPS scan contour plot are shown in Figure 2.3, note that four features are identical and separated by π.

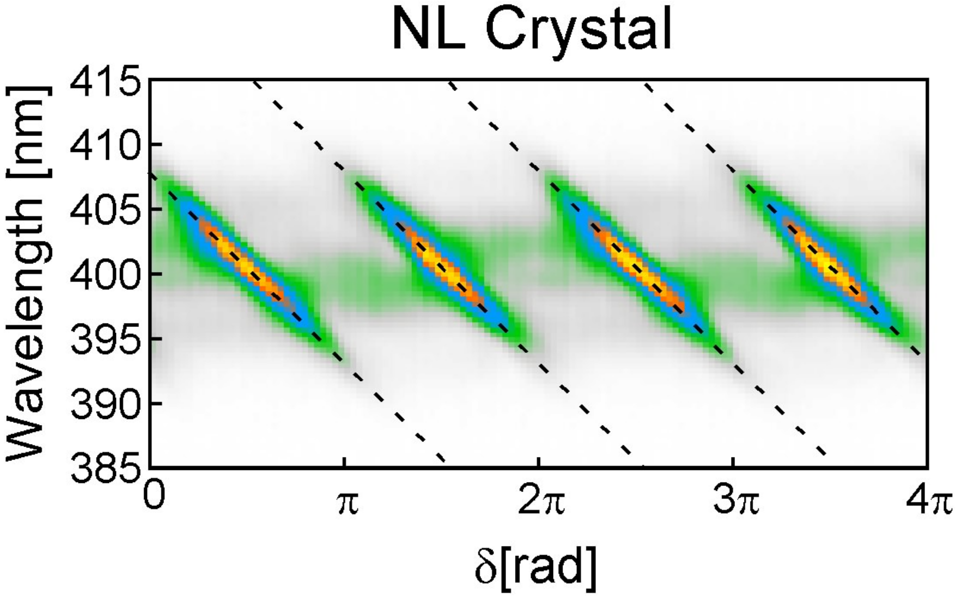

Figure 2.3 MIIPS setup and a MIIPS scan contour plot for compensated pulses. For interpretation of the references to color in this and all other figures, the reader is referred to the electronic version of this dissertation.

2.2.1 Remote MIIPS

In order to demonstrate the capability of MIIPS to deliver pulses with desired phases at the sample, pulse characterization and compression were performed using MIIPS on a remote target, which in this case was a 1 cm diameter pellet made of compressed KDP powder. The scattered frequency-doubled light generated at the target was collected and dispersed by a compact spectrometer. Group velocity dispersion measurements were carried out tracking changes in the compensation phases when MIIPS was carried out at different distances from the laser source.

The spectral phase of the pulse at 2.8 m from the exit aperture of the amplifier was measured first. The residual spectral phase, shown in Figure 2.4, contains all distortions from the oscillator, amplifier and optics after the beam leaves the amplifier. The beam was then directed to intermediate distances 7.6, 13.3, 18.3, 22.7 and 28.9 m, away from the amplifier. The same number of mirrors (protected silver) was used in all the experiments to preserve a constant non-air contribution to the phase distortion. The accumulated phases for the shortest and longest distance are plotted in Figure 2.4. From measurements made at intermediate distances we obtained a value for the second derivative of the phase ϕ'' at 800 nm, and from the slope of these values we obtain the group velocity dispersion of air (see Figure 2.4 insert). A linear fit of the data yields 20.1 ± 1.5 fs^2/m, which is in good agreement with previously published values (Pitts *et al.*, 2004). This measurement was performed at 21 ^oC, under 35% relative humidity. After correction using MIIPS, the residual phase distortions were on the order of 0.1 rad across the entire bandwidth of the pulse. The maximum phase distortion that can be compensated by the present setup is ~ 45000 fs^2, enough to compensate propagation through 2 km in air. This range can be easily expanded using different focusing optics, a different spatial light modulator, or taking advantage of the compression optics in the amplifier to reduce linear chirp, leaving high order phase distortions for automated compression. MIIPS per se has no range limit as long as sufficient signal can be detected.

To demonstrate accurate delivery of arbitrarily shaped pulses to a remote target, the pulses were first compensated and then a binary phase (Figure 2.5, top) or a sinusoidal function (Figure 2.5 bottom) was introduced by the pulse shaper. When the shaped pulse interacts with the remote target, frequency-doubled light is scattered and its spectrum is recorded. The remote signal (black dots) at 28.9 m is in excellent agreement with the signal obtained from 2.8 m (red line, Figure 2.5) indicating that accurately phase shaped pulses were delivered at the remote target. MIIPS corrects the dispersion accumulated by the laser pulses as they travel to the target, resulting in the excellent agreement.

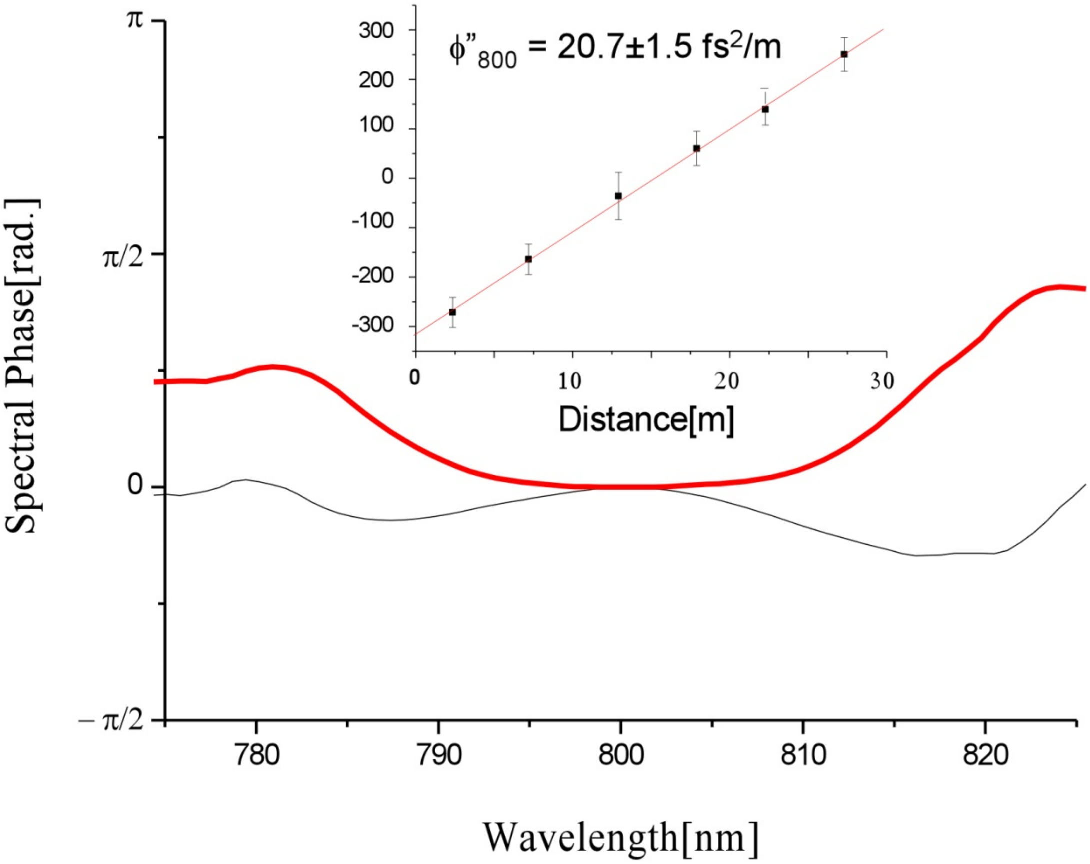

Figure 2.4 Accumulated phase caused by propagation of femtosecond pulses in air. The black line is the retrieved phase measured 2.8 m from the amplifier. The red line is the retrieved phase after the pulses propagate in air 28.9 m from the output source. Inset: Measurement of the group velocity dispersion of air at 800 nm, obtained from the slope from a number of intermediate measurements. For interpretation of the references to color in this and all other figures, the reader is referred to the electronic version of this dissertation.

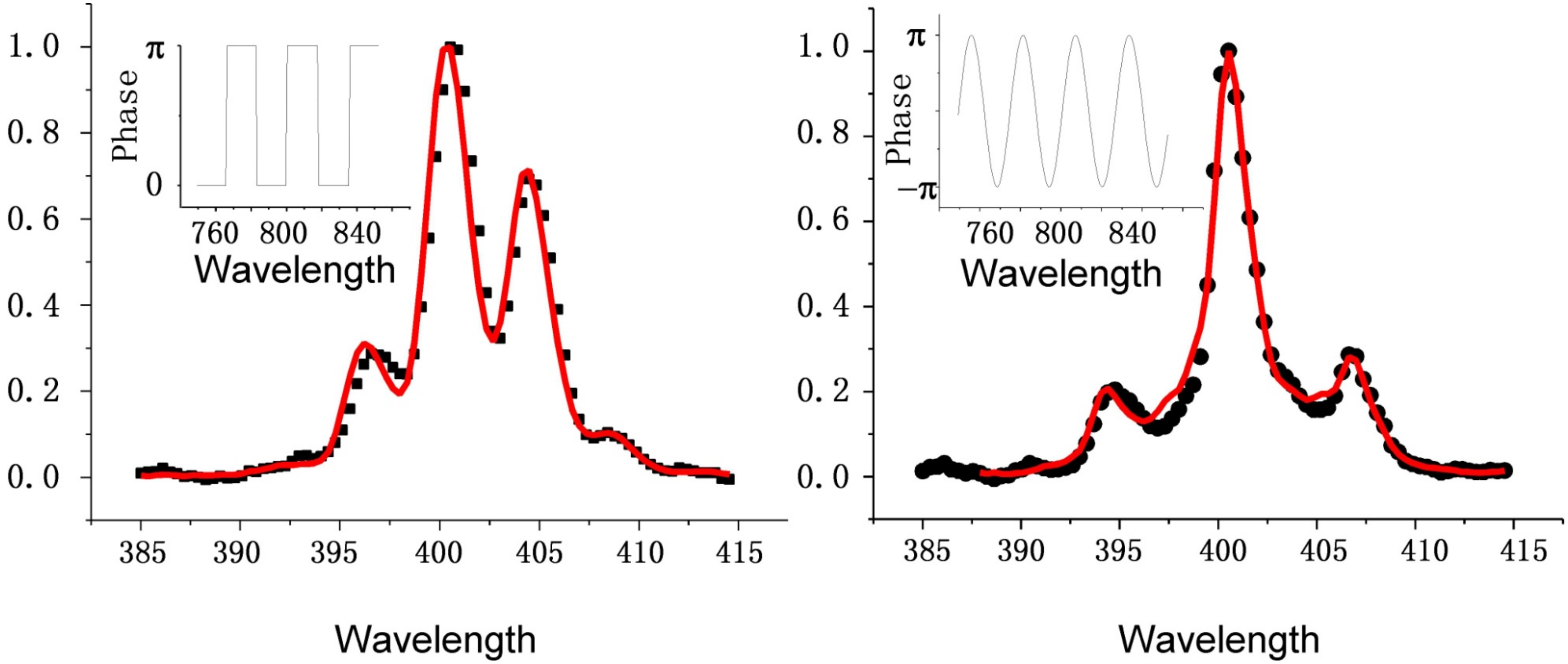

Figure 2.5 Frequency doubled spectra of pulses shaped with a binary (top) and a sinusoidal (bottom) phase functions recorded at a distance of 2.8 m (red light) and 28.9m (black dots). The excellent agreement between the near and remote measurements indicates that phase distortions were successfully corrected. For interpretation of the references to color in this and all other figures, the reader is referred to the electronic version of this dissertation.

2.3 The Time-of-flight Mass Spectrometer

A schematic of the TOF mass spectrometer used for the experiments presented in this dissertation is shown in Figure 2.6. The mass spectrometer has a linear geometry with a 0.5 meter field-free drift region. A base pressure of 10^{-7} Torr is maintained by a three stage differentially pumping scheme with a mechanical roughing pump, a diffusion pump, and a turbo pump. The sample is allowed to effuse into the chamber by an inlet valve up to a pressure of 10^{-5} Torr during experimentation. The pressure is an equilibrium reached by the vapor of the sample (cooled by an ice bath) and the fast pumping speed of a 4″ turbo molecular vacuum pump. This ensures very fast flow and prevents the accumulation of photoproducts in the chamber, which is confirmed by observing the fast decay of the signal when closing the valve (See Figure 2.7). When the sample valve is closed all ion signals disappear in less than one second and the pressure drops to 10^{-7} Torr. The sample molecules are ionized by the laser beam, focused by a lens at the entrance of the time of flight chamber. The focusing lens is also used as the window of the chamber to minimize self focusing effects that could appear if an external lens were used, as distortions of the light field by phase modulation have been found to affect MS measurements (Muller *et al.*, 2000; Sussman *et al.*, 2008; Tang *et al.*, 2005). In most experiments, the beam was attenuated to 170 μJ/pulse and no phase distortions due to the self-focusing were observed.

The repeller plate is maintained at 2.5 kV. The extraction plate is 1 cm away from the repeller plate and is maintained at 1.6 kV, with a 5/8 inch diameter circular wire grid. For some experiments, the extraction plate was replaced by a blank plate with a 0.7 mm diameter extraction pinhole. It was found that the pinhole led to a three-fold loss of signal but no difference was found in the fragmentation patterns observed for TL or shaped pulses. The loss of signal may be caused by the horizontal recoil of the fragment ions. Unless noted, the experimental results presented here were obtained with an extraction mesh. In order to examine volume effects, expected at higher intensities, an extraction plate with a 0.9 mm slit perpendicular to the laser beam was used. These measurements are presented in Chapter 3. The extracted molecular ions pass through the extraction grid into the acceleration region. The ions are detected using a micro-channel plate (MCP) detector coupled to a 500 MHz digital oscilloscope (Infiniium 54820A, HP). The MCP sensitivity has some m/z dependence (Fraser, 2002; Krems *et al.*, 2005) which at our conditions is minimal and was not taken into account. The unit mass resolution of our TOF system is approximately 250.

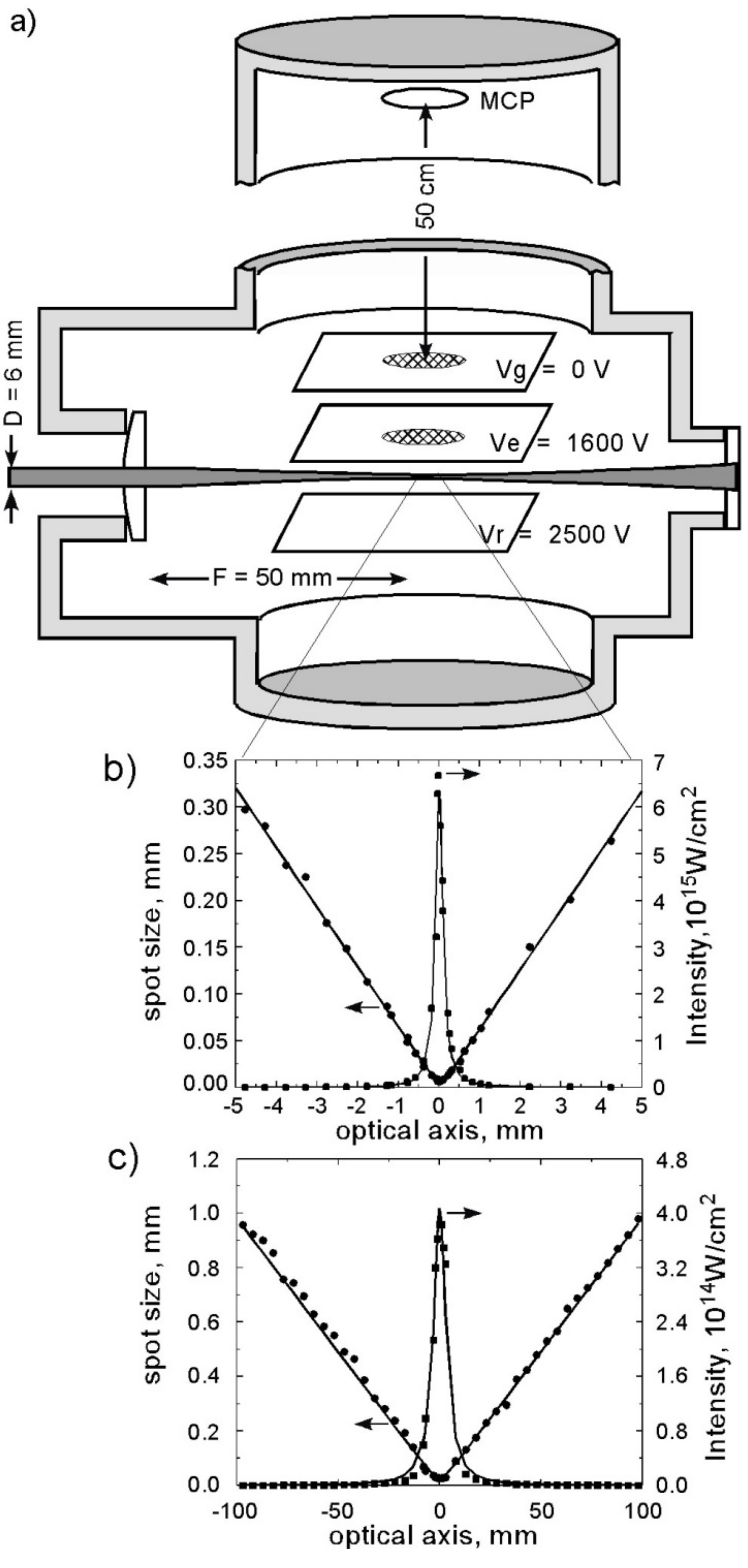
a)
MCP
50 cm
Vg = 0 V
Ve = 1600 V
Vr = 2500 V
D = 6 mm
F = 50 mm
b)
spot size, mm
0.00
0.05
0.10
0.15
0.20
0.25
0.30
0.35
Intensity, 10^{15}W/cm^2
0
1
2
3
4
5
6
7
-5
-4
-3
-2
-1
0
1
2
3
4
5
optical axis, mm
c)
spot size, mm
0.0
0.2
0.4
0.6
0.8
1.0
1.2
Intensity, 10^{14}W/cm^2
0.0
0.8
1.6
2.4
3.2
4.0
4.8
-100
-50
0
50
100
optical axis, mm

Figure 2.6 a) A schematic of the time of flight mass spectrometer. The laser beam is introduced into the chamber through a lens to minimize phase distortion. Ions, generated between the repeller/extractor pair at high voltage, accelerate to the flight tube, where they are registered by the dual micro channel plate detector. b) Graph showing the measured spot sizes of the beam waist along the optical axis of the laser for the 50 mm focal length lens with a Rayleigh length of 66 µm, together with the calculated peak power for 170 µJ TL pulses. c) Graph showing the same as in b) but for the 300 mm focal length lens with a Rayleigh length of 2.2 mm.

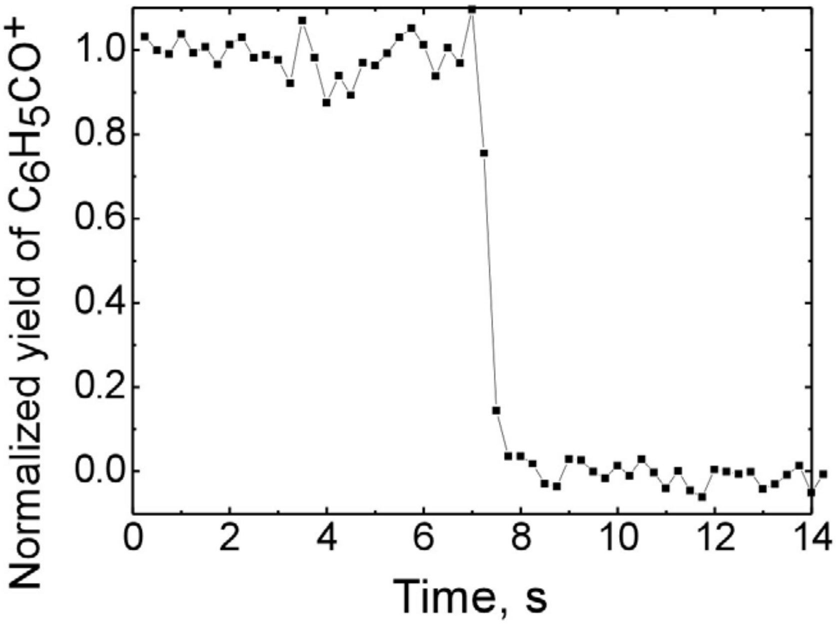

Figure 2.7 The intensity of $C_6H_5CO^+$, the most abundant photoproduct from acetophenone, drops to zero within a half second after closing the valve, which confirms the fast flow of our system.

Two different focusing conditions were used for our experiments. Normally a 50 mm focal length lens was used. In some experiments presented, a 300 mm focal length lens was used for lower intensities and to explore the influence of volume effects. The spatial profile of the beam was measured using a beam profiler (Coherent). The beam profile can be approximated to a Gaussian function and the beam propagation ratio (M^2) was found to be 1.04 and 1.5 for the 300 mm and 50 mm lenses respectively. The spot size of the beam was measured by scanning a blade across the beam. The minimum spot size ω_0 was 6.4 μm and 25.9 μm for the 50 and 300 mm lenses, respectively. The spot size of the beam increases away from its minimum value with a Rayleigh range (z_R) of 66 μm and 2.2 mm for the 50 and 300 mm lenses. The spot size dependence along the optical axis is shown in the Figure 2.6b and Figure 2.6c. For both focusing lenses, together with the prediction for the Gaussian beam (line). The maximum intensities I_0 of the beam were calculated with the formula $I_0 = 4\left(\ln\left(2\right)\right)^{0.5} \pi^{-1.5} \times W \times \tau^{-1} \times \omega_0^{-2}$, where W is energy of the pulse (J), τ is the duration (FWHM) of the pulse, and ω_0 is spot size (radius where the intensity decreases by e^2 times. The calculated dependence of the maximum field intensity along the optical axis is shown in Figure 2.6c together with a simulation (Lorentzian line shape). In order to check the accuracy of our intensity measurements, the ionization threshold for the atoms using the 50 mm focal length lens was measured. The obtained value (1287×10^{12} W/cm^2) is in good agreement with of the value (1158×10^{12} W/cm^2) reported by Hankin et al (2001).

According to modern theories, the threshold for molecular ionization (I_S) is between 1.0×10^{14} and 1.5×10^{15} W/cm^2 (Sussman *et al.*, 2008; Uiterwaal *et al.*, 2004). The peak field intensity (I_f) for the 35 fs TL at the focal region, shown in Figure 2.6b is 7×10^{15} W/cm^2. The volume of the sample (V_i) above ionization threshold (I_i) calculated using formula from a review (Posthumus, 2004) is $V_i=2/9\pi\omega_0^2 z_R(I_f/I_i)^{3/2}$. At the pressure of 10^{-5} Torr the calculated volume V_i~10^{-8}cm^3 results in 10^5 molecules being ionized. Approximately 75% of the ions from this volume are detected by the TOF mass spectrometer. Mass spectra in the range of pressure from 10^{-6} Torr up to 2.2×10^{-5} Torr were collected and no change was found in the relative yields of ions with pressure. The combination of very high laser intensity and very high sample pressure resulted in space-charge broadening of some peaks. This condition was avoided in the experiments presented here.

Chapter 3 Control of Laser-Matter Interaction: A Comprehensive Study

As introduced earlier, the quest for controlling chemical reactions with lasers is one fraught with dreams, breakthroughs, and disappointments. It involves a complex time-dependent interaction between light and matter in which energy redistribution and decoherence play a significant role. The continued interest in this area is reflected by the high number of publications in peer reviewed journals, which now exceeds 30 articles per year. The following are molecules that have been studied to date with shaped pulses and MS: S_8 (Wells *et al.*, 2005), CH_4(Mathur *et al.*, 2004), C_6H_{12} (Dela Cruz, J. M. *et al.*, 2005), C_7H_{14} (Dela Cruz, J. M. *et al.*, 2005), C_8H_{10} (Dela Cruz, J. M. *et al.*, 2005), C_2H_6O (Itakura *et al.*, 2003; Yazawa *et al.*, 2006), $C_2H_7O_3$ (Pastirk *et al.*, 2005), $C_3H_6O_3$ (Brixner *et al.*, 2003), C_4H_6O (Levis *et al.*, 2001), C_8H_8O (Graham *et al.*, 2003; Levis *et al.*, 2001; Pastirk *et al.*, 2006a), $C_8H_{10}O$ (Pastirk *et al.*, 2006a), C_5H_5N (Pastirk *et al.*, 2005), $C_8H_{11}N$ (Pastirk *et al.*, 2006a), C_5O_5F (Assion *et al.*, 1998; Bergt *et al.*, 2002; Bergt *et al.*, 1999), $C_3H_3OD_3$ (Cardoza *et al.*, 2005a), CH_2ClBr (Brixner *et al.*, 2001), CH_2BrI (Cardoza *et al.*, 2005a), $C_3H_3OF_3$ (Cardoza *et al.*, 2005a, 2005b; Cardoza *et al.*, 2004; Langhojer *et al.*, 2005; Levis *et al.*, 2001), $C_3H_3OCl_3$ (Cardoza *et al.*, 2005a; Cardoza *et al.*, 2004), $C_3HBr_2OF_3$ (Cardoza *et al.*, 2006), $C_7H_5FeO_2Cl$ (Assion *et al.*, 1998; Bergt *et al.*, 2002; Bergt *et al.*, 1999; Brixner *et al.*, 2001), $C_7H_5FeO_2Br$ (Bergt *et al.*, 2002), $C_5H_5FeO_2I$ (Bergt *et al.*, 2002), $C_7H_7NO_2$ (Dela Cruz, J. M. *et al.*, 2005; Lozovoy, V.V. *et al.*, 2006c; Shane *et al.*, 2006).

For all the molecules that have been studied the absolute yield of the molecular ion is always maximized when transform limited (TL) pulses are used. This universal observation has a simple explanation: when the pulses are shorter than 100 fs, the strong off-resonance field plucks out an electron from the molecule yielding the molecular ion, a process known as field ionization. Another general result, gleaned from a number of published projects, is that the relative yield of heavy fragments to lighter fragments is maximized for TL pulses, and minimized for longer pulses. This observation can be confirmed, for example, from the work by Kosmidis and Ledingham on nitrotoluene (Kosmidis *et al.*, 1997; Kosmidis *et al.*, 1994b; Ledingham *et al.*, 1995; Tasker *et al.*, 2002) or the Dantus group on para-nitrotoluene (Shane *et al.*, 2006).There are a few exceptions to this rule, for example benzene, acetone and tricarbonyl-[η5-1-methyl-2,4-cyclopentadien-1-yl]-manganese, which will be shown in this chapter.

The goal of laser control in the context of this research is to increase the yield of a desired fragment ion while suppressing the yield of other undesired fragment ions. This goal is illustrated by a simple cartoon in Figure 3.1. One can assess ‘selectivity’ simply by obtaining the ratio between the intensity of two fragment-ion lines in a mass spectrum. Based on the previous observations, the experiment could be trivialized as simply making the pulse as short or as long as possible to observe the greatest change in the aforementioned ratio. By phase modulation one can stretch the pulse from tens of femtoseconds to tens of picoseconds. If, as discussed above, the greatest control is achieved for near TL or maximally stretched pulses, then linear chirp ought to provide a simple one-parameter approach to optimization. Beyond this relatively obvious conclusion, here we look for evidence of a type of shaped pulse that is capable of introducing energy into the molecule in such a way that arbitrary selective bond fragmentation is caused. The elusive pulse among tens-of-thousands of shaped pulses was searched experimentally following a number of strategies inspired by physics, spectroscopy and reaction dynamics, as well as the evidence of selectivity not only between two discrete lines but within the entire mass spectrum. The question this work trying to answer is: how do different phase modulation strategies affect molecular fragmentation?

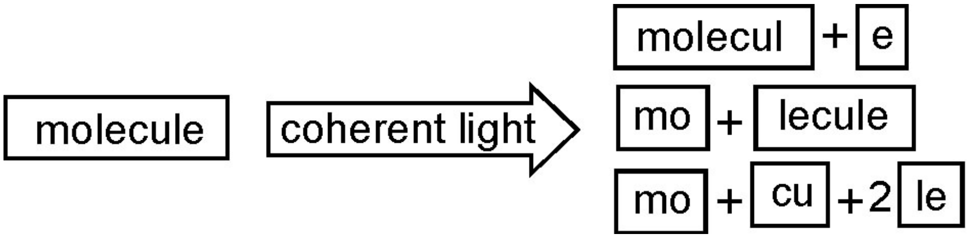

Figure 3.1 Cartoon illustrating different pathways for coherent laser control of a chemical reaction. The yield of each product depends on the time-frequency profile of the laser pulse.

This chapter presents a comprehensive and systematic search for selective fragmentation of gas phase molecules, analyzed using time-of-flight mass spectrometry (TOF-MS). *p*-NT was chosen as an example of a medium-sized molecule with known spectroscopy; additionally, the functionalized aromatic ring gives *p*-NT relative structural complexity. Furthermore, this molecule has been used to refine explosives detection. The mass spectrum of *p*-NT measured with 70 eV electron impact (NIST, 2005) is presented in Figure 3.2a, with the molecular ion at m/z 137. The absorption spectrum (NIST, 2005) is presented in Figure 3.2b, and the excited states S_2 and S_3 are identified based on the literature (Abbott *et al.*, 2002). The ionization energy (IE) and appearance energy (AE) of many ionic fragments have been measured with synchrotron radiation (Sheng *et al.*, 1997) and are presented in Figure 3.2b. As seen in Figure 3.2b at least three photons are required for excitation of the lowest singlet state, six photons for the ionization of the parent ion, and seven to ten photons to access the different fragmentation pathways leading to ionic products.

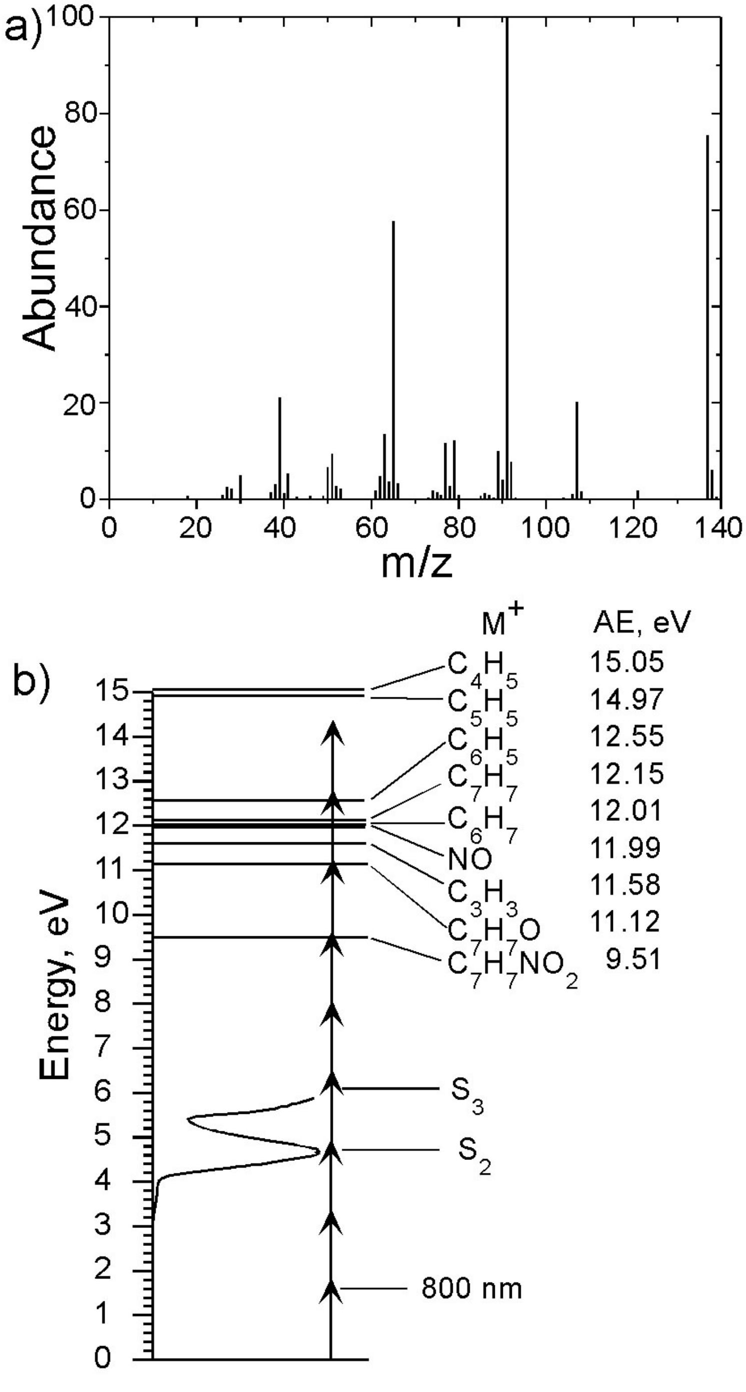

Figure 3.2 a) Mass spectrum of *p*-NT at 70 eV electron impact ionization. b) optical absorption spectra and appearance energies of main fragmentation products by optical synchrotron excitation of *p*-NT.

3.1 Experimental

3.1.1 Typical Shaped Pulses

The lasers and the pulse shapers were described in Chapter 2.

Figure 3.3 shows some of the typical shaped pulses produced by the system. The left column shows the spectrum of the pulses (dashed line) centered around 800nm, along with the phase functions applied to the pulses (solid line). The right column shows the calculated effect of the phase modulation on the pulses in the time domain. Each row shows the effects of a different kind of pulse shaping used in our experiments. The shaped pulses shown have a second harmonic spectrum whose integrated intensity is 25% that of transform limited pulses.

The amplitude of the complex fundamental spectrum is the square root of the measured power spectrum in the frequency domain $I(\omega)$ and the phase $\phi(\omega)$ introduced by the pulse shaper. The complex spectrum of the electric field is given by

$$E(\omega) = \sqrt{I(\omega)}\exp\,[i\emptyset(\omega)] \qquad (1)$$

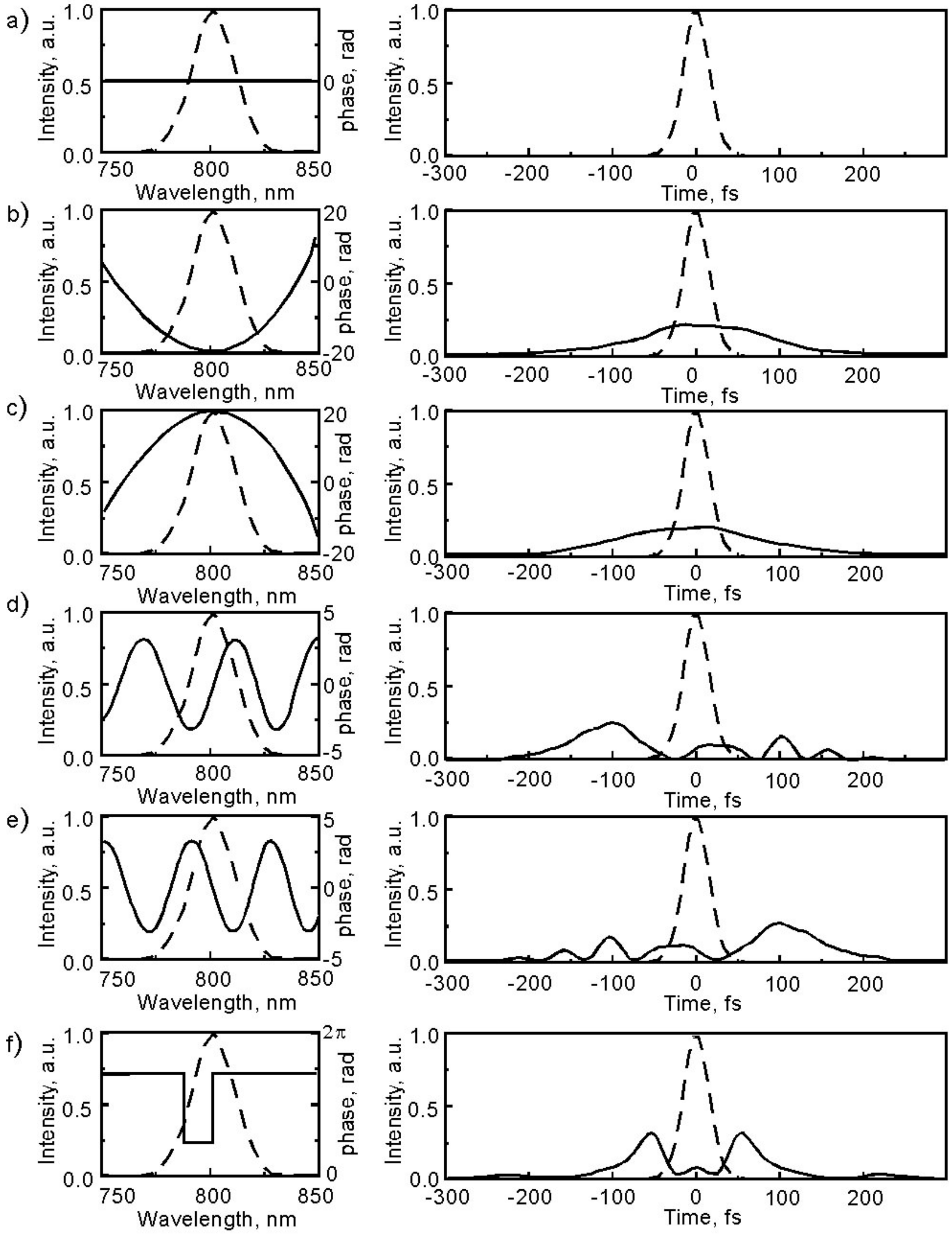
a)
b)
c)
d)
e)
f)
Intensity, a.u.
phase, rad
Wavelength, nm
750
800
850
Time, fs
-300
-200
-100
0
100
200
1.0
0.5
0.0
20
0
-20
5
-5
2π

Figure 3.3 Typical field shapes of phase modulated femtosecond laser pulses. Left column: spectral power (dashed line) and phase (solid line); right column: calculated time profile of the intensity. a) phase compensated TL pulse (dashed line), the starting point for the generation of shaped laser pulses. b-c) positively and negatively chirped pulses with sinusoidal phase function $\phi = \pm 2500\text{fs}^2/2(\omega - \omega_0)^2$. d-e) laser pulse with sinusoidal phase function $\phi = \pm\pi\sin[35\text{fs}(\omega - \omega_0)]$. f) binary phase modulation where phase is evenly modulated in the frequency domain with the string $\pi\pi\pi00\pi\pi\pi$.

To calculate the field in the time domain, we take the inverse Fourier transform of the complex fundamental spectrum.

$$E(t) = \int E(\omega)\, exp\,[-i\omega t] d\omega \qquad (2)$$

Figure 3.3a shows the experimentally measured spectrum (left, dashed line) and the phase used for shaping it. Figure 3.3b shows the calculated time profile of our TL pulses with 30 nm full width at half maximum (right, dashed line) and the resulting intensity of the modulated pulses $I(t)=|E(t)|^2$. Figure 3.3b and Figure 3.3c show the effect of applying positive and negative quadratic chirp to a TL pulse. Formally, the phase function for quadratic chirp is $\phi(\omega) = 0.5\phi''(\omega-\omega_0)^2$ with ϕ'' in units of fs^2. Applying chirp to a Gaussian pulse yields a time profile that is still Gaussian, but stretched out in time, and therefore reduced in intensity. The slight deviation from a Gaussian time profile showed here results from the fact that our experimental spectral profile was not perfectly Gaussian. In Figure 4b, ϕ''= 2500 fs^2, while in Figure 4c, ϕ''= -2500 fs^2.

Figure3.3d and Figure3.3e show the effect of sinusoidal phase modulation, where the period γ, or the phase shift δ were varied, according to $\phi(\omega) = \alpha\sin[\gamma(\omega-\omega_0)-\delta]$. Applying sinusoidal phase modulation causes the time profile of the pulse to spread, as well as to deviate from TL. In the examples shown, phase modulation produces a series of pulses of either decreasing amplitude (Figure3.3d, where $\alpha=\pi$, γ=35 fs, and $\delta=0$) or increasing amplitude (Figure3.3e, where $\alpha=\pi$, γ=-35 fs, and $\delta=0$). Figure3.3f shows an example of the effect of binary phase shaping. In binary phase shaping, the spectral phase is only allowed to take a value of 0 rad (assigned a value of “0”), or π rad (assigned a value of “1”) at discrete blocks of frequencies within the pulse spectrum. The phase function can then be represented as a binary string of 0s and 1s. This representation is similar to that used in areas of signal processing and mathematics for related problems. Binary phase functions can produce a variety of time profiles, but these time profiles will always be symmetric about $t = 0$. In general, the more the phase switches between 1 and 0, the more the time profile will be stretched, and the peak intensity will be reduced. The binary phase function shown in Figure 4f can be represented by the 8-bit string 11100111.

Each of these different phase functions controls a different plausible mechanism that could influence different photofragmentation pathways and cause selective bond cleavage. Chirped pulses cause a linear delay between high and low frequencies within the bandwidth of the laser pulses. This temporal progression has been linked to pump-dump processes in the excitation of a laser dye in solution (Cerullo *et al.*, 1996). Sinusoidal modulation causes trains of pulses. Varying the time delay between these pulses, by varying the modulation frequency, may drive coherently vibrations that again could be implicated in selective bond cleavage. These resonant frequencies have been implicated in control experiments (Wohlleben *et al.*, 2005). Changing the phase of a single sinusoidal phase modulation can be used to control the frequencies at which multiphoton excitation can take place. This type of phase modulation has been used to control two and three photon excitation in atoms (Meshulach *et al.*, 1998) and in large molecules in solution (Dela Cruz, J. M. *et al.*, 2004; Lozovoy, V. V. *et al.*, 2003; Walowicz *et al.*, 2002). Finally, binary phases were examined because of their ability to control the amplitude of multiphoton excitations and to control selective stimulated Raman transitions

(Comstock *et al.*, 2004; Lozovoy, V. V. *et al.*, 2005b; Lozovoy, V. V. *et al.*, 2006d).

In order to test our pulses, SHG spectra for a chirp scan from -20,000 fs^2 to +20,000 fs^2 were recorded, integrated and compared to theoretical simulation, shown in Figure 3.4. The excellent agreement between experimental data and theoretical simulation confirms our ability to deliver pulses with desired phases, including transform limited pulses, to the target accurately.

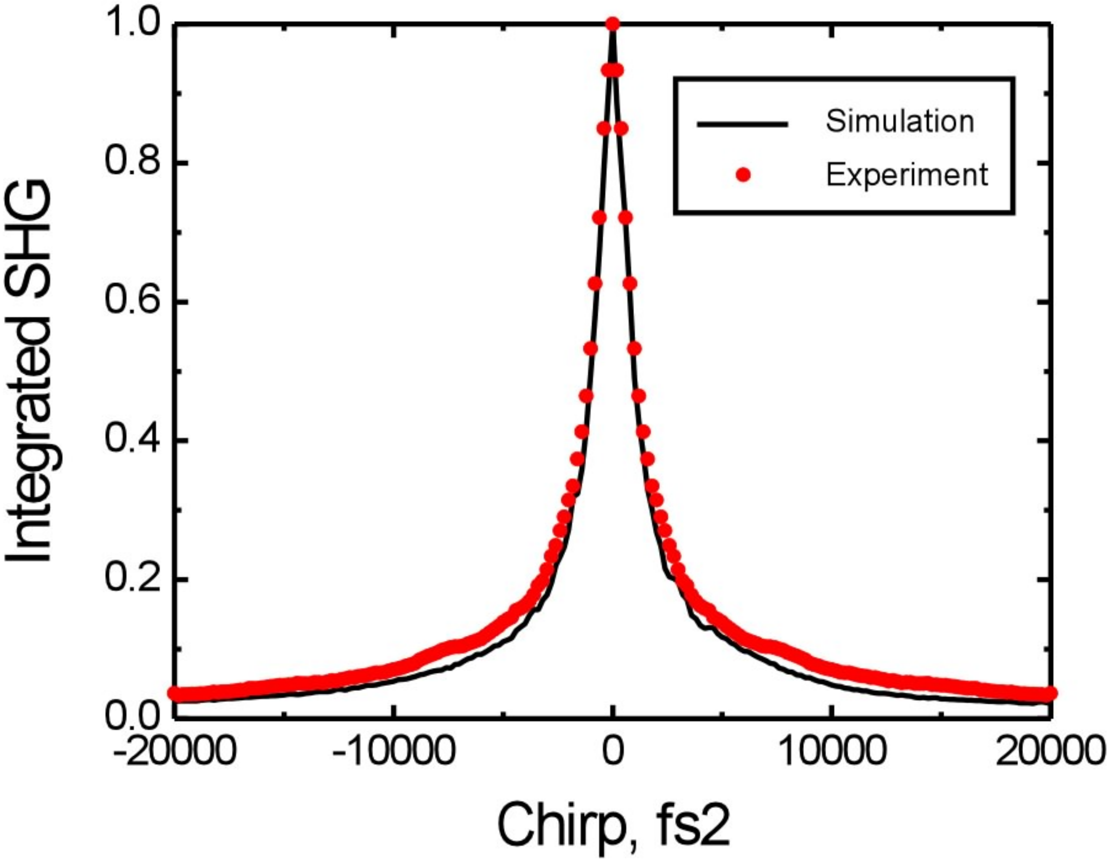

Figure 3.4 Integrated SHG for a chirp scan from -20,000 fs^2 to +20,000 fs^2 starting with 35 fs TL pulses. Red dots are experimental data and the solid line is the theoretical simulation. For interpretation of the references to color in this and all other figures, the reader is referred to the electronic version of this dissertation.

3.1.2 Mass spectrometry

The time-of-flight mass spectrometer used for this study was described in Chapter 2. The Raw mass spectrum of *p*-NT obtained with TL 6×10^{15} W/cm^2 pulses is presented and the main fragment-ions are labeled in Figure 3.5a.After identification of several “fingerprint” ions in the raw MS the ion drift time can be transformed to an *m/z* scale. Mass spectra obtained for TL 6×10^{14} and 1×10^{13} W/cm^2 are shown in Figure 3.5b and Figure 3.5c, respectively.

A bar diagram is calculated from integrals under the corresponding peaks in the MS data. Because pulse shaping affects the MS, the results are presented as percentage of total ionization (Y, %) (Watson, 1997). Standard deviations in the bar-graph (see Figure 3.6a) are small and were calculated using 6 to 10 repetitions of the experiments. Figure 3.6 demonstrates the MS spectrum following excitation with TL pulse and for pulses stretched up to 635 fs by a quadratic phase modulation $\phi''=\pm8000$ fs^2 introduced by Shaper I. To assess the selectivity the intensity of fragment ions with *m/z* 91 and *m/z* 39 (see Figure 3.6) were compared. Control over all the different fragments ions will be presented in the later sections of this article. As can be immediately seen from Figure 3.6 the shapes of the MS spectra are different between TL and chirped pulses and do not depend on the sign of the phase modulation.

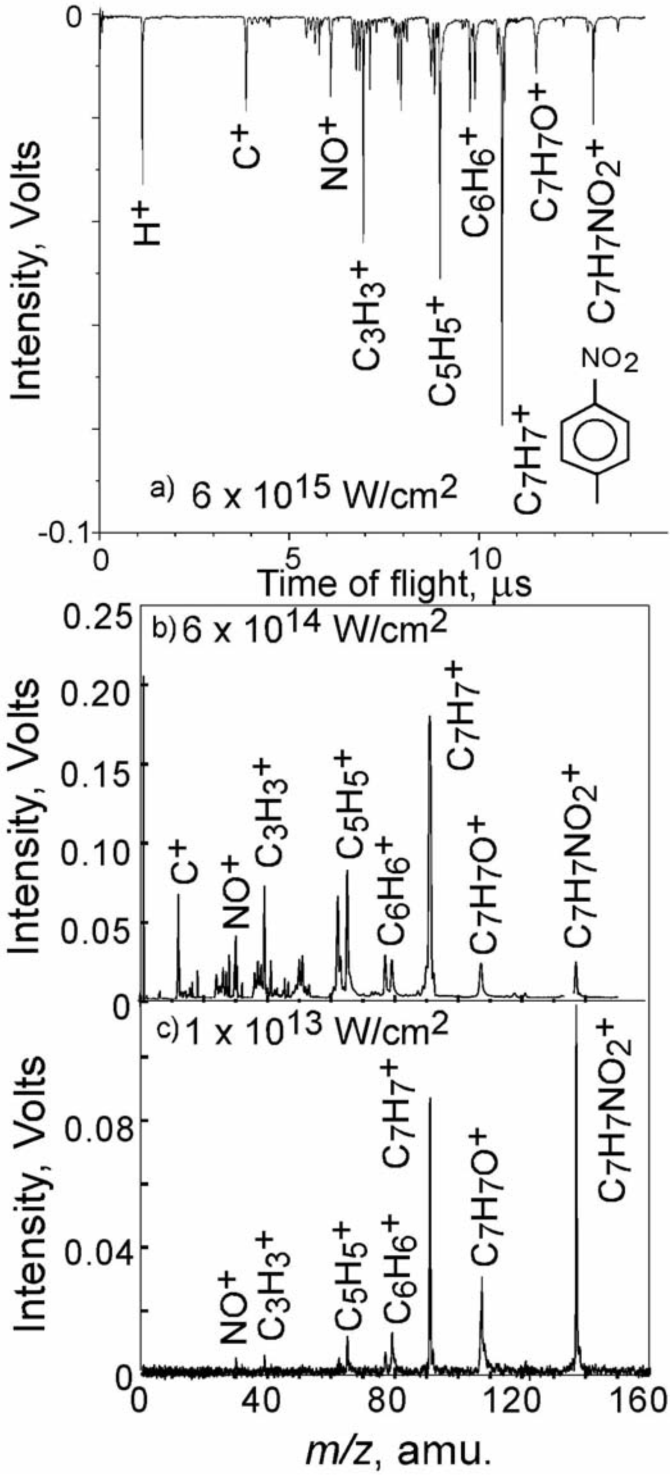

Figure 3.5 Mass spectra for *p*-NT. (a) Oscilloscope trace of the time of flight mass spectrum of *p*-NT under TL optical excitation for 6×10^{15}. Mass spectra obtained for TL 6×10^{14} (b) and 1×10^{13} W/cm^2 (c).

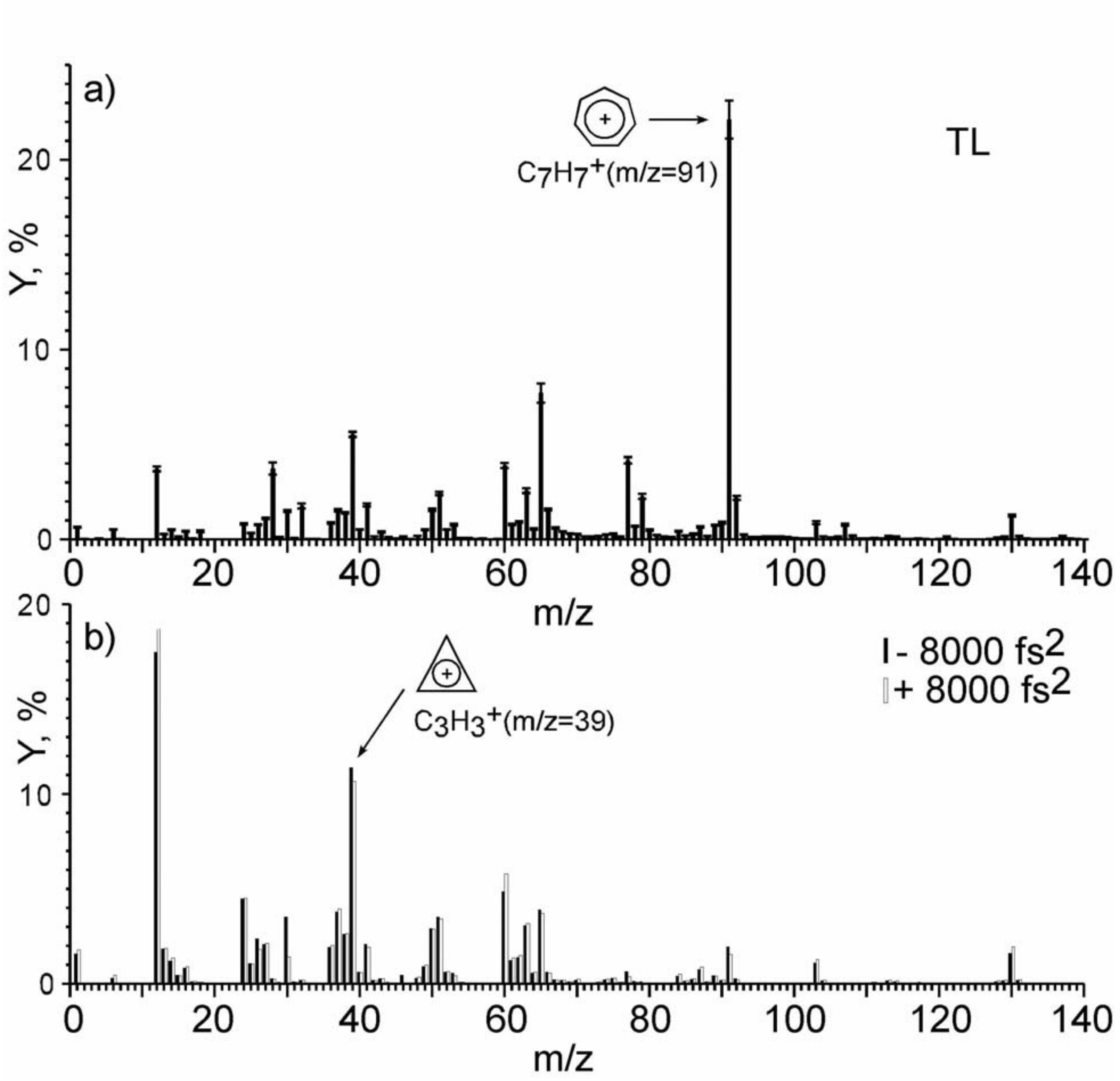

Figure 3.6 Bar diagrams of the mass spectra of *p*-NT. a) percentage of total ionization for each *m/z* value at TL excitation; standard deviations of these measurements are marked as error bars. b) Mass spectra using positively and negatively chirped pulses. The two most abundant molecular products, which are used for selectivity analysis, are identified in the spectra.

Contamination due to the accumulation of photoproducts in the chamber could be a serious problem resulting in misleading conclusions. To prevent this source of error, a pressure of 10^{-5} Torr is maintained when running the experiments by equilibrating the vapor of the sample and the fast pumping speed of the 4 inch turbo molecular vacuum pump. The fast flow is confirmed by observing the fast decay of the signal when closing the valve (See Figure 3.7).

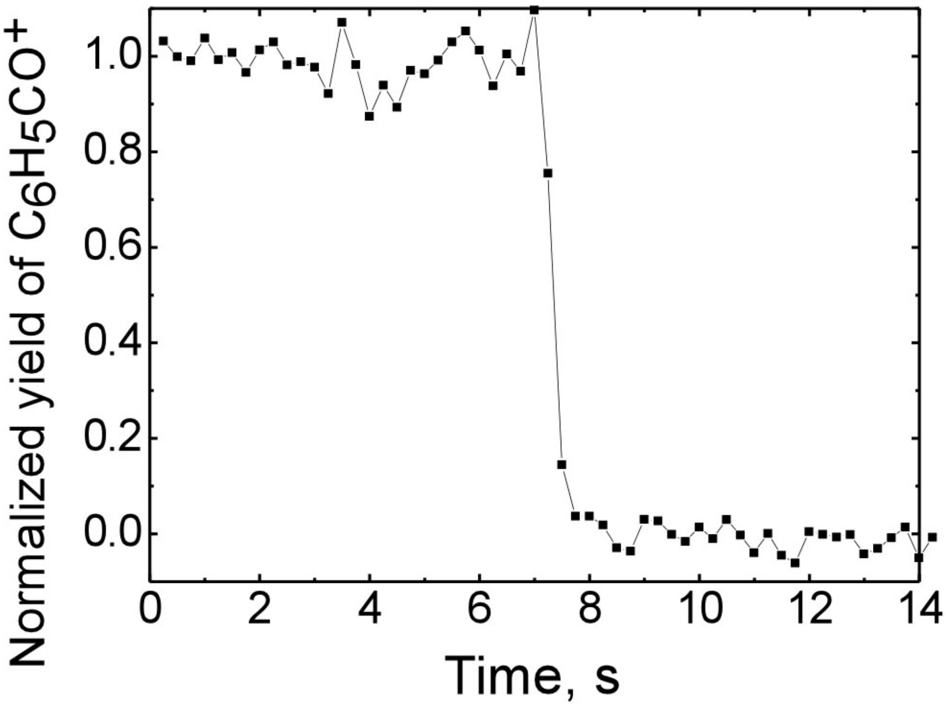

Figure 3.7 The intensity of $C_6H_5CO^+$, the most abundant photoproduct from acetophenone, drops to zero within a half second after closing the valve, which confirms the fast flow of our system.

3.1.3 Effect of focusing

MS results can be influenced by the focusing parameters (Posthumus, 2004; Robson *et al.*, 2005; Zhang *et al.*, 1994). In order to make sure that the results obtained are general and can be used to explain experiments carried out elsewhere, how changes in the focusing parameters affect the observed results was explored.

Laser intensity dependence measurements were carried out on *p*-NT using both short and long focusing geometries. The measurement with the longer focal length were made using a slit to limit the z axis contribution to volume effect (Hankin *et al.*, 2000, 2001; Wang *et al.*, 2005). From the measurements presented in Figure 3.8a we find the expected initial rise of the signal and it's change to a linear dependence. From these data we obtain a value for the I_{sat} of 1.7×10^{14} W/cm^2 which is in the range of expected values for organic molecules. The interpretation of I_{sat} has been discussed in detail by Corkum (Hankin *et al.*, 2000, 2001). In the simplest approximation (sudden model) I_{sat} is assumed to indicate a value where 100% of the species in the focal volume are ionized. In the case of multiphoton ionization I_{sat} is defined as the intensity at which 43% of the molecules in the laser irradiated volume are ionized (Hankin *et al.*, 2000, 2001). As can be expected, above I_{sat} one can expect high signal-to-noise ratios because signals are quite robust. At values below I_{sat} pulse shaping causes a significant drop in the signal, greatly reducing the reliability of the measurements. Most of the experiments presented here were carried out above I_{sat} under the conditions shown in Figure 3.5b, without the extraction plate slit. If laser controlled chemistry will have a practical application, it is only above I_{sat} that a significant yield of products could be achieved. This is why laser control above I_{sat} is considered here. A discussion and experimental evaluation of the findings near and below I_{sat}, including a quantitative analysis of volume effects is given later.

Having chosen the shorter focal length arrangement we explored effects caused by changing the diameter of the beam before the focusing lens while adjusting the power of the laser to keep the energy of the pulse constant. These measurements probe effects of the Rayleigh length of the beam on our findings. It's observed that the MS yield increased as the input beam diameter decreased (see Figure 3.9a). This observation can be explained by realizing that decreasing the input beam causes an increase in the spot size and Rayleigh length. These increases cause the irradiated volume, where the field strength exceeds the threshold for ionization, to increase. Therefore, more molecules can be ionized. It is important to note that, the ratio between the fragment ions with *m/z* 91 and *m/z* 39, and in general the overall shape of the mass spectrum, was found to be independent on the diameter of the laser beam or the average laser power (Figure 3.9). Therefore, the conclusion is that although focusing parameters can change the overall signal level and the volume from which the ions are generated, these changes do not influence the ability of the laser parameters to change the fragmentation pattern which is used here as a measure for selectivity. The changes observed as a function of intensity for both short and long focusing conditions will be discussed later.

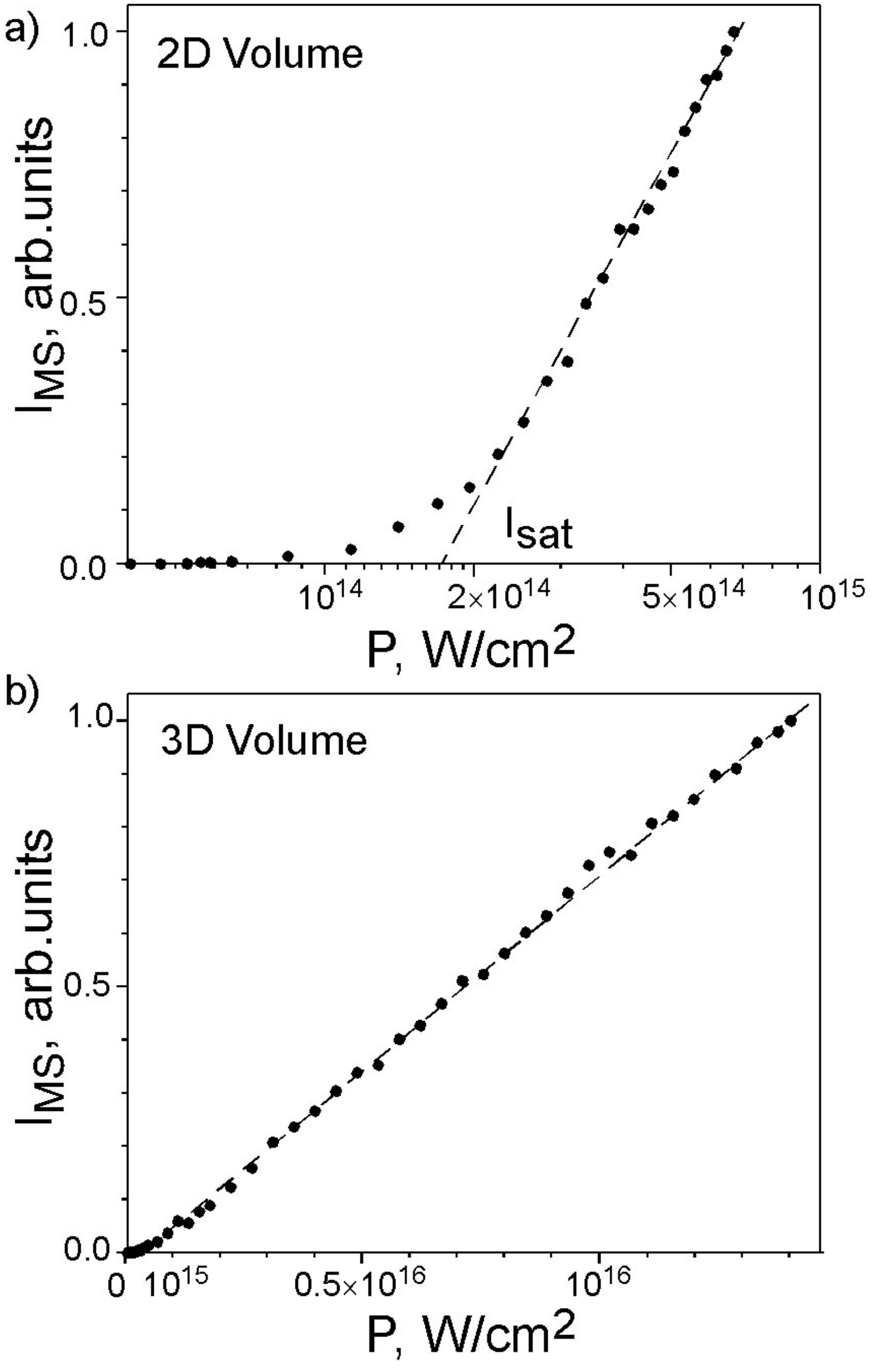

Figure 3.8 Power dependence of the total yield of ionization of *p*-NT. a) Experiment carried out using the 300 mm focal length lens and a 0.9 mm slit on the extraction plate. b) Experiment carried out using 50 mm focal length lens with a wire grid extraction plate.

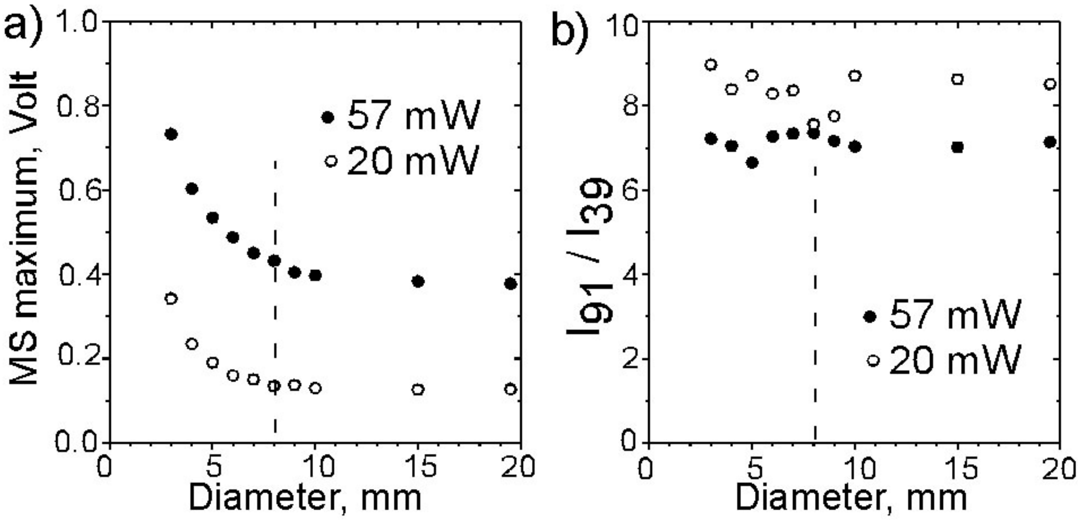

Figure 3.9 a) Dependence of strongest line (m/z=91) total TOF MS yield on the diameter of the iris used to cut the beam, shown at two different laser powers.The dashed line is the beam waist size of the collimated beam used in all subsequent experiments. b) Ratio between integrated MS signals from two products at different powers and beam diameters.

3.1.4 Chemicals

Experimental samples: *para*-nitrotoluene (*p*-NT, Aldrich 99%), *meta*-nitrotoluene (*m*-NT, Aldrich 99%), *ortho*-nitrotoluene (*o*-NT, Aldrich 99+%), 1-methyl-2,4-dinitro-benzene (DNT, Aldrich 97%), benzene (Aldrich 99+%), toluene (J T Baker 100%), naphthalene (Aldrich 99.7%), azulene (Aldrich 99%), acetone (Mallinckrodt 99.8%), acetyl chloride (Aldrich 99+%), acetophenone (Fluka >99.5%), *p*-chrolobenzonitrile (Aldrich 99%), N,N-dimethylformamide (DMF, Spectrum Chemicals 99.8%a), dimethyl phosphate (DMP, Aldrich 98%), 2-chloroethyl ethyl suifide (h-MG, Aldrich 98%), and tricarbonyl-[(1,2,3,4,5-η5)-1-methyl-2,4-cyclopentadien-1-yl]-manganese (MMT, Aldrich 99.5%) were used without further purification.

3.2 Results

3.2.1 Effects of power, bandwidth and carrier frequency of TL pulses

The first set of experiments explored the effect of power, pulse duration and carrier frequency for TL pulses on the fragmentation and ionization of *p*-NT. The power of the pulse was changed using a zeroth-order half-wave retardation plate and a calcite polarizer. The pulse duration and carrier frequency changes were achieved using amplitude modulation in pulse Shaper II. The group velocity dispersion on the pulse for each setting was compensated for each measurement using MIIPS (Coello *et al.*, 2008; Dantus *et al.*, 2007; Lozovoy, V. V. *et al.*, 2004; Xu *et al.*, 2006). The results of these experiments are collected in Figure 3.10. Column I shows the dependence of the integrated SHG obtained after a frequency doubling crystal (I_{SHG}) and is used as a diagnostic, Column II shows the integrated yield of all ions (I_{MS}), and

Column III shows the percentage of total ionization (Y,%) of two different fragment ions (C_7H_7 and C_3H_3) as functions of the scanned parameters. Column IV shows the integrated ion intensity (I_{MS}) plotted against the measured integrated SHG (I_{SHG}). Column V shows how the ratio between the yields of the two fragment ions (m/z=91 divided by m/z=39) depends on the integrated ion intensity. The intensities I_{SHG} and I_{MS} were normalized to the value measured for TL pulses. The first row (a) presents results as a function of average power (at constant spectral shape corresponding 35 fs time duration); the second row (b) presents results as a function of spectral width of the pulse while the intensity of the laser is held at 50 mW; The third row (c) presents results as a function of position of the pulse maximum while the FWHM of the spectral width is restricted to 15-17 nm.

The results from the first row in Figure 3.10 show the expected quadratic dependence of the SHG intensity on the intensity of the laser. In this range, 10^{15} - 10^{16} W/cm^{2}, the total ion intensity was found to increase linearly with the power of the pulse. Despite the order of magnitude change in laser intensity and the similarly large change in the excitation volume, the ratio between the two different fragment ions stays constant. The results in the second row show the dependence on bandwidth. It can be seen that the total ion yield tracks the integrated SHG signal, which is confirmed by the nearly linear relationship between the two in column IV. The yield of the heavy and light ions changes as a function of bandwidth. The broader bandwidth (TL) pulses favor the larger ions. The results in the third row explore possible effects caused by the carrier frequency. Most importantly, the ratio between the two different fragment ions remains constant, indicating selectivity is not a function of carrier frequency.

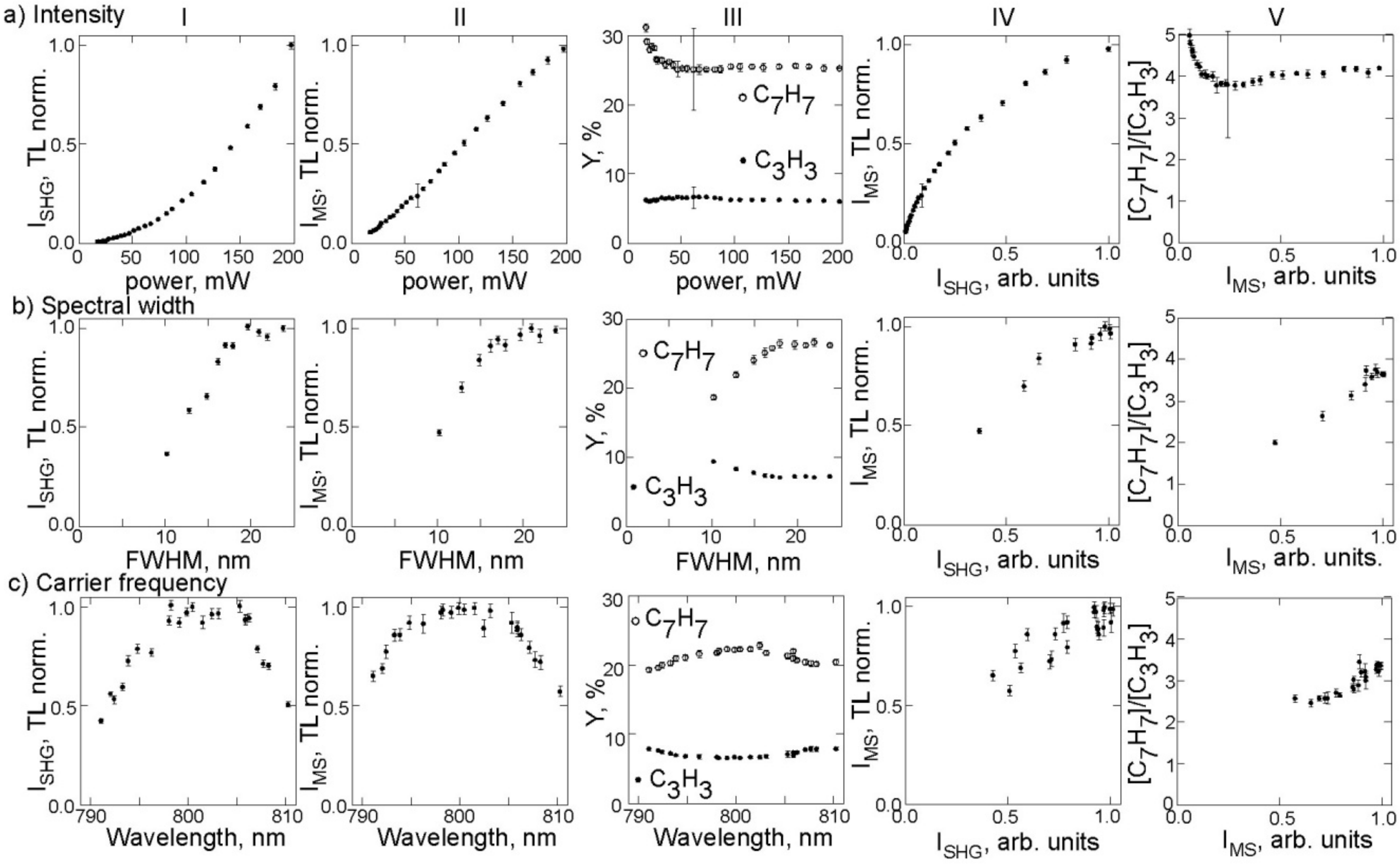
a) Intensity
I
II
III
IV
V
I_{SHG}, TL norm.
I_{MS}, TL norm.
Y, %
$[C_7H_7]/[C_3H_3]$
power, mW
I_{SHG}, arb. units
I_{MS}, arb. units
○ C_7H_7
● C_3H_3
b) Spectral width
FWHM, nm
I_{MS}, arb. units.
c) Carrier frequency
Wavelength, nm
0.0
0.5
1.0
0
10
20
30
1
2
3
4
5
50
100
150
200
790
800
810

Figure 3.10 Experimental fragmentation results with a) different pulse energies but constant duration, b) different spectral widths at constant 50 mW laser energy, and c) different carrier frequencies at constant 35 fs pulse duration and 50 mW laser energy. The columns denote: I. Dependence of the energy of the SH generated in the nonlinear crystal. II. Dependence of the total yield of all positively charged ions. III. Yield (percentage of total ionization) of two major fragments. IV. Total yield of all fragments as a function of intensity of SHG in the crystal. V Selectivity (ratio between fragments) as a function of total yield of all fragments. All results are given with standard deviation of measurements as error bars obtained from 10 runs, averaging 128 laser pulses each. Yields are normalized to the maximum value.

3.2.2 Effects of quadratic and sinusoidal phase modulation on SHG, total fragmentation yield and selectivity

In the second set of experiments changes that are caused by phase only modulation were explored, with the amplitude kept constant. The experimental results are summarized in Figure 3.11. The average power of the beam was 170 mW at 1 kHz, and pulse duration of the corresponding TL pulse was 35 fs. Column I shows I_{SHG}. Column II shows total ionization yield I_{MS}. Column III shows relative yields of two fragments. Column IV shows the relation between total ionization yield and the intensity of the SHG. Column V shows the ratio of the two fragments as a function of total ionization yield. Quadratic $\phi=0.5\phi''(\omega-\omega_0)^2$ or sinusoidal $\phi=\pi\sin[\gamma(\omega-\omega_0)+\delta]$ phase functions were introduced using Shaper I. The results in the first row (a) show the effects caused by linear chirp, more precisely known as quadratic phase modulation (ϕ''). It can be seen that I_{MS} and I_{SHG} have a very similar dependence which is confirmed in panel IV. An overall laser control factor R_{max}/R_{min} = $([C_7H_7]/[C_3H_3])_{max}/([C_7H_7]/[C_3H_3])_{min}=30$ was measured, achieved here by simple chirp. Interestingly, it can be observed that the light and heavy fragment yields have a linear relationship as evidenced by panel V. The second row (b) shows the effects caused by changing the period of a sinusoidal phase modulation (γ, while keeping $\delta=0$). Positive as well as negative values were scanned in order to explore possible effects of temporal symmetry of the pulse. For sinusoidal modulation the pulse in the time domain changes depending on the sign, for example see Figure 3.3d and Figure 3.3e. Once again it's seen that I_{MS} and I_{SHG} have a very similar dependence which is confirmed in panel IV. An overall laser control factor $R_{max}/R_{min}=10$ was measured. It's also seen that the light and heavy fragment yields have a linear relationship as evidenced by panel V. The slight asymmetry between positive and negative γ appears as a slight deviation in the linear relationship between I_{MS} and I_{SHG}. This deviation is probably caused by the imperfection of the phase modulator, particularly the effect of phase wrapping (Dantus *et al.*, 2004) in the SLM after the distortion compensation and additional phase function are implemented. The third row (c) shows the effects caused as sinusoidal phase functions are introduced with different values for δ while keeping γ=35 fs. It's seen that changing δ causes small changes in all the observed variables compared to the other modes of phase modulation. Changes in δ cause changes in the frequencies at which multiphoton transitions can take place (Lozovoy, V. V. *et al.*, 2003; Walowicz *et al.*, 2002). The modest laser control factor $R_{max}/R_{min}=1.5$ observed here indicates that resonant multiphoton transitions play a minimal or no role in the fragmentation of this molecule under the conditions of our experiments.

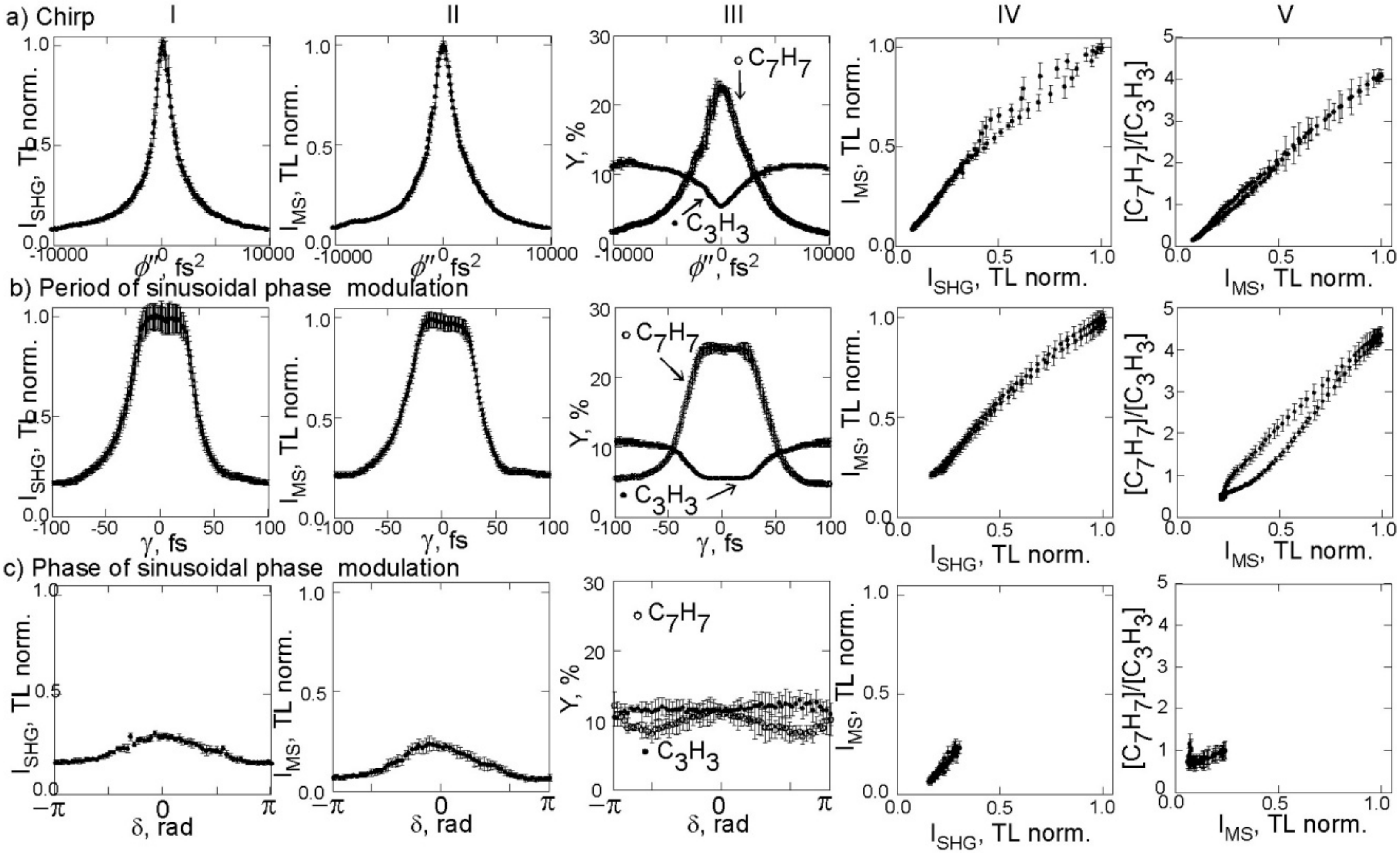
a) Chirp
I
II
III
IV
V
I_{SHG}, TL norm.
I_{MS}, TL norm.
Y, %
C_7H_7
C_3H_3
ϕ'', fs^2
-10000
0
10000
I_{SHG}, TL norm.
I_{MS}, TL norm.
$[C_7H_7]/[C_3H_3]$
b) Period of sinusoidal phase modulation
γ, fs
-100
-50
0
50
100
c) Phase of sinusoidal phase modulation
δ, rad
$-\pi$
π
0.0
0.5
1.0
0
10
20
30
1
2
3
4
5

Figure 3.11 Experimental results on fragmentation using phase only shaped femtosecond pulses with a) differing amounts of quadratic chirp ω, with phase functions given by $0.5\phi''(\omega-\omega_0)^2$, b) sinusoidal phase modulation with different periods γ, with phase functions $\pi\sin[\gamma(\omega-\omega_0)]$, c) sinusoidal phase modulation with different phase delays δ, with phase functions $\pi\sin[35\text{ fs }(\omega-\omega_0)+\delta]$. The columns denote: I. Dependence of the energy of the SH generated in the nonlinear crystal. II. Dependence of the total yield of all positively charged ions. III. Percentage of ionization of two main fragments. IV. Total yield of fragments as a function of intensity of SHG in the doubling crystal. V. Selectivity as a ratio between fragments as a function of total yield of fragments. All results are given with standard deviation of measurements as error bars obtained from 10 runs, averaging 128 laser pulses each. Yields are normalized to the value obtained at TL excitation.

3.2.3 Effects of binary phase on SHG, total fragmentation yield and selectivity

In the third set of experiments the effects caused by binary phase modulation using Shaper I (before the amplifier) and Shaper II (after the amplifier) were explored. For these experiments 8-bit functions were used. The central 6 logical bits correspond to groups of binned pixels in the central part of the spectrum (the region for which the spectral intensity was greater than 25 percent of the maximum. The blue and red spectral wings of the pulse were assigned as the 0th and 7th bits of the 8 bit sequences, where logical 0 corresponds to phase value of 0 rad and logical 1 corresponds to phase value of π rad. The average power of the beam was 100 mW, and pulse duration of the corresponding TL pulse was 35 fs. The columns in Figure 3.12 follow the same arrangement as in Figure 3.10 and Figure 3.11. The results demonstrate that phase modulation by Shaper I and II are equivalent. Interestingly, once again it's seen that the measured I_{MS} and I_{SHG} have a linear dependence which is confirmed in panel IV. The laser controllability factor R_{max}/R_{min} observed for 8 bit binary phase shaping was 20 for the Shaper I and 10 for Shaper II. This difference may be caused by slight beam distortions caused by the limited height of the liquid crystal mask which is smaller than the beam diameter and apertures the beam.

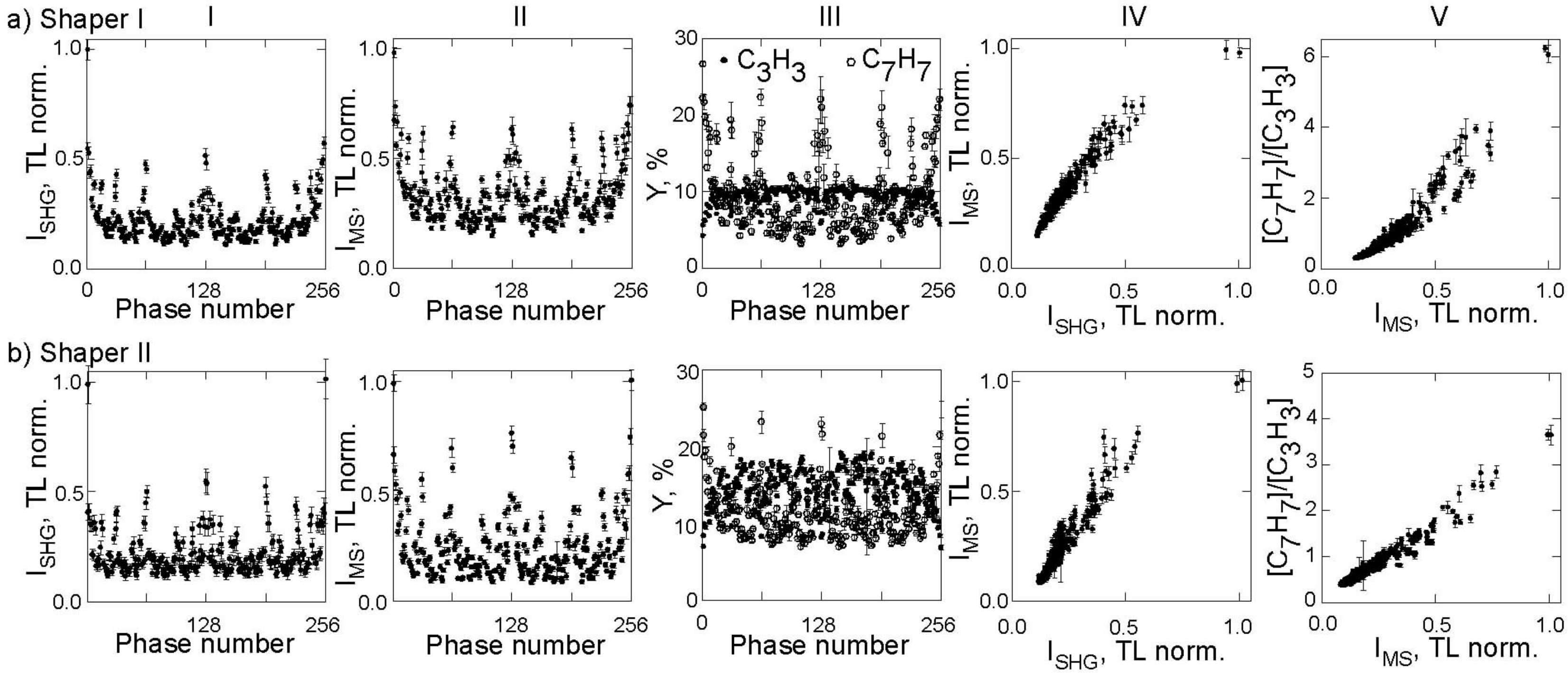
a) Shaper I
I
II
III
IV
V
I_{SHG}, TL norm.
I_{MS}, TL norm.
Y, %
C_3H_3
C_7H_7
$[C_7H_7]/[C_3H_3]$
Phase number
0
128
256
0.0
0.5
1.0
0
10
20
30
2
4
6
b) Shaper II
1
3
5

Figure 3.12 Experimental results on fragmentation using binary phase modulated femtosecond pulses. a) using shaper between oscillator and amplifier, b) using shaper after the amplifier. The columns denote: I. Dependence of the energy of the SH generated in the nonlinear crystal. II. Dependence of the total yield of all positively charged ions. III. Percentage of ionization of two main fragments. IV. Total yield of fragments as a function of intensity of SHG in the doubling crystal. V. Selectivity as a ratio between fragments as a function of total yield of fragments. All results are given with standard deviation of measurements as error bars obtained from 10 runs, averaging 128 laser pulses each. Yields are normalized to the value obtained at TL excitation.

3.2.4 Effect of laser pulse energy density

Experimental measurements with four different phase functions were repeated using four different laser pulse energies, ranging from 2×10^{15} to 1.5×10^{16} W/cm^2 when TL, in order to determine if molecular fragmentation depends on the laser pulse energy density. As can be seen in Figure 3.13, the relative yield of C_7H_7 and C_3H_3 ions is independent from the energy of the pulse for all types of phase modulation. These results may seem to contradict results in the literature for which laser pulse intensity did change the relative yield of fragment ions. Given that a complete review of all such observations is beyond the scope of this article, the explanation is limited to only the current results. The experiments presented here were carried out with very well-behaved pulses. Given our ability to eliminate all phase distortions from our pulses, they are free from a pedestal or wings, therefore as the intensity is increased there is no drastic change in the field. Conversely, for pulses that have a pedestal, increasing the intensity results in substantially different fields interacting with the molecules and hence to different results. Notice that the results given in Figure 3.13, were repeated with four different sets of shaped pulses; a. chirp, b. binary, c. sinusoidal period, and d. sinusoidal phase. In all cases, laser pulse intensity had no influence on relative yield. Of course, the signal intensity changed drastically and so did the volume probed in each case, however, the relative yields remained constant for all laser intensities. The overall laser control factor measured were 7.5 for chirp, 11 for binary, 7.5 for sinusoidal period, and 3 for sinusoidal phase, which were found to be independent of laser intensity. The controllability parameter for chirp modulation here is 4 times smaller than that found in Figure 3.11 because for these measurements the maximum chirp (5,000 fs^2) was 4 times smaller than in the previous experiment (20,000 fs^2). These results prove that energy density is not responsible for the changes observed in the fragmentation patterns.

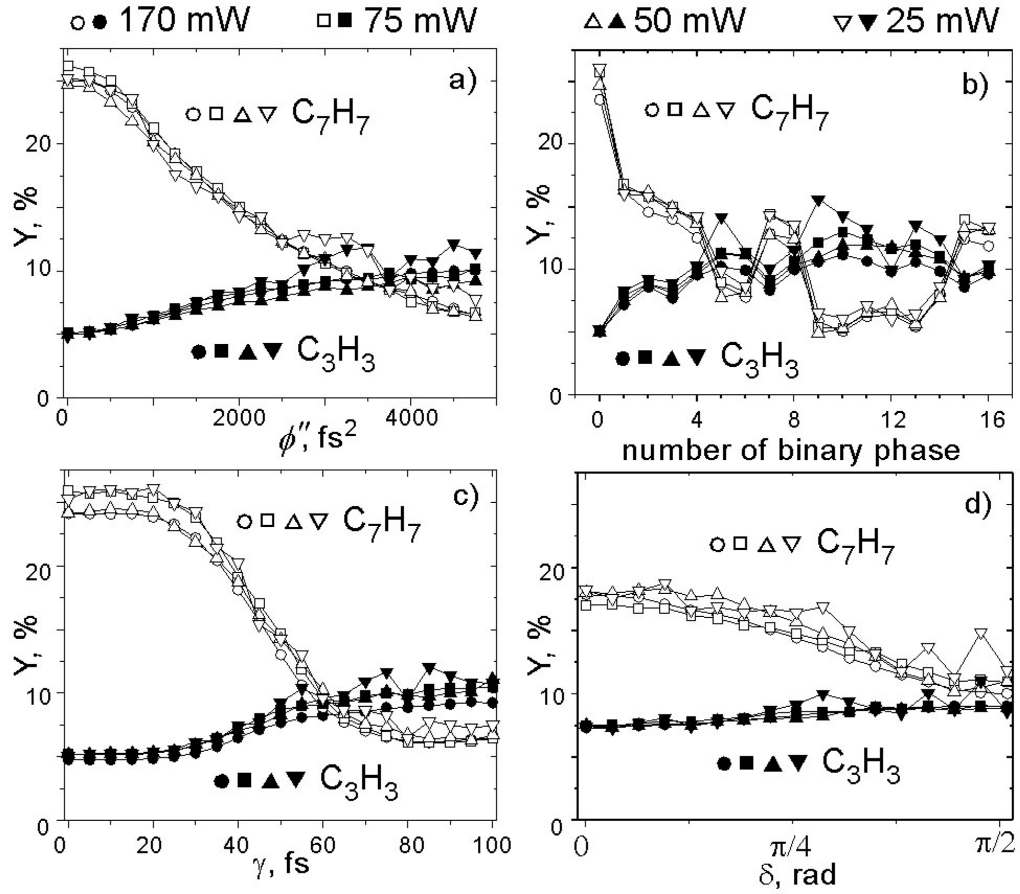

Figure 3.13 Percentage of total ionization measured at different laser powers (dot, squares, up and down triangle for 170, 75, 50 and 25 mW respectively) for two main fragments of dissociation of *p*-NT; C_7H_7 (open symbols) and C_3H_3 (filled symbols). Experiments were carried out using different types of phase modulation including; a) quadratic phase modulation $0.5\phi''(\omega-\omega_0)^2$, b) 8 bit binary phase modulation, c) sinusoidal phase modulation with different period $\pi\sin[\gamma(\omega-\omega_0)]$, d) periodical phase modulation with scanning phase $\pi\sin[35\text{ fs }(\omega-\omega_0)+\delta]$. The difference of the signal for different power is no more than the standard deviation of the measurements.

3.2.5 Dependence of fragmentation pattern on phase function used

As seen in Figure 3.6b and Figure 3.11a.I-III, both the sign of the quadratic phase modulation and the sign of the period of a sinusoidal phase modulation does not affect the results. However, the modulation parameters do affect the total yield of fragments. It is very interesting that for all types of modulation the total yield of fragmentation and ratio between heavy and light fragments are found to be linearly proportional to the measured SHG in the crystal, or total ionization yield, as seen in columns IV and V of Figure 3.10, Figure 3.11, and Figure 3.12.

In order to compare the results among different pulse shaping phase functions, the normalized integrated ion signal I_{MS} was used as an independent parameter, with $I_{MS} = 1$ for TL pulses. The extent of phase modulation causes I_{MS} to decrease. Different methods of phase modulation used include: a) quadratic phase modulation, $\phi(\omega) = ½\phi''(\omega-\omega_0)^2$; b) periodic phase modulation, $\phi(\omega) = \alpha\sin[\gamma(\omega-\omega_0)]$; and c) binary phase modulation, in which the binary phase number is defined as $BPN=\Sigma_i\phi_i/\pi$. The relative yield of six different $C_nH_n^+$ ions normalized to their yield when using TL excitation was compared and plotted against I_{MS}. The first column of Figure 3.14 shows the change in the yield for each of these fragment ions for each method of phase modulation. Notice the clear evidence for the elimination of C_2H_2 units are reflected in the alternating intensities of the different fragment ions ($C_7H_7^+$, $C_5H_5^+$, $C_3H_3^+$). In Figure 3.14, very similar (essentially identical) trends are observed for every single fragment despite the use of three very different forms of phase modulation. The similarity in the yields as a function of I_{MS} between the very different pulse shaping experiments is unexpected. Note that the laser control factor is about 5 in the four cases. However, it appears from the second column of Figure 3.13 that the extent of fragmentation depends on I_{MS} but does not depend on the function used to shape the pulses. As we can see from

Figure 3.3, different types of modulation produce very different fields, but the relative yields of fragments depend only on the overall efficiency of the field to produce ions and not on the detailed temporal or spectral behavior of the field. As observed earlier, this efficiency (I_{MS}) is also proportional to the integrated yield of SHG (I_{SHG}). It's confirmed from Figure 3.14 that in general as the pulse is shaped the relative yield of smaller ions increases while that of heavy ions decreases.

a) Linear chirp

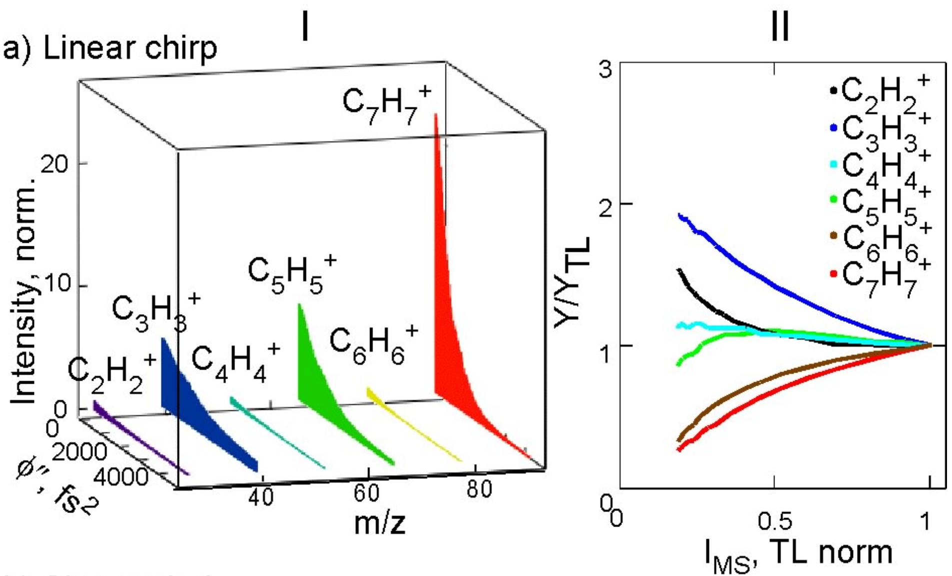

b) Sine period

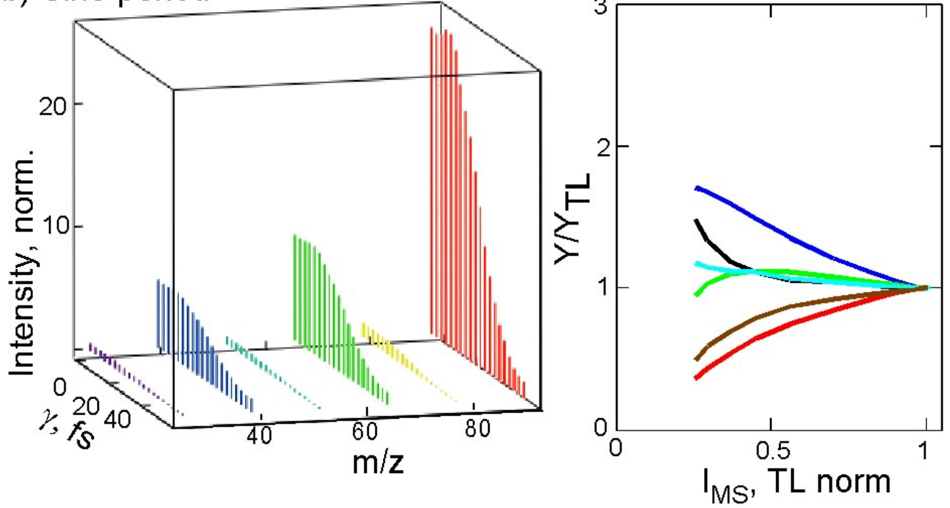

c) Binary phase

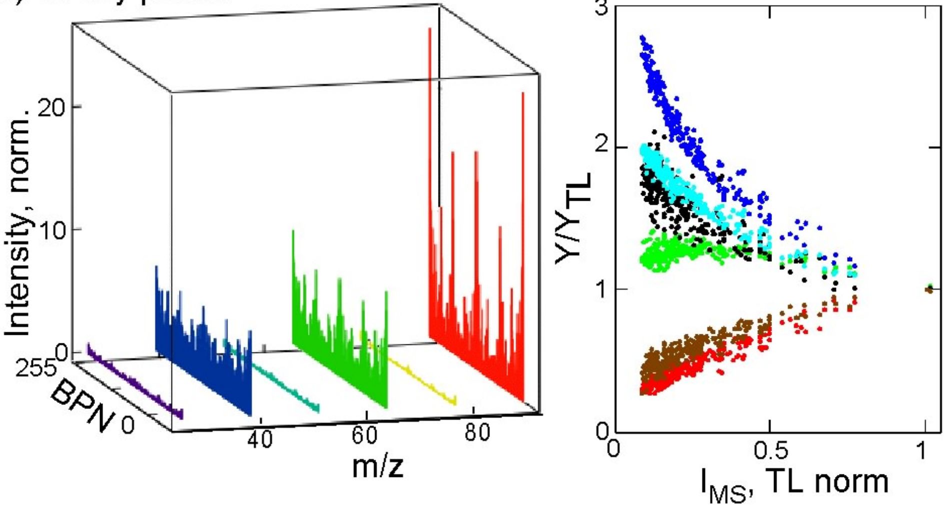

Figure 3.14 Comparison of effects of different types of phase modulation on fragmentation of *p*-NT. Experiments were done using a) quadratic phase modulation $0.5\phi''(\omega-\omega_0)^2$, b) sinusoidal phase modulation with different period $\pi\sin[\gamma(\omega-\omega_0)]$, c) 8 bit binary phase modulation. In column I, mass spectra of selected ions (C_nH_n) are presented as functions of the scanning parameters of phase modulation. In column II, the intensity of selected lines is presented as functions of total fragmentation yield, with the data on both axis normalized on the value at TL excitation. The difference between normalized functions is no more than the precision of measurements. For interpretation of the references to color in this and all other figures, the reader is referred to the electronic version of this dissertation.

3.2.6 Statistics of total ion yield and ratio between ion yields

All the findings so far seem to support the hypothesis that regardless of the pulse shaping phase function, a single laser characterization parameter, such as the resulting I_{MS} or I_{SHG}, can be used to determine the fragmentation pattern and hence the laser control factor for a given ratio between two fragment ions. An experiment was designed that would stringently test this hypothesis. This experiment is unusual because it is designed to find any pulse that violates the hypothesis. This requires us to evaluate an entire set of pulses that have a particular I_{MS} and I_{SHG}, and determine if any show a different fragmentation, as measured by a product ratio that is outside of the experimental noise.

For this experiment shaped pulses with pre-calculated (10-bit) phase functions that generate only 10%-20% of the SHG corresponding to TL pulses were used. In these experiments we used a limited range of the available spectrum. The wings of the spectrum were suppressed to produce a shape that more closely resembles a flat spectrum. For our simulations, Galois fields were used, where the spectral component of the electric field can only be positive or negative at the flat spectrum (Lozovoy, V. V. *et al.*, 2006d). Statistical analysis of 537 different phases is presented in the Figure 3.15. For all the hundreds of measurements a linear dependence of I_{MS} versus I_{SHG} is observed, see Figure 3.15a. The statistical signature for linear dependence is the Pearson correlation coefficient (r), which is very close to unity for this experiment. Figure 3.15b shows the results for all experiments that fell inside the window for I_{MS} and I_{SHG} defined by standard deviation of experimentally measured I_{MS} and I_{SHG}. These measurements were sorted according to ascending ratio. All the phase functions produced MS with a ratio $[C_7H_7]/[C_3H_3]$ described by a normal Gaussian distribution shown in Figure 15c. This agreement between the measurements and the predicted value implies that statistically there is no difference in the selectivity of fragmentation outcome as a result of pure phase modulation regardless of the phase function used.

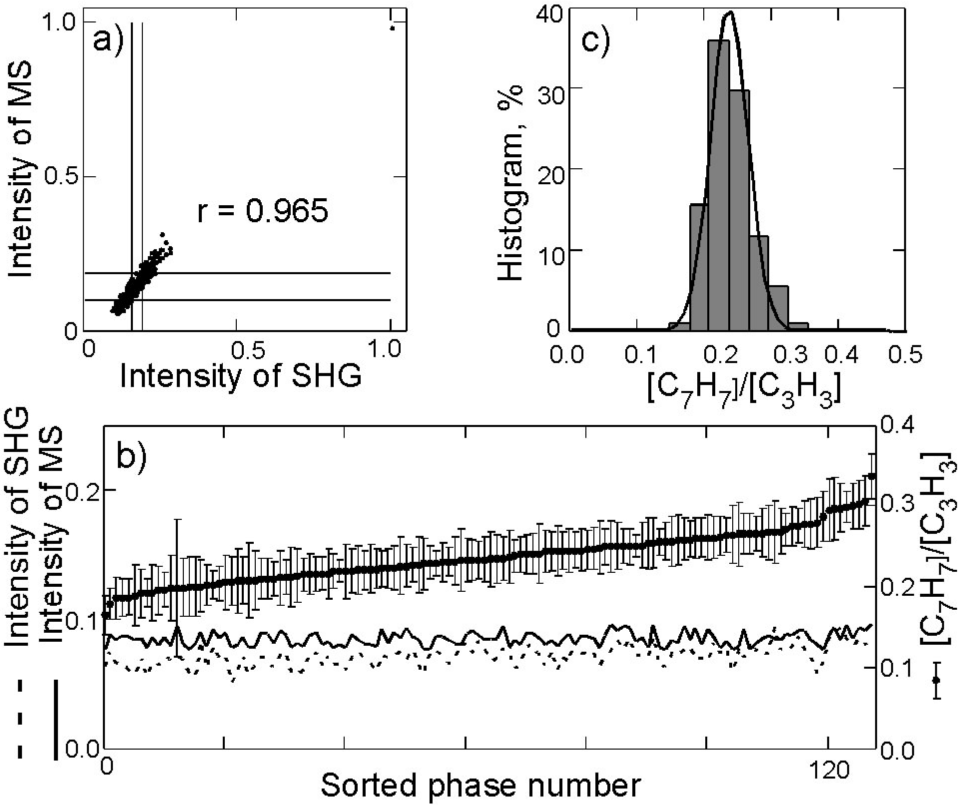

Figure 3.15 Statistical analysis of total yields of fragments and ratio between selected fragments for 537 different types of binary phase functions. a) Total yield of all ions as a function of corresponding SHG intensity. The lines delineate the region for which 128 different shaped pulses are within the standard deviation of our measurements and were chosen for further analysis. b) Ratio between the yields of mass 91 and 39 (points with error bars) together with the total intensity of the mass spectrum (solid line) and SHG (dotted line) sorted in ascending order of ratio. c) Histogram of the ratios in panel b. Notice that all measurements fall within the Gaussian noise spectrum that is consistent with the standard deviation of our measurements.

3.2.7 Dependence of the mass spectrum on different shaped pulses

For these experiments the MS spectra for a number of very different phase modulated pulses producing the same I_{SHG} and I_{MS} were compared. These measurements were designed to test if I_{SHG} was reliable for predicting the fragmentation and ionization of p-NT. Figure 3.16 shows the raw MS spectrum for each of the laser pulses. Different types of modulations were used including binary phase modulation ($\pi\pi\pi00\pi\pi\pi$), positive and negative linear chirp ($\pm 2650\ fs^2$), and periodical phase modulation of different sign ($\pm\pi\sin[35fs\times(\omega-\omega_0)]$). The calculated time-frequency behavior of the pulses, Wigner function, is shown in Figure 3.17. The time profiles for these pulses are very different but all of them generate ¼ the SHG from TL pulses. As was shown above, the total ion yield is directly proportional to the total SHG and in these experiments the total yield of all ions is 1/4 of the yield generated by TL pulses. As can be seen from Figure 3.16 the MS of ions generated by these very different five pulses are indistinguishable (maximum of 0.2 deviation in the laser control factor for $[C_7H_7]/[C_3H_3]$) despite very different time-frequency behavior of the five different fields. Given that more than order magnitude control in this ratio can be achieved, we consider this 0.2 difference insignificant. The maximum deviation observed was between binary and sinusoidal modulation. A reason for the deviations causes by binary phases is discussed below.

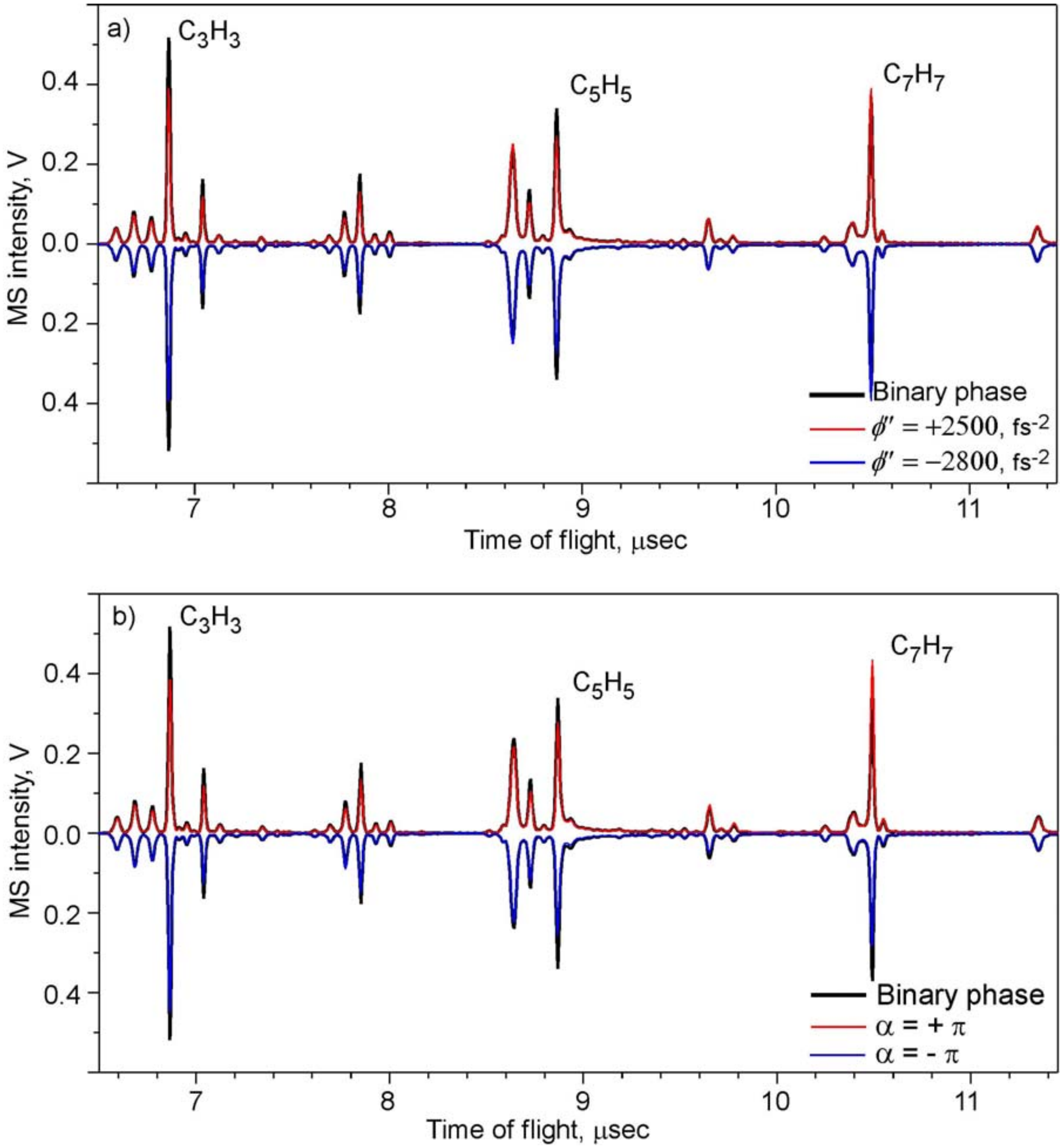

Figure 3.16 Raw oscilloscope traces measured from our TOF MS showing part of the mass spectrum of *p*-NT obtained for different types of phase modulation that yield ¼ of the ions that are observed for TL excitation. The black line on both panels corresponds to the MS for binary phase modulation, when the phase is evenly modulated in frequency domain with the binary string $\pi\pi\pi00\pi\pi\pi$. a) red and blue lines are for positive and negative chirped pulses $\phi=\pm\frac{1}{2}\phi''(\omega-\omega_0)^2$. b) red and blue lines are for positive and negative sinusoidal phase function $\phi=\pm\alpha\sin[35fs(\omega-\omega_0)]$. All types of phase modulation provide the fragmentation pattern depends only from total yields of all fragments relative to TL excitation. For interpretation of the references to color in this and all other figures, the reader is referred to the electronic version of this dissertation.

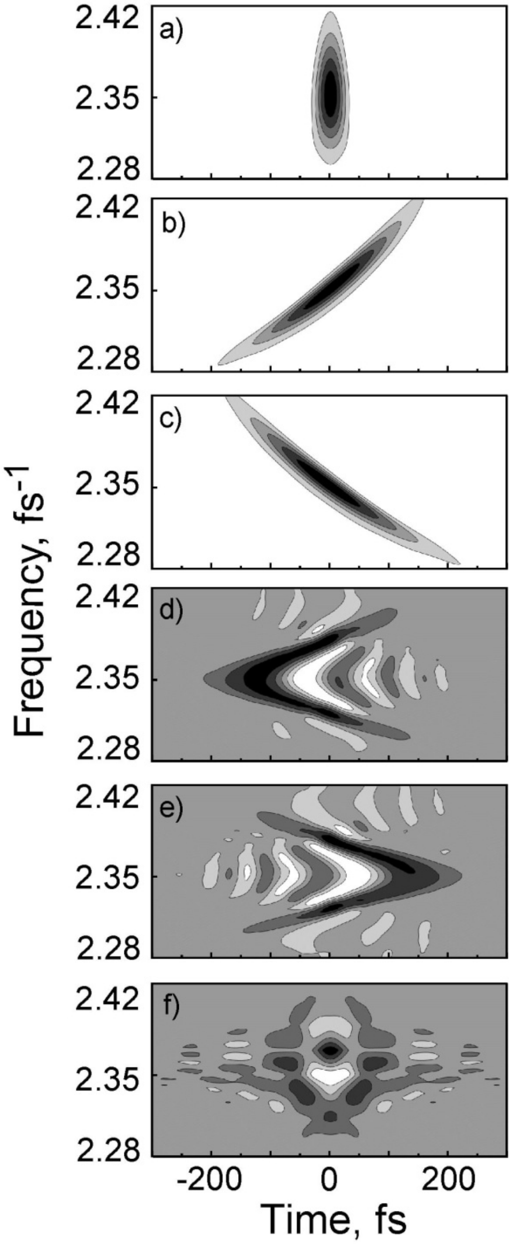

Figure 3.17 Calculated Wigner functions of the phase modulated femtosecond laser pulses, used for Figure 16, in the time and frequency domains. a) phase compensated TL pulse. b-c) positively and negatively chirped pulses with phase function $\phi=\pm\frac{1}{2}2500\text{fs}^2(\omega-\omega_0)^2$. d-e) laser pulse with sinusoidal phase function $\phi=\pm\pi\sin[35\text{fs}(\omega-\omega_0)]$. f) binary phase modulation when phase is evenly modulated in frequency domain with binary string ππππ00πππ.

3.2.8 Predictability of mass spectra for *p*-NT

On the basis of the observations above, we propose that each molecule undergoes a characteristic photofragmentation chain that is activated by the laser pulse and varies monotonically with a laser parameter, which in this case is I_{SHG} or I_{MS}. This implies that the extent of pulse shaping, measured as the normalized I_{MS} or I_{SHG}, will allow one to predict the resulting mass spectrum regardless of phase function used to modulate the pulse (chirp, sinusoidal, etc.).

This predictability hypothesis was tested on p-NT by subjecting it to a number of intense pulses shaped with different phase functions. For all cases, the results obtained as a function of linear chirp (see Figure 3.18) are plotted as a line. Results from (a) different periodicity of the sinusoidal modulation, (b) the location of the phase mask δ, (c) split pulses in the time domain, (d) binary phase modulation, (e) hundreds of pulses with different arbitrary phase modulation and (f) hundreds of different phases resulting from a Taylor expansion series, are plotted as a function of I_{MS}. It's found that the fragmentation in all cases is very similar to that found for linear chirp (lines). The visible systematic deviations (20-30%) for different phase modulation observed (for case (c), values obtained for I_{MS} <0.4) and for the discontinuous phases are caused by slight amplitude changes that occur when discontinuous phase functions are implemented on the SLM. The effects of amplitude and phase-amplitude modulation are discussed in the next subsection. The data in Figure 3.18 reveals that for any phase shaped pulse, if the normalized I_{SHG} or I_{MS} is known we can predict the resulting mass spectrum within a few percent. Similarly, we expect that each molecule will have a monotonic fragmentation pattern, which once determined by linear chirp dependence, for example, will allow one to predict the resulting mass spectrum for any phase shaped pulse.

In order to have a more complete evaluation, a set of orthogonal polynomial functions inspired by the first five states of a harmonic oscillator is designed and tested. Evaluation of that entire search space yielded once again results that are consistent with those found for the other phase functions shown in Figure 3.18.

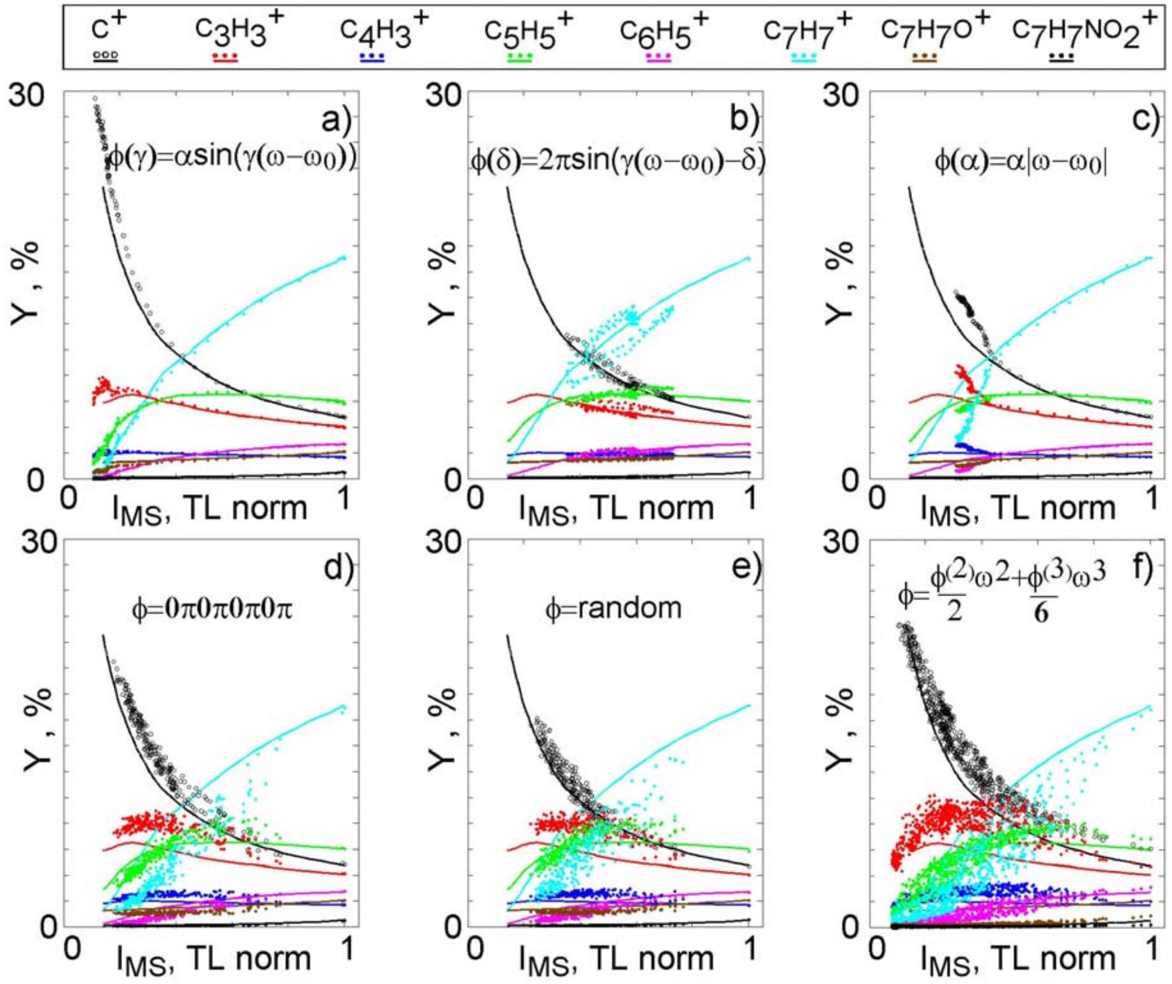

Figure 3.18 Relative intensities of some MS lines (Y) of *para*-Nitrotoluene plotted as functions of relative total intensity, I_{MS}. The graphs show the comparison of different types of phase modulation (points) with quadratic phase modulation of different positive chirp values from 0 to 10,000 fs^2 (lines). a) Sinusoidal phase modulation $2\pi\sin[\gamma(\omega-\omega_0)]$ with different positive periods γ from 0 to 200 fs. b) Sinusoidal phase modulation $2\pi\sin[35fs(\omega-\omega_0)-\delta]$ with different phase delays δ from 0 to 4π. c) Phase modulation with function $\alpha|\omega-\omega_0|$ which provides splitting of the pulse to the two parts with delay time (2α) from -800 to 800 fs. d) Full set of 256 phases of binary ($0,\pi$) phase modulation by binning 8 pixels per bit in the central part of spectrum. e) 256 random phases from 0 to 2π by binning 8 pixels over the whole spectrum. f) All possible combination of three terms of the Taylor expansion, where the nonlinear terms of the expansion are in the range $\pm1.6\text{x}10^4 fs^2$, $\pm8\text{x}10^5 fs^3$, $\pm4\text{x}10^7 fs^4$ for the second, third and fourth order of phase modulation respectively. There is a minor quantitative difference found for discontinuous phase functions but the fragmentation pathways always vary monotonically as a function of I_{MS}. For interpretation of the references to color in this and all other figures, the reader is referred to the electronic version of this dissertation.

3.2.9 Effects arising from spectral amplitude shaping

In all the measurements presented (Figure 3.10-12) I_{MS} was found to be proportional to I_{SHG}. Here we explore if this direct proportionality applies to amplitude shaping. Analysis of measurements obtained for 256 8-bit binary amplitude shaped pulses, for which the amplitude of different pixels was set to 0 or 1, is presented below. The dependence of I_{MS} and I_{SHG} versus the intensity of the fundamental pulse was plotted in the Figure 3.19a. From the log-log plot it's found that I_{MS} is close to the fourth order dependence on the intensity of the fundamental pulse. This observation is unexpected given the well known square dependence of I_{SHG} on $I_{Fundamental}$. The difference in this experiment is that the binary amplitude modulation causes both a loss in intensity of the fundamental and a lengthening of the pulse. The two-fold effect causes a nonlinear dependence with n>2. It's confirmed by numerical simulation that the intensity of SHG generated by binary amplitude modulated pulses is proportional to the intensity of the fundamental in order n=3 to n=4, where the smaller number corresponds to a single block of bits set to 0 and the larger number is found for amplitude functions with alternating on-off bits. These values are in agreement with the data measured. Our amplitude modulation measurements are very different than pulse attenuation, where all frequencies are attenuated by a certain amount. In that case the familiar n=2 dependence is observed. We note in Figure 3.19a that I_{SHG} and I_{MS} have exactly the same dependence on $I_{Fundamental}$, as observed earlier for phase modulation. Figure 3.19b shows the intensity of two individual fragment ion peaks with m/z of 91 and 39, as a function of I_{SHG}. In the log-log plot it's seen that the dependence is to the fourth power at the lowest intensities but it quickly saturates and reaches linear dependence. The change may be a signature of different mechanisms of ionization/fragmentation for low and high intensities.

Experiments on laser control have usually combined phase and amplitude modulation with the hope that this more general combination will optimize a desired quantum mechanical pathway. When the system being controlled can be excited linearly by the laser (resonant excitation), amplitude modulation controls the population transfer to every excited state within the laser bandwidth. When the excitation is through a nonlinear interaction, for example multiphoton excitation, phase can be used to control the amplitude at specific frequencies very efficiently without amplitude modulation (loss of photons) (Lozovoy, V. V. *et al.*, 2005b; Lozovoy, V. V. *et al.*, 2006d). Here we explore the combination of phase and amplitude modulation systematically for *p*-NT (a molecule without excited states within one photon excitation by the laser) to find if there is a departure from pure phase modulation. For these experiments 32 different 5-bit amplitude modulated pulses (using Pulse Shaper II) were tested, and for each of them mass spectra for 50 different phase functions were measured (introduced by Pulse Shaper I) using quadratic phase modulation from 0 to 10,000 fs^2. The results from these measurements are plotted in Figure 3.20. First, we find in Figure 20a that the total ion yield, I_{MS}, is essentially linear with the integrated SHG intensity, as for all pure phase and pure amplitude modulation similar to the results shown before.

In Figure 20b the percentage of total ionization measured for *m/z* 91 and 39 is plotted. The lines correspond to laser without amplitude modulation. The first observation is that amplitude modulation causes an overall shift in the relative ion yield curves, but the changes in relative yield are systematic and follow the same monotonic trend as found for all the previous experiments above. This suggests that there is no quantum mechanical pathway that has been blocked by the amplitude modulation. In a sense, the amplitude modulation is working as an additional pulse lengthening effect that shifts the dependence on I_{MS} but doesn't affect the fundamental fragmentation pathways. The second observation is that the changes in the trends, lower values for *m/z* 91, and higher values for *m/z* 39, are consistent with the observation in subsection 3.2.8, where heavily modulated pulses and discontinuous phase functions were found to deviate from the trends observed for chirped pulses. The experimental data in Figure 3.20b, therefore, gives us the confidence to claim that there was nothing special in the experimental points that deviated from the trend when discontinuous phase modulation functions were used (see Figure 3.18). The deviations were caused by inadvertently introduced amplitude modulation.

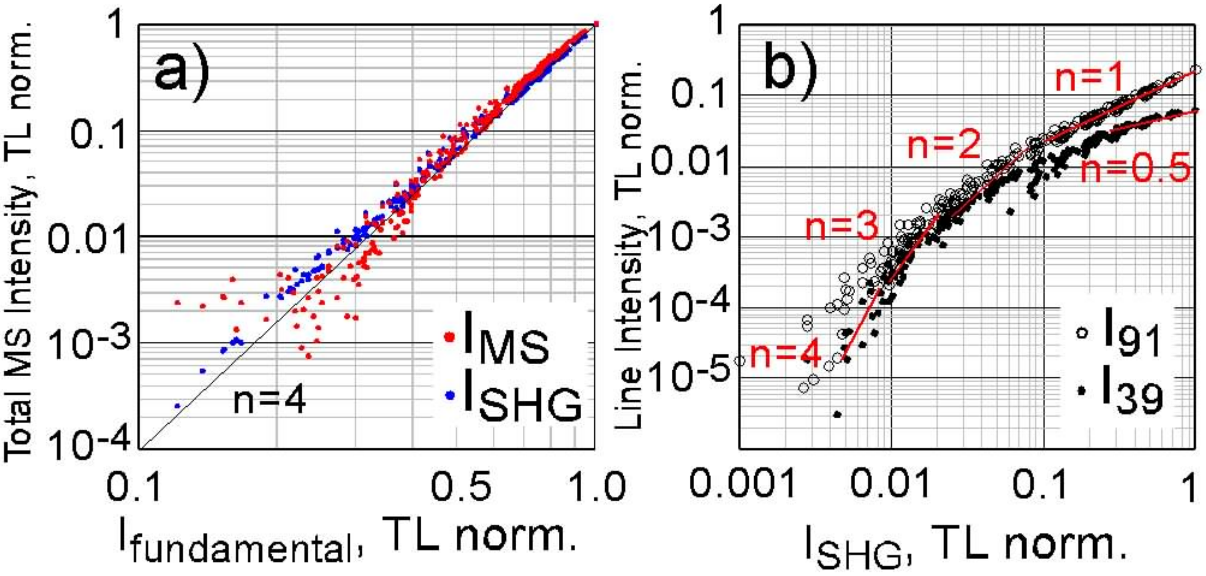

Figure 3.19 a) Dependence of total yield of fragments (red) and SHG from a crystal (blue) as a function pure binary amplitude modulation, plotted as a function of laser intensity. b) Intensity of the fragments ions with m/z=91 and 39 of *p*-NT as a function of SHG intensity obtained for the amplitude modulation experiments. For interpretation of the references to color in this and all other figures, the reader is referred to the electronic version of this dissertation.

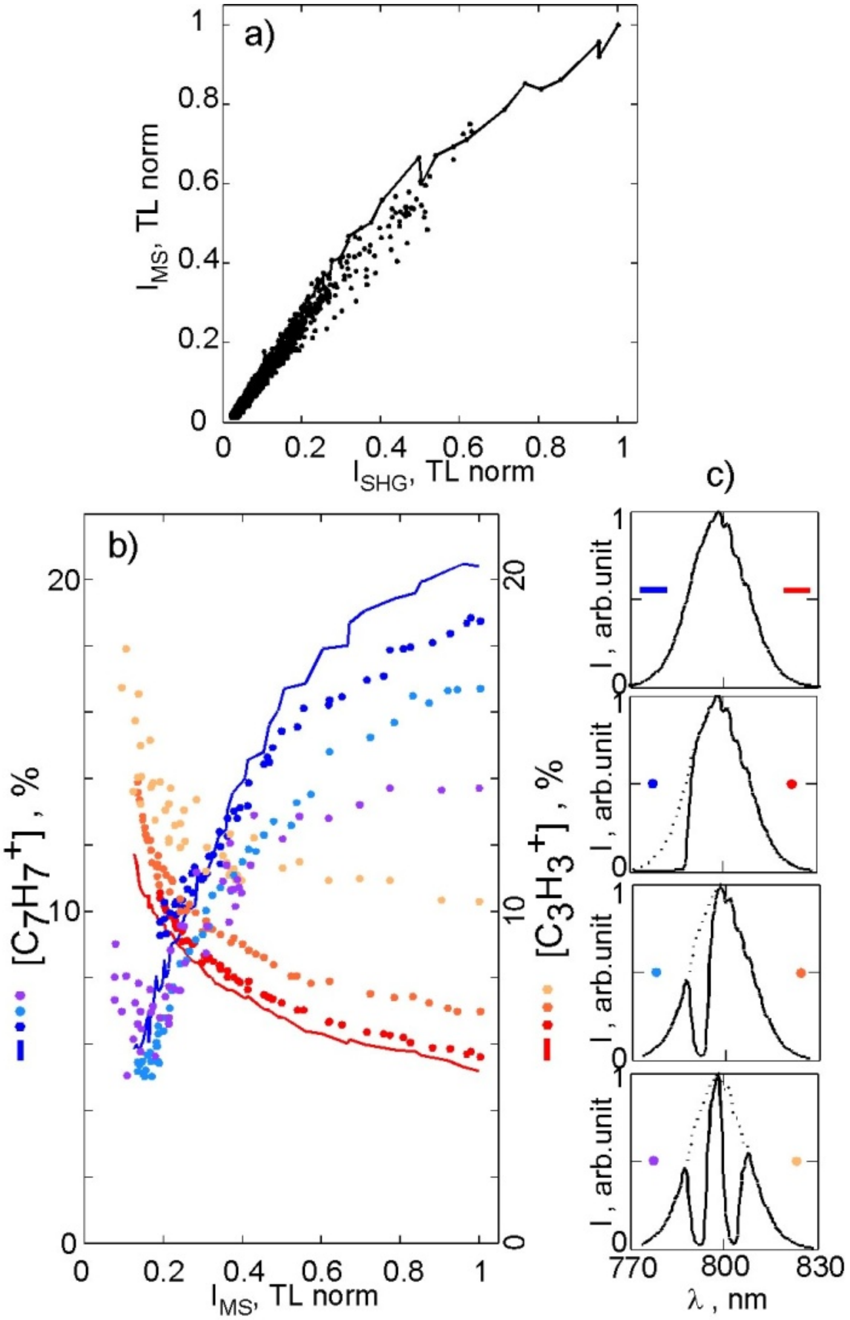

Figure 3.20 a) Total fragment ion yield as a function of total SHG intensity for amplitude and phase modulated pulses. b) Percentage of total ionization of fragments with *m/z* 91 (blue colors) and *m/z* 39 (red colors) for *p*-NT as a function of the total ion yield normalized for TL excitation. c) Spectra of the amplitude modulated pulses corresponding to each case. For interpretation of the references to color in this and all other figures, the reader is referred to the electronic version of this dissertation.

3.2.10 Generalization of our findings to other molecules

To further test our hypothesis that the laser induced fragmentation and ionization pattern can be predicted once we learn how it depends on I_{MS}, the behavior of sixteen different molecules upon pulse shaping with two very different phase functions is tested. In Figure 3.21 the total ion yield I_{MS} is compared for quadratic phase modulation (continuous line, where ϕ'' was up to 10,000 fs^2) and for sinusoidal phase modulation (dots) given by $2\pi\sin[\gamma(\omega-\omega_0)]$, where γ is scanned from 0 to 100 fs. First, I_{MS} is observed to directly proportional to I_{SHG} for all molecules and is practically independent from the phase function used. This behavior is not limited to *p*-NT.

Finally the fragmentation patterns for the 16 different molecules is explored and tested, for the observations made for *p*-NT, that it changes monotonically and predictably as a function of I_{MS} despite the phase function used to shape the pulses. The data is shown in Figure 3.22, where the relative product ion yields measured for the linear chirp (lines) and the period of a sinusoidal function (dots) are found to be practically identical when plotted against I_{MS}. Some slight deviations are observed when pulse shaping is such that less than 0.3 of I_{MS} is detected, this is caused by unwanted amplitude modulation as discussed above. Experiments with other phase functions such as binary, Taylor expansion were carried out and for all the molecules the results were essentially the same as those presented in Figure 3.22. The results of these experiments strongly support our conclusion that the fragmentation pattern varies monotonically and predictably with I_{MS}. Once the fragmentation pattern as a function of I_{MS} has been determined, as shown here by scanning linear chirp, then the fragmentation pattern for any other phase function can be predicted to be essentially the same.

The data in the first three panels of Figure 3.22 illustrates how the yield of particular fragment ions changes for molecular isomers. For example, the molecular ion of *m*-NT is much more sensitive to pulse duration than that from *p*-NT (Figure 3.22.1 and Figure 3.22.2). More examples of isomer identification have been discussed elsewhere (Dela Cruz, J., M. *et al.*, 2007; Dela Cruz, J. M. *et al.*, 2005; Pastirk *et al.*, 2005). Differences in the femtosecond laser mass spectra of isomers is not new (see for example (Fuss *et al.*, 2000; Kosmidis *et al.*, 1997; Kosmidis *et al.*, 1994b; Tonnies *et al.*, 2001; Weickhardt *et al.*, 2002)). What is new is that by shaping the pulse we can distinguish one molecule from another by the changes in the yield of a single fragment ion. The relative yield of fragment with *m/z* 39 responds differently to pulse shaping. For the nitrotoluenes (Figure 3.21.1-3) it decreases with increasing I_{MS}, for chlorobenzonitrile it is insensitive to pulse shaping (Figure 3.21.12) and increases for benzene (Figure 3.21.5). These differences can be used for molecular identification purposes (Dela Cruz, J., M. *et al.*, 2007; Dela Cruz, J. M. *et al.*, 2005; Lozovoy, V., V. *et al.*, 2006a; Lozovoy, V. V. *et al.*, 2005a; Lozovoy, V.V. *et al.*, 2006c; Pastirk *et al.*, 2005; Shane *et al.*, 2006). A parameter that integrates the changes in the molecular response upon pulse shaping, for example measuring variance, allows us to add an extra dimension to mass spectrometry that can be used to improve molecular identification (Pastirk *et al.*, 2006a).

One of the molecules tested was acetophenone (shown in Figure 3.21.11), a molecule that had been studied with shaped laser pulses (Graham *et al.*, 2003; Levis *et al.*, 2001; Levis *et al.*, 2002). Notice that no toluene *m/z* 92 was observed for any of the different pulses as claimed by Levis and Rabitz. There is evidence strongly suggesting the formation of toluene observed in the initial publication is due to contamination (Zhu *et al.*, 2009).

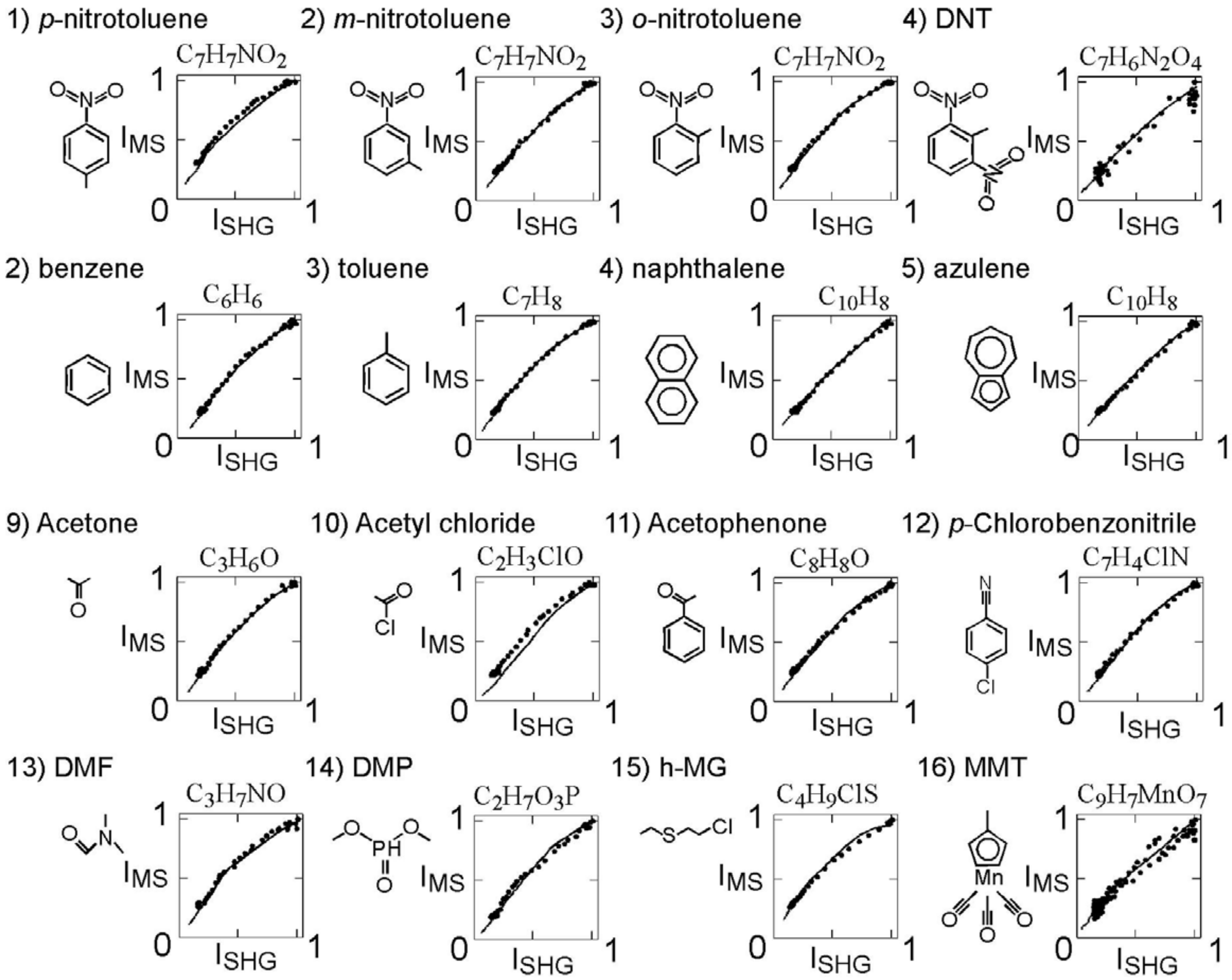

1) *p*-nitrotoluene

2) *m*-nitrotoluene

3) *o*-nitrotoluene

4) DNT

2) benzene

3) toluene

4) naphthalene

5) azulene

9) Acetone

10) Acetyl chloride

11) Acetophenone

12) *p*-Chlorobenzonitrile

13) DMF

14) DMP

15) h-MG

16) MMT

Figure 3.21 (1-16) Total yield, I_{MS}, as a function of SHG intensity, I_{SHG}, measured for sixteen different molecules. Comparison of linear chirp when ϕ'' is scanned from 0 to 10,000 fs^2 (lines) with periodical phase modulation $2\pi\sin[\gamma(\omega-\omega_0)]$ for γ scanned from 0 to 100 fs (points).

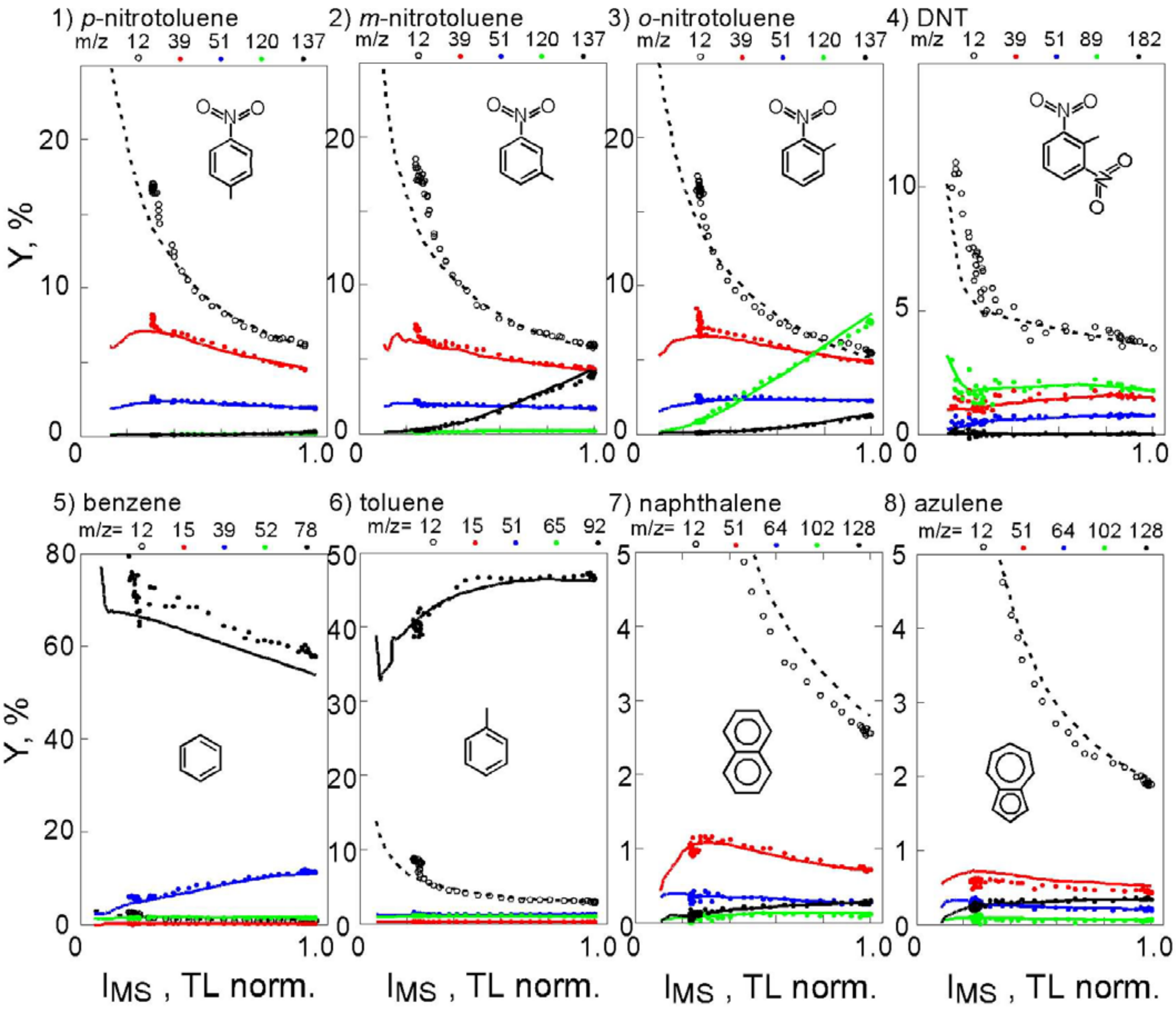
1) *p*-nitrotoluene
m/z 12 39 51 120 137
2) *m*-nitrotoluene
m/z 12 39 51 120 137
3) *o*-nitrotoluene
m/z 12 39 51 120 137
4) DNT
m/z 12 39 51 89 182
Y, %
0
10
20
5
1.0
5) benzene
m/z= 12 15 39 52 78
6) toluene
m/z= 12 15 51 65 92
7) naphthalene
m/z= 12 51 64 102 128
8) azulene
m/z= 12 51 64 102 128
80
60
40
30
50
1
2
3
4
I_{MS}, TL norm.

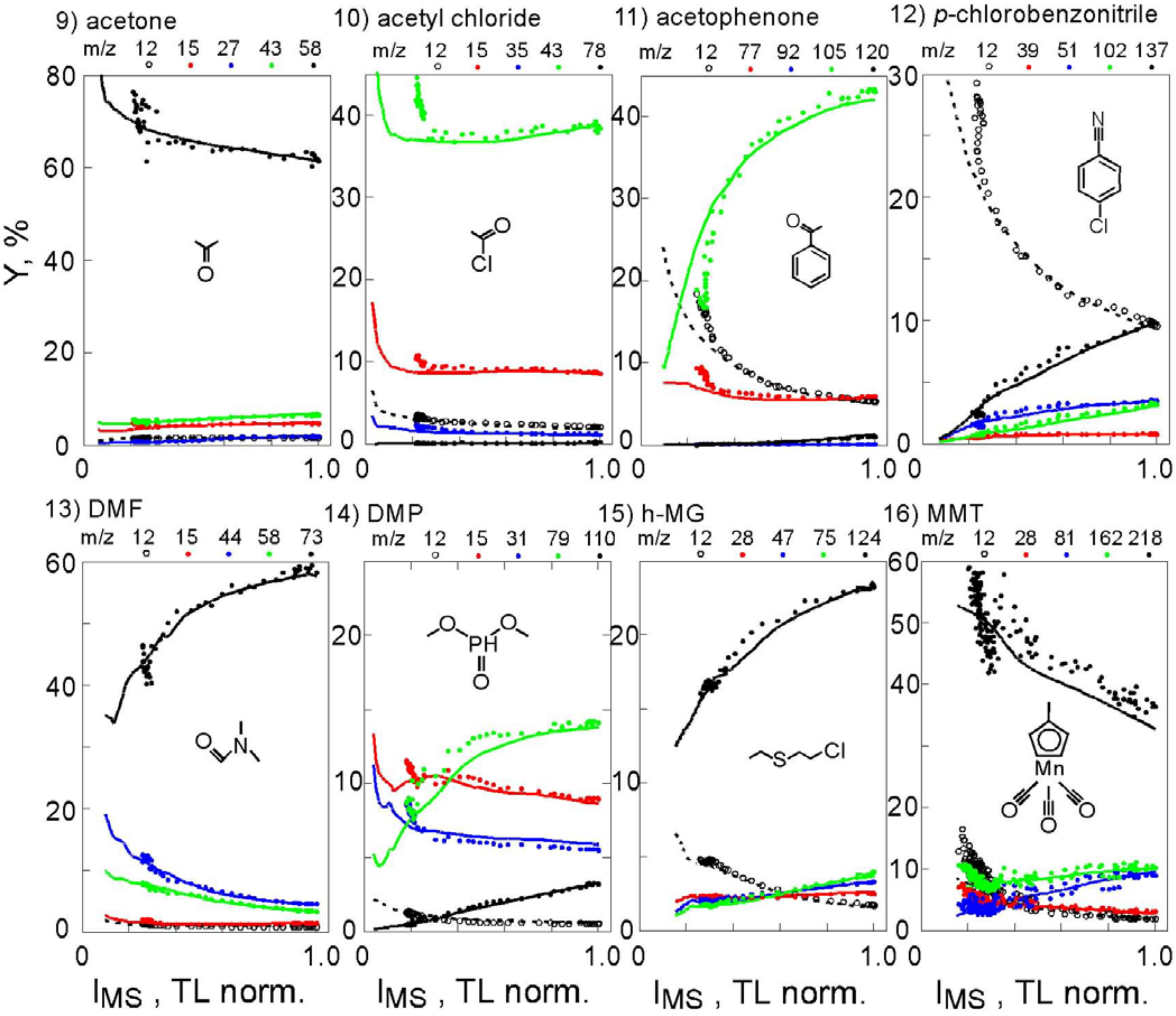
9) acetone
m/z 12 15 27 43 58
10) acetyl chloride
m/z 12 15 35 43 78
11) acetophenone
m/z 12 77 92 105 120
12) *p*-chlorobenzonitrile
m/z 12 39 51 102 137
13) DMF
m/z 12 15 44 58 73
14) DMP
m/z 12 15 31 79 110
15) h-MG
m/z 12 28 47 75 124
16) MMT
m/z 12 28 81 162 218
Y, %
0
20
40
60
80
10
30
50
1.0
I_{MS} , TL norm.
O
Cl
N
PH
S
Mn

Figure 3.22 (1-16) Relative intensity of the more prominent MS lines (Y) including C^+ (open black) and molecular ion (black dot) as a function of total yield of all ions (I_{MS}) for sixteen different molecules as a function of linear chirp when ϕ'' is scanned from 0 to 10,000 fs^2 (lines) and as a function of periodic phase modulation $2\pi\sin[\gamma(\omega-\omega_0)]$ for γ is scanned from 0 to 100 fs (points). For interpretation of the references to color in this and all other figures, the reader is referred to the electronic version of this dissertation.

3.2.11 Intensity and volume effects

The experimental findings presented above for *p*-NT were presented at a laser control conference and they generated concern among some colleagues that the observations were merely a volume effect. Experiments in strong fields, especially when the laser intensity exceeds I_{sat}, are performed with lasers having a Gaussian intensity profile, therefore the signal obtained contains a range of intensities. Higher intensities are reached only in the center of the beam, and produce a minor contribution, while the greater volume outside the focus produces a major contribution. Taking into considerations that changing the laser Rayleigh parameter as shown in Figure 3.9; changing the laser intensity as shown in Figure 3.10 (top row); and changing the laser intensity as shown in Figure 3.13, caused no difference in the observed laser control as a function of pulse shaping, gives us confidence that volume effects are not responsible for the observed changes in fragmentation patterns. In light of this concern additional experiments were carried out to evaluate to what extent our findings could be influenced by volume effects. The method used is based on the clever observation by Ben-Itzhak that for Gaussian beam profiles, when collecting data through a slit perpendicular to the laser excitation, subtraction of lower intensity data can be used to isolate effects caused by the higher excitation (Wang *et al.*, 2005). This method has been tested and is rigorous for two-dimensional slices when using Gaussian pulses.

Two-dimensional volume effects were explored using the long-focal length setup using a 0.9 mm slit perpendicular to the beam propagation. These parameters are well in the range required for eliminating volume effects by subtraction (Wang *et al.*, 2005). First the yields of three different fragment ions were measured as a function of power density (data shown in

Figure 3.23). It's confirmed that I_{sat} for *p*-NT is about 10^{14} W/cm^2. Having the power dependence, it's possible to evaluate the differential changes in ion yield for the different fragment ions. These findings, shown in the top row in Figure 3.23, show two regimes. Below I_{sat}, there is a systematic rise in the appearance of the ions. Above I_{sat}, there appears to be no significant change outside the noise in the yield of these fragments. Note that this being a differential measurement it is very sensitive to noise.

Volume effects were also explored which may have played a role for the short focusing geometry. In this case, given the very short Rayleigh length, slit was not applied. Therefore, this is outside the two-dimensional case. Once again, in these data, shown in the bottom row of Figure 3.23, that beyond I_{sat}, differential increases in energy cause essentially no change in the yield of the different fragment ions. Given the order of magnitude changes in the relative fragment ion yields reported in the study as a function of pulse shaping, the minimal change in the differential yield indicates that the observed effects on pulse shaping are not caused by volume effects, in either of the focusing configurations explored in this work.

Having determined that volume effects can be neglected in the experiment above I_{sat}, the effect of pulse shaping was measured (sine function open circles and chirp filled circles) at different laser intensities, data shown in Figure 3.24. These data were obtained using the longer focal length geometry. At the higher intensities, the data reproduces the results found earlier, namely, extensive changes in the yield of $C_nH_n^+$ fragment ions upon pulse shaping, and no difference between the two different types of phase functions. At I_{sat}, the effect of pulse shaping is essentially lost. Finally, at very low intensities, noise overwhelms the possible changes as a function of pulse shaping.

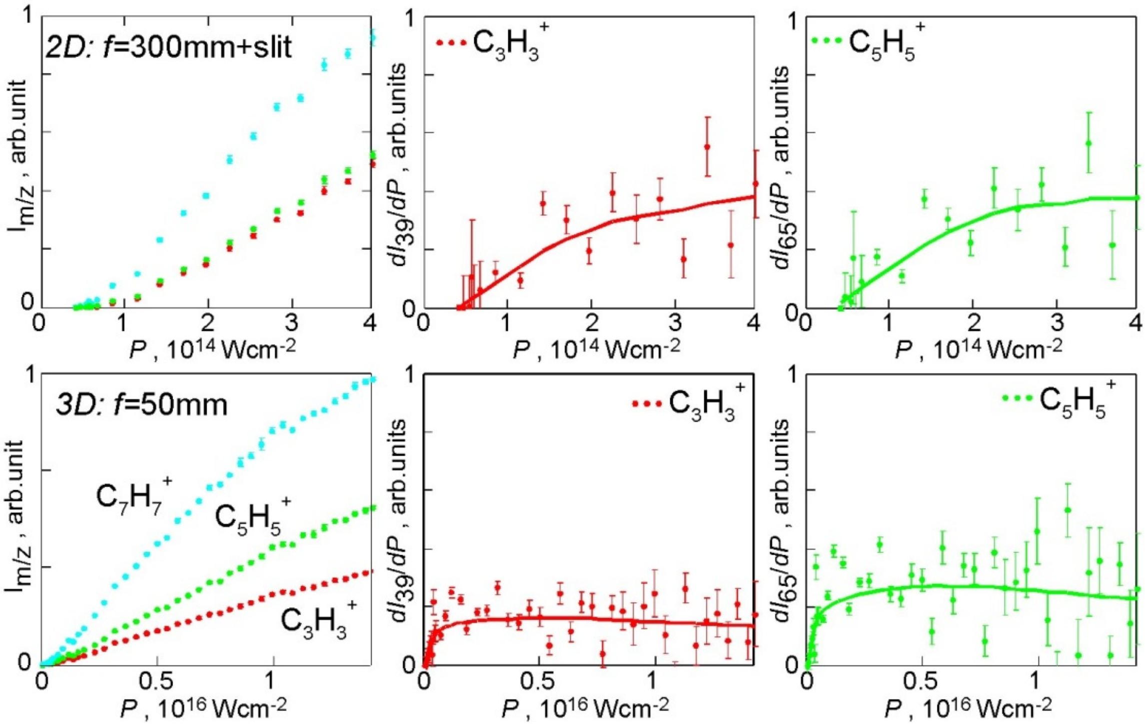

Figure 3.23 Volume effect. The dependence of the relative yield of three fragments *m/z* 39, 65, 91 from *p*-NT as a function of power density. Upper row: experiment was carried out using 300 mm focal length lens and 0.9 mm slit in the extraction plate. Lower row: experiment was carried out using 50 mm focal length lens and mesh in the extraction plate. The lines are smooth functions obtained from the experimental points. For interpretation of the references to color in this and all other figures, the reader is referred to the electronic version of this dissertation.

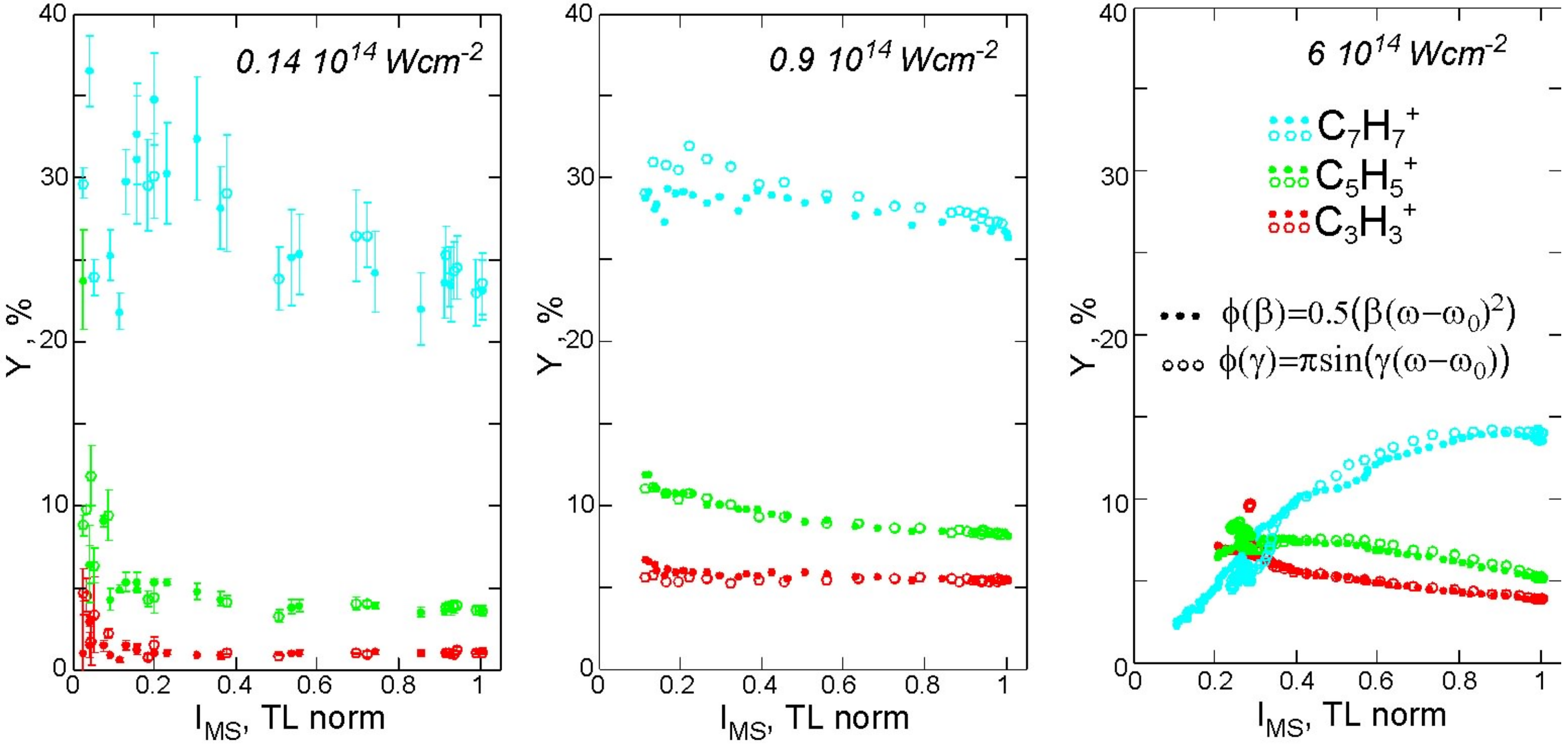

Figure 3.24 Controllability of fragmentation at different power densities. The dependence of the relative yield of three fragments *m/z* 39, 65, 91 from *p*–NT were measured as function of integrated yield of all ions, I_{MS}, for different power densities using chirped pulses (filled dots) and sinusoidal phase modulation with different period (open cycles). Note that at the three different power densities the fragment ion yield is independent from the type of phase modulation used. For interpretation of the references to color in this and all other figures, the reader is referred to the electronic version of this dissertation.

3.3 Discussion

3.3.1 Femtosecond laser induced photochemistry of *p*-NT

The photochemistry of *p*-NT (Baer *et al.*, 1988; Beynon *et al.*, 1973; Brown, 1970; Bursey *et al.*, 1966; Cassady *et al.*, 1993; Choe *et al.*, 1991; Harris *et al.*, 1981; Lablanquie *et al.*, 1993) and its analogue, nitrobenzene (Brill *et al.*, 1999; Cooper *et al.*, 2001; Galloway *et al.*, 1993; Galloway *et al.*, 1994; Hwang *et al.*, 1996; Kosmidis *et al.*, 1994a; Marshall *et al.*, 1992; Moini *et al.*, 1987; Nishimura *et al.*, 1986; Osterheld *et al.*, 1993; Panczel *et al.*, 1984) have been the subject of intensive research, with some results that have been considered controversial, but the major transformations are well established. The findings here is presented in light of the more widely accepted model for the fragmentation of *p*-NT and the ladder switching mechanism shown in Figure 3.25. This model can be rationalized using one or more models of photoionization and photodissociation collected in Table 1. The first step occurs in the rising edge of the pulse and involves field ionization. The threshold was measured here for field ionization at 800 nm for *p*-NT to be 1.7×10^{14} W/cm^2, a number that is reasonable given the literature (Hankin *et al.*, 2001; Uiterwaal *et al.*, 2004) where a large number of experimental and theoretical values for field ionization thresholds are given. Only for pulses with heavy amplitude modulation, when we simultaneously reduced the fundamental amplitude by 5 times and increased the pulse duration by 10 times, does the intensity become lower and a deviation from the typical fragmentation pattern becomes apparent (see Figure 3.18a). For the shortest and most intense pulses the signature of double ionization and Coulomb explosion were observed and this data, representing <5% of the total ion yield for the highest intensity experiments, is not discussed here.

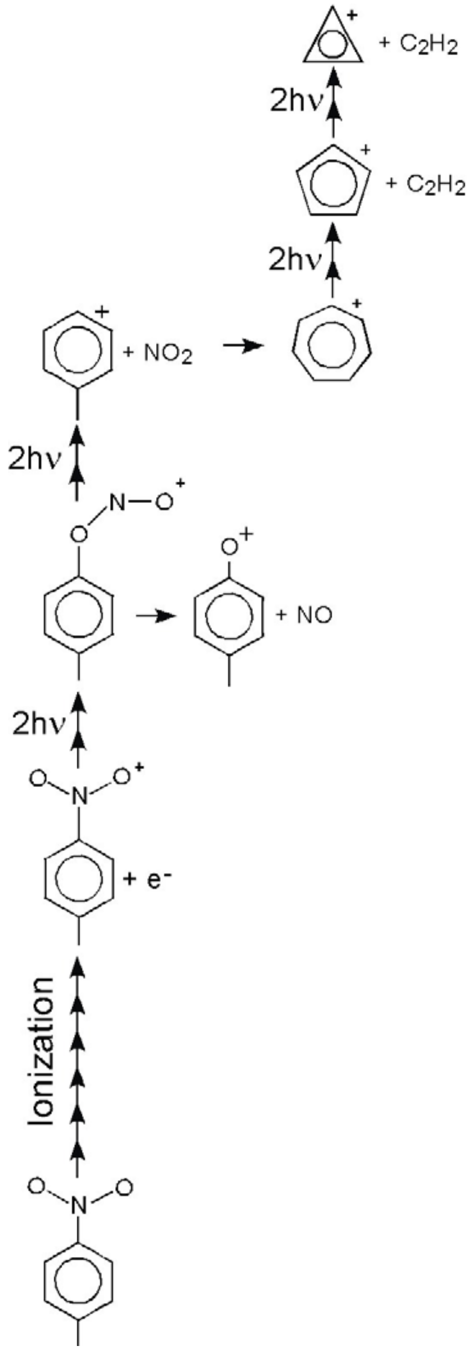

Figure 3.25 Ladder switching mechanism of photodissociation of *p*-NT upon femtosecond IR excitation. The first step is fast field ionization. The second step is photoisomerization, from which NO or NO_2 elimination takes place, followed by further steps involving C_2H_2 loss. Pulse shaping enhances ladder-switching processes while TL pulses enhance ladder climbing.

Table 1 Models of ionization and dissociation in femtosecond fields

#		**Models of dissociation**	**Molecules and references**
1	ADI	Dissociation followed by ionization	C_3H_6O[105] NO_2[106]
2	AID	Ionization followed by dissociation	C_6H_6[107] C_nH_m[108] $C_nH_mCl_kF_1$[109] $M(CO)_n$[110] C_3H_6O[105] $C_3H_3OF_3$[105] C_8H_8O[105]
3	CE	Coulomb explosion	C_2H_4[111,112] C_3H_6[111,112] C_2H_6O[113] CH_4O[114]
4	ERC	Electron re-collision	H_2[115] CH_4[39] C_6H_6[116,117] C_7H_8[63] H_2O[117] CH_4O,[118] C_2H_4O[118] $C_6H_{14}O$[118]
5	FAD	Field assisted dissociation	CH_4[119] C_2H_4O[120] CH_2I_2[121] $C_2H_6O_3$[122]
6	FID	Field induced dissociation	C_6H_6[123,124] C_6H_5X[123] $C_{10}H_8$[123] $C_{14}H_{10}$[123]
7	IED	Inner valence electron excitation	CH_4[125] C_6H_6[126]
8	MDI	Multielectron dissociative ionization	H_2[127] N_2[127] O_2[127] Cl_2[127] I_2[127] CH_3I[128] C_3H_7I[128] C_4H_9I[128] C_6H_8[76,129]
9	NCL	Nonadiabatic charge localization	$C_{14}H_{10}$[130]
10	NED	Nonadiabatic excitation-dissociation	C_6H_6[131,132] $C_{10}H_8$[131,132] $C_{14}H_{10}$[131,132] $C_{18}H_{22}$[131,132] $C_{14}H_{12}$[131,132] $C_{14}H_{18}$[131,132]
11	NME	Nonadiabatic multielectron excitation	C_6H_8[133,134] $C_{10}H_{12}$[133,134] $C_{40}H_{56}$[133,134] C_8H_8[133,134]

The observed low relative yield for the molecular ion seems to indicate that the parent ion is unstable. However, it's known from electron impact MS (see Figure 3.2a) that the parent ion is stable. Therefore, differences between electron impact and femtosecond ionization indicate the molecular ion is not stable in the presence of the laser field. This observation is confirmed by comparing the mass spectrum of p-NT obtained with 35 fs TL pulses at peak intensities of 10^{13} and 10^{14} W/cm^2 (data not shown). At the lower intensity the parent ion reaches as much as 30% relative yield, this value decreases with laser intensity.

After *p*-NT is field ionized, I_{MS} is observed to be linearly proportional to the relative SHG intensity, I_{SHG}, suggesting a two-photon bottleneck exists, and it is plausible that it is related to the loss of the molecular ion. For *p*-NT, the isomerization in which CH_3-ϕ-NO_2 transforms to CH_3-ϕ-O-NO has been found to have an energy barrier and does not take place in solution. This energy is supplied by the strong laser field. Experimental data and calculations reveal that one 800 nm photon is not enough to form the isomer but two photons are sufficient for isomerization. As a result the *p*-NT ions undergo isomerization which promptly results in the elimination of NO or NO_2. Under thermal equilibrium the main channel is NO elimination followed by sequential CO elimination. In the presence of a strong field, the preferred decay channel is NO_2 elimination, while under electron impact, the molecular ion is stable. After NO_2 elimination, the $C_7H_7^+$ ion, initially in the benzyl form, appears and transforms into the more stable seven-member ring, tolyl ion, which is the most likely the form that is detected. In the presence of the strong electromagnetic field, sequential absorption of photons releases C_2H_2 fragments thereby forming the $C_5H_5^+$, $C_3H_3^+$ and finally C^+ ions. The observation that longer pulses (with a lower I_{SHG} and/or I_{MS}) produce more fragmentation can be understood dynamically. The longer the pulse the more time the atoms have to change their configuration. When plotted against chirp, as Figure 3.14a, the relative intensity of smaller fragments increases with chirp, the larger fragments decreases with chirp and intermediate fragments, like $C_5H_5^+$, first increases and then decreases. The observed fragmentation mechanism is consistent with ladder climbing followed by ladder switching. For the longer pulses, the field remains sufficiently strong to cause the formation of fragment ions by ladder switching processes.

For *p*-NT, the fragmentation pattern from electron impact mass spectrometry is very similar to the fragmentation pattern observed for femtosecond pulse excitation below I_{sat}, the molecular ion decreases in intensity as the laser intensity increases. The similarity would suggest that electron recollision, ERC model in Table 1, has an important role in the laser induced fragmentation and ionization process. ERC is expected to play an important role for TL pulses, when post-ionization excitation is minimal. We examined the fragmentation pattern as a function of polarization for TL pulses. By changing the polarization from linear to circular, modulation of the probability electron-nuclei collisions in analogy to the high-harmonic generation process would be expected. These changes in polarization were found to have no effect on the fragment ion pattern. This suggests that ERC does not play a major role in determining the fragmentation pattern in our experiments, or that electron-nuclei collisions are not needed for the electron to transfer energy to the molecule.

A number of models have been proposed that consider multielectron excitation (IED, MDI, and NME in Table I). It is possible that multielectron excitation is favored by shaped pulses, which are longer, and therefore lead to further fragmentation. We had expected that certain shaped pulses would enhance specific pathways that result when specific electronic excitation pathways are accessed. However, no evidence is found that such selective excitation takes place for any of the different shaped pulses used. There is sufficient evidence here to suggest that δ scanning and binary phases would result in excitation of multiphoton processes at different wavelengths. However, no evidence for having accessed different electronic states is present in the fragmentation patterns observed. Similarly several pulse shapes were tested, such as sinusoidal functions that create trains of pulses with the idea of driving a vibrational coherence. No evidence of coherent vibrational motion was found.

Developing a precise model of ionization and fragmentation for *p*-NT is beyond the scope of this article. This complete dataset is hoped to be used by scientists and theoreticians who are devoted to determining the entire mechanism of ion fragmentation. Here I only focus on the main observation of our study. The detailed time-frequency dependence of the shaped laser pulses plays a minor role (if any) in influencing the fragmentation pattern. Thousands of experiments were carried out trying to find evidence of one or more specially shaped pulse that are capable of causing bond selective fragmentation of *p*-NT to yield one or two product ions in a pattern that deviates from that which is observed as a function of chirp. No evidence is found for such a pulse in any of our experiments. A model for fragmentation-ionization by intense and shaped near IR pulses is thus proposed. In this model, molecules have a prescribed fragmentation pattern, or fragmentation cascade, that depends on their atomic and electronic structure. In this proposed model the yield of all fragments is interrelated. TL pulses will maximize the observation of the heavier fragments including the molecular ion if stable under laser irradiation. The longer the shaped pulses the more extensive the fragmentation cascade will be producing smaller fragments down to single atom ions. This can be understood in terms of a ladder switching model. The increased fragmentation observed for shaped pulses can also be interpreted in terms of a dynamic energy flow from the Franck-Condon excited states to hundreds of degrees of freedom, this flow reaching all parts of the molecule when the pulses are lengthened by pulse shaping. In order to predict how far in the fragmentation cascade the molecule will follow, it is sufficient to know I_{MS} or I_{SHG} normalized to TL. All the measurements with phase shaped pulses confirm this model. This model envisions the creation of a wave packet encompassing thousands of quantum (rotational, vibrational, electronic, and translational) states, which undergoes ultrafast delocalization. The speed of delocalization reduces and perhaps eliminates the possibility of a time-dependent interplay between the complex laser pulse and the molecular dynamics. More detailed study on the model is presented in the next chapter.

3.3.2 Possible applications

So far, mass spectrometry (MS) has been widely used as a tool of molecule detection and identification in real-time. In most standard implementation of MS, mass spectra are typically obtained from the energetic ionization process involving collision between neutral molecules and electrons that are typically accelerated to energies between 50 to 150eV, normally 70eV for most organic compounds. Excess energy is transferred to the molecule to generate fragmentation of ions. Such fragmentation can be very useful in providing structural information. However, there are several limitations of this approach. First, the analysis can become very difficult for complex mixtures. Moreover, it is often the case that different species of the same basic molecule type yield practically identical fragmentation patterns, for example isomers and enantiomers. Various techniques have been developed to try to overcome these limitations including GC-MS (gas chromatography-MS) or another MS (GC-MS-MS) (Gross *et al.*, 1982); however, they inevitably complicate the process and increase the response/analysis time.

In our case the electron gun and the GC column are replaced with a femtosecond laser. The results shown previously indicate that the photo fragmentation pattern of molecules is determined by their atomic and electronic structure. In Figure 3.22.1, Figure 3.22.2 and Figure 3.22.3, we see that different isomers have very different fragmentation patterns. The fundamental reason for this can be traced back to the restricted energy flow (IVR) which depends on molecular geometry (selection rules) (Gruebele *et al.*, 1998). From a practical point of view, this implies that shaped pulses can be used as a tool for analytical chemistry, such as for isomer identification (Dela Cruz, J., M. *et al.*, 2007; Pastirk *et al.*, 2007). In order to maximize reproducibility and minimize the number of shaped pulses used, it’s essential to eliminate the phase deformations in the laser system to ensure TL pulses at the sample. Measuring the outcome from two shaped pulses allows quantitative identification of mixtures (Dela Cruz, J., M. *et al.*, 2007; Pastirk *et al.*, 2007). Phase functions that can be reproduced accurately will give the most reliable and reproducible results.

3.3.3 General observations on pulse shaping and fragmentation

The spectra shown in Figure 3.22 contain a wealth of information. For certain molecules, such as acetone, acetyl chloride, benzene and toluene, the fragmentation pattern is relatively insensitive to pulse shaping when compared to the rest of the molecules. The fragmentation of azulene and naphthalene, molecules with very different spectroscopy and ionization potential, is quite similar. For acetone, benzene and the organometallic compound MMT, the molecular ion increases as I_{MS} decreases, this trend is the opposite of that observed for all the other molecules. Finally, most aromatic molecules produce C^+ ions readily, but benzene does not. These and many other observations may be the object of further in-depth studies.

3.3.4 Achieving control with a single parameter

In this study only a finite (~10^4) number of differently phase-shaped pulses were evaluated out of the possible 10^{200} different phase-shaped pulses that could be synthesized by our pulse shaper. This number being the number of permutations possible with 100 pixels and 100 different phase values per pixel. Despite the limited sampling, we consider that it is prudent to conclude that a single laser parameter such as I_{SHG} can be used to determine the fragmentation pattern of a molecule. This is justified by the following arguments. First, the phases that were tested cover the most likely excitation pathways that could lead to influencing selective photochemistry. Different values of chirp and split pulses were evaluated, which would cover any pump-probe scenario involving higher and lower frequencies within the bandwidth of the pulse. The period of a sine function was examined, which would address the influence of pulse sequences that could coherently drive a vibrational frequency in the molecule. The phase of a sinusoidal function was examined, which is known to control multiphoton excitation. Binary phase functions were evaluated, which cause large frequency-dependent changes in the amplitude of multiphoton excitation, and produce complex pulse sequences that can selectively drive stimulated Raman transitions. Experiments were carried out which varied systematically the second, third, and fourth order terms of the Taylor expansion parameters. The entire sets of random phases, and random binary phases were also evaluated. But, as indicated in the text, the resulting photofragmentation from all the different experiments was found to depend on the normalized I_{MS} or I_{SHG} values and not on how the pulse was shaped.

Because I_{MS} is proportional to I_{SHG}, which is roughly inversely proportional to the duration of the pulse, our model can be refined to one in which the pulse duration is the single parameter that determines the extent of fragmentation in a molecule subjected to a strong near-IR field. Because some pulses are highly modulated in the time domain, their time duration can be estimated from I_{SHG}. The results in Figure 3.11b where we changed the pulse duration by restricting the bandwidth of the pulse can be referred to as a proof to this statement. In that case the ratio between the heavier and lighter mass fragments changed just like that when phase modulation was used. Therefore all the findings here support the conclusion that the extent of fragmentation, which depends monotonically from I_{MS} and I_{SHG}, depends mainly from the pulse duration. It follows, that the observed results for sixteen different compounds can be understood in terms of prompt field ionization with subsequent multiphoton fragmentation processes, as stated earlier for *p*-NT fragmentation.

It's necessary here to avoid the possible confusion between pulse duration and peak intensity, which arises because peak intensity depends on three parameters: pulse energy, pulse duration, and focusing. In Section 3.1.3, it's shown that the fragmentation pattern was independent from focusing, and hence peak intensity. In that case, the diameter of the focal spot was increased by one order of magnitude, without affecting the ratio between two fragments. In Section 3.2.4, ample experimental evidence was shown that fragmentation does not depend on pulse energy. In those experiments the fragmentation patterns as a function of four different pulse shaping functions were showed not to change as the laser pulse energy was changed from 25 to 170 μJ. In Section 3.2.1 it's shown that lengthening the pulse by reducing its bandwidth lead to changes in the fragmentation pattern as measured by the ratio between two masses. In the rest of the phase shaping experiments presented throughout this article, the overwhelming data support our observation that pulse duration and not peak intensity caused the desired measure of selectivity.

The findings here are not entirely surprising. The dependence of fragmentation on pulse duration had been observed at least two decades ago. In the early days only two points were available, a nanosecond laser versus a picosecond laser (Szaflarski *et al.*, 1988; Weinkauf *et al.*, 1994; Yang *et al.*, 1985). More importantly, the observation that mass spectrum fragmentation patterns change with chirp was independently found by several research groups working with femtosecond lasers. In 1998 Pastirk et al. (1998) showed that chirp could be used to enhance the concerted elimination of I_2 from CH_2I_2. For example, Levis found that the fragmentation of *p*-nitroaniline changed substantially as a function of chirp (Levis *et al.*, 2002). However, the highlight of that article was that closed-loop control was capable of more sophisticated control compared to chirp. Jones studied the chirp dependence on the fragmentation of S_8 and then used a closed-loop learning-algorithm approach (Wells *et al.*, 2005). He found that smaller fragments were produced with longer pulses and that the same dependence was found using the learning algorithm. A more recent study on the open and closed-loop dissociative ionization of ethanol by Yazawa et al (2006) found that a systematic approach, simple chirp, or pulse sequences, yielded the best results. The overall pulse duration was found to be the essential factor for determining the relative yield and that the spike-like temporal profiles within a pulse did not affect the yield (Yazawa *et al.*, 2006). Unfortunately these findings are usually dismissed as a trivial dependence on peak intensity, and some groups have preferred the mystery of the closed-loop approach.

If the complex time-frequency properties of the shaped near-IR pulses could direct energy flow or coherently drive a vibrational wave packet and cause bond selective fragmentation and ionization we would have found at least one pulse producing a very different fragmentation ratio than that found in Figure 3.15; but we didn't. Therefore, there is no evidence in the entire dataset presented showing that complex pulses can cause different fragmentation patterns than those determined by the particular I_{SHG} or I_{MS} of that pulse. This conclusion is based on the statistical analysis of all the data. If a closed-loop approach had been used for the experiments shown in Figure 3.15, requiring that for all shaped pulses I_{MS} stays constant, we would have concluded that the relative yield between the two fragments was controlled by as much as a factor of two. However, the values are well within the Gaussian noise spectrum presented in Figure 3.15c, and the correct interpretation is that there was no control outside what could be predicted given the value of I_{MS}.

If vibrational coherence played a role in the laser control experiments presented here, scanning the time between multiple sub-pulses in a shaped pulse should reveal this type of coherence. The measurements on different molecules presented in Figure 3.22, comparing a sinusoidal modulation with linear chirp, were designed to probe vibrational coherence. However, there was no instance where such a vibrational resonance was observed in all the molecules studied. This experimental evidence strongly indicates that vibrational coherence does not play a role in the fragmentation process.

In the language of learning algorithms, if there is an optimal solution and there is a gradient toward this solution the search space is dubbed convex. Convex problems are easily solved by learning algorithms. Here we argue that laser controlled fragmentation under the conditions considered here can be represented as a convex problem. Minimum fragmentation corresponding to TL pulses, while maximum fragmentation corresponds to the longest pulses accessible by the pulse shaper. This observation explains why learning-algorithm based searches have been able to advance successfully despite the enormous search space and the experimental noise associated with molecular fragmentation. If the search space was more like a needle-in-the-haystack, where one or more specific shaped pulses are greatly different than all others, even those that are quite similar, then learning-algorithm based searches would have much more difficulty optimizing different product yields. Given that the number of phase shaped pulses that can produce a given value of ionization probability grows exponentially as I_{MS} approaches zero, a random search quickly finds a pulse with minimal—close to the noise level—ionization yield.

Despite all the evidence shown it may not be obvious why fragmentation and ionization does not seem to depend on parameters such as time delay between sub-pulses. The primary reason is that there is a ~9 eV energy barrier that needs to be surmounted to achieve ionization of the molecules. The laser intensity needed for ionization causes excitation in a large number of intermediate rovibronic states, some of which include dissociation continua. Therefore, the resulting coherent superposition undergoes very fast delocalization and the ability to observe wave packet revivals as are observed in pump-probe experiments involving a single electronic state is lost.

3.4 Conclusion

In this chapter I have discussed the prospects of laser controlled chemistry resulting from the interaction between isolated molecules and strong (10^{14}-10^{16}) W/cm^2 non-resonant laser pulses shaped by different phase and amplitude functions. Detailed analysis of the systematic experimental results had led to uncover a number of trends. It's found that the total yield of ions, relative to transform limited pulses, is directly proportional to the integrated second harmonic of the laser pulse for any type of phase-and-or-amplitude modulation.

When the total yield of ions relative to transform-limited pulses is known, the fragmentation pattern for a given molecule is found to be limited within a plane defined by the total ion yield, and the resulting fragmentation pattern—the relative ion yield for each m/z. Such a plane is illustrated for pNT in Figure 3.26. For any type of phase function the resulting fragmentation ratio is always found to fall in this plane. All of the experimental evidence from this work indicates that despite large differences in the particular time-frequency details of a given shaped pulse, the fragmentation always falls within the molecular fragmentation plane, and no shaped pulse capable of causing a fragmentation pattern that deviates from that given by this plane. Had we found evidence of bond-selective cleavage, we would have found a pattern in which a significant percent of the yield would be dominated by the desired fragment ion. Unfortunately no such observation for any of the molecules or for any of the pulses tested.

To determine the laser fragmentation pattern for a given molecular dissociation with intense fields, one needs less than one hundred measurement. There is no need to evaluate the astronomical number of possible shaped pulses that can be synthesized experimentally by the pulse shaper. Fragmentation pathways under an intense laser field depend only on the molecule and the most one can do is control where in the fragmentation plane the excitation takes place. Apparently the extent of fragmentation seems to depend on the laser-molecule interaction time. This observation is consistent with the absorption-ionization-dissociation mechanism. At the intensities investigated in this work, field ionization takes place for TL pulses, and shaped pulses enhance fragmentation, producing cations that decrease in size follow a photofragmentation chain while the field is present.

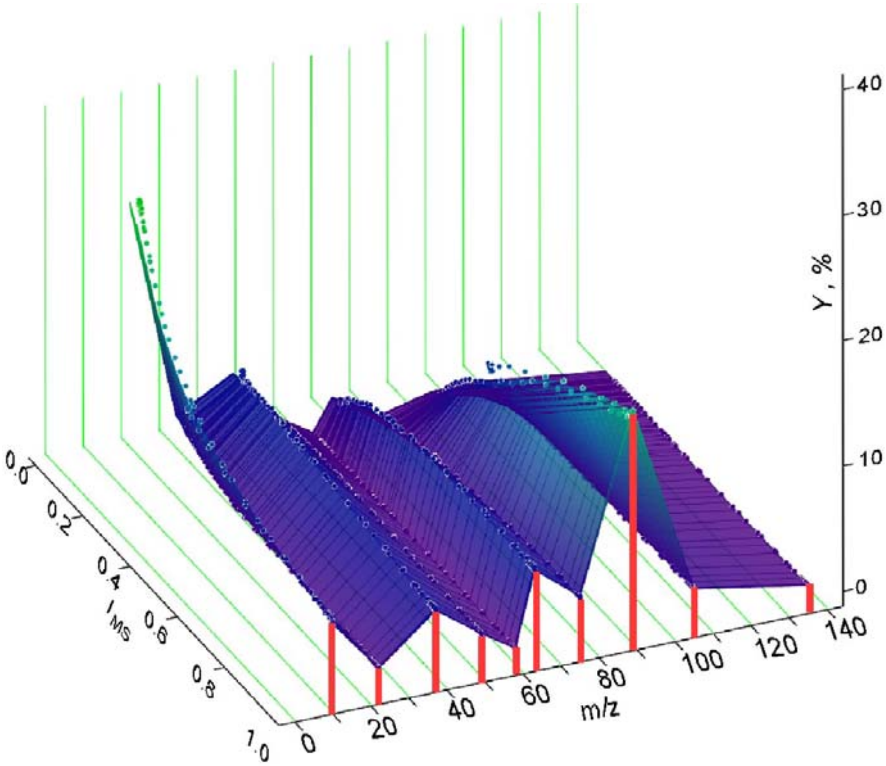

Figure 3.26 Laser control fragmentation plane for *p*-NT. The three dimensional figure is generated by plotting the mass spectrum in the x-axis, the normalized total ion yield in the y-axis, and the relative ion yield in the z-axis. The plane is a surface that wraps over the main ion peaks measured as a function of positive chirp. The points shown, belong to additional experimental measurements: using different sinusoidal phase functions and changing the time between two pulses. For interpretation of the references to color in this and all other figures, the reader is referred to the electronic version of this dissertation.

To avoid misinterpretations of the conclusions, it should be made clear that the findings are valid for amplified near-IR phase shaped femtosecond laser pulses on isolated molecules. All the observations here are also restricted by the fact that only the nascent ions are monitored, so the fate of the neutrals can't be determined. For experiments involving nonlinear optical processes such as harmonic generation or multiphoton excitation (not shown here), phase modulation can exert a high level of control that is well understood (Lozovoy, V. V. *et al.*, 2005a, 2006b). However, here I only focus on the interaction between intense (shaped) near-IR pulses and isolated molecules.

Our experimental data in Figure 3.22 indicates that a single parameter can be used to explore the entire range of changes in the fragmentation of isolated molecules using near-IR pulses above I_{sat}. This observation allows us to define a 'laser control fragmentation plane' that maps the fragmentation patterns (*m/z*) as a function of the total ion yield (I_{MS}), which is illustrated in Figure 27 for *p*-NT. Having defined this plane, it can be stated that all of the pulse shaping experiments presented here for *p*-NT fall within this plane except for statistical noise or for cases in which the shaper introduced a systematic error due to amplitude modulation as discussed in section 3.2.9.

Although all of the experiments shown indicate that laser control of chemical reactions with a single intense near-IR pulse fall within the laser control fragmentation plane illustrated in Figure 3.26, one may argue that there ought to be at least one class of pulses capable of achieving selective bond cleavage, well above the statistical noise, and thus generate a fragmentation pattern that significantly deviates from the laser control fragmentation plane.

Experimentally refuting the existence of such a class of pulses would take an infinite number of experiments given the essentially infinite resolution that can be achieved by the pulse shaper. Realistically, the bandwidth of the pulses is limited, the number of pixels is limited, the noise of the experiment makes minute changes in phase immeasurable, and experimental timescale is also limited. The molecular system has a finite coherence lifetime and a finite initial distribution of states that also place limits on the degree of finesse that would make sense to explore. All can be said at this time, is that all the experiments presented here show no deviation from the laser control fragmentation plane, or in other words, the fragmentation observed for any shaped pulse is very similar to that found for a positively chirped pulse that creates an equivalent total ion yield.

The fragmentation of isolated molecules when exposed to an intense near-IR femtosecond shaped pulse can be mapped as a function of the normalized total ion yield. Given this conclusion, a number of scientific challenges can be considered: first and foremost, providing a mechanism that explains this behavior; second, finding non-statistical deviations to this behavior; third, designing new experimental approaches to laser control.

After a thorough examination of different sets of experiments on the effects of phase and amplitude shaped pulses on a molecular fragmentation, no evidence for coherent control in the fragmentation of isolated molecules by shaped near-IR pulses is found. This implies that electronic and vibrational coherences seem to dissipate though wave packet delocalization and have minimal influence on the photofragmentation pathways. Accordingly, the present study promises a robust method for controlling molecular fragmentation with potential analytic and synthetic application.

Chapter 4 Control of Laser-Matter Interaction: Photo dissociation of Acetophenone and Its Derivatives

It has been over two decades since ultrafast lasers were used to explore the photo-dissociation dynamics of molecules. During this time, important lessons have been learned about direct and indirect bond breakage, curve crossing dynamics, and dynamics over saddle points. Over a decade ago, some interest shifted from probing the dynamics to controlling the dynamics. Of particular interest were studies in which an intense non-resonant laser field is shaped prior to interacting with isolated molecules and the subsequent yield of fragment ions, detected using a mass spectrometer, was found to vary according to the phase and amplitude of the shaped laser pulses. Including the work presented in Chapter 3, experimental evidence indicates that pulse duration can account for the majority of the changes in fragmentation observed (Kosmidis *et al.*, 1997; Kosmidis *et al.*, 1994b; Ledingham *et al.*, 1995; Lozovoy, V. V. *et al.*, 2008; Shane *et al.*, 2006; Tasker *et al.*, 2002). In this chapter, results studying the dynamics occurring soon after isolated molecules interact with an intense non-resonant laser field are presented. This study reveals dynamics that take place over a range that extends through four orders of magnitude in time, which provide information about how molecules interact with intense laser fields and how pulse shaping influences the yield of different fragment ions.

Early femtosecond photo-dissociation dynamics studies were carried out using a pump laser that was tuned to the desired electronic potential energy surface (PES) and the dynamics occurring on the PES were subsequently probed by a probe laser pulse tuned to detect the photofragments (Dantus *et al.*, 1987, 1988; Rosker *et al.*, 1988). Since the early days it was noted that femtosecond lasers, even when not resonant with an electronic transition would be able to cause excitation, fragmentation and ionization. A distinction was made between long pulse excitation, where the process could be characterized by multiphoton transitions and short pulse excitation, where the process was characterized by fast field ionization followed by fragmentation. The former process became known as ladder switching which indicated photo-dissociation takes place at a comparable rate with transitions to upper excited states (Szaflarski *et al.*, 1988; Yang *et al.*, 1985).

Direct ultrafast excitation to selected PES allowed direct probing of wave packet dynamics. Bound and quasi-bound states arising from the crossing of electronic states led to the observation of coherent oscillations. Extrapolating from these early studies, one would expect that a shaped pulse could be used to time a number of discrete transitions among two or more PES in order to direct the photo-dissociation reaction and control the product formation. Control of a wave packet requires a collection of sub-50fs pulses at a number of different wavelengths in the 260-532nm spectral region. A laser source capable of creating three or more pulses by pulse shaping a single input pulse in the UV-Vis wavelength range is still outside of present technical capabilities, although significant progress is being made on shaped UV sources and their use for controlling chemical reactions (Greenfield *et al.*, 2009; Kotur *et al.*, 2009; Pearson *et al.*, 2007). The widely available near-IR femtosecond shaped sources have already inspired numerous laser control experiments in which significant changes over product distribution have been observed (Assion *et al.*, 1998; Brif *et al.*). Efforts to explain the observed changes in the yield of different photo-fragments in terms of transitions timed to trigger transitions between different PES acting on the evolving localized wave packet were complicated by the lack of information about excited state potential energy surfaces, and their transition dipoles as a function of different reaction coordinates. The new interpretation of strong non-resonant photo-dissociation discussed in chapter 3 recognizes that the laser pulse causes field ionization, and the time during which the field acts on the nascent ion is more likely regulating ladder climbing and ladder switching events (Lozovoy, V. V. *et al.*, 2008).

In the results presented in this chapter, a series of pump-probe experiments were performed on acetophenone (1), partially deuterated acetophenone (2), 2-methyl-acetophoenone (3), 3-methyl-acetophenone (4) and 4-methyl-acetophenone (5), as shown in Figure 4.1. The results obtained by electron ionization mass spectrometry are compared to those obtained by femtosecond photoionization using near-IR ultrashort pulses. These results, together with the time resolved measurements and comparison between the different derivative compounds, allow us to propose that pulse shaping acts by controlling ladder climbing and ladder switching processes that take place during the strong-field excitation of this family of polyatomic molecules.

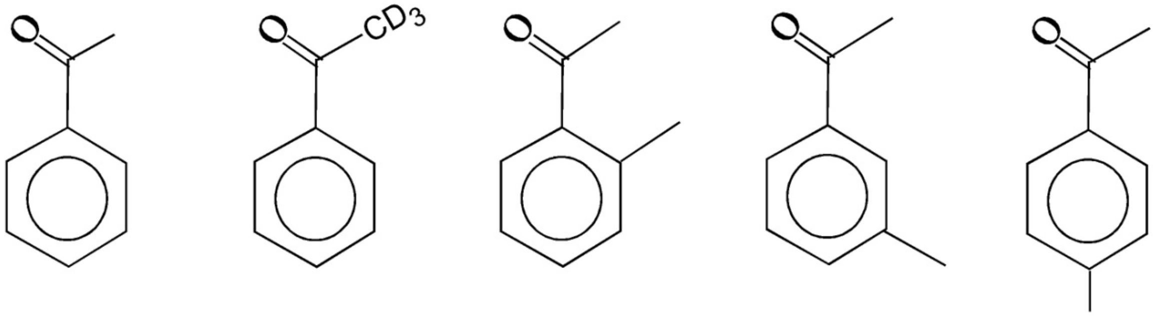

1 2 3 4 5

Figure 4.1 Structures of the acetophenone, D3-acetophenone, and three methyl-acetophenone isomers. 1. acetophenone 2. β,β,β-deuterated acetophenone 3. 2-methyl acetophenone 4. 3-methyl acetophenone 5. 4 methyl acetophenone.

4.1 Experimental

The mass spectrometer and the laser system are the same as those described in Chapter 2. The output pulses were split by a 50/50 beam splitter and spatially recombined with an adjustable delay before entering the mass spectrometer. For some experiments, a ten cm path length water filled glass cell was placed in one of the arms to introduce +2500 fs^2 linear chirp, which broadened the probe pulses to ~200 fs pulse duration. The schematic of the setup is shown in Figure 4.2. Neutral density filters were placed in the beam paths to adjust the laser irradiance such that energy/pulse was always the same. A 50 mm focal length lens was used to focus the pulses into the chamber of the mass spectrometer and cause ionization and dissociation of gas phase acetophenone molecules. Typical pulse energy at the focus was attenuated to 100 μJ/pulse, giving a maximum intensity of 4×10^{15} W/cm^2 for TL pulses using the formula $I_0 = 4\left(\ln\left(2\right)\right)^{0.5} \pi^{-1.5} \times W \times \tau^{-1} \times \omega_0^{-2}$, where W is the pulse energy (J), τ is the time duration of the pulse(s) and ω_0 is the radius at the focus when intensity drops by $1/e^2$ (cm) (also called focal spot size). No efforts to mitigate the Gaussian intensity distribution inherent with laser excitation were needed for these experiments. The intensity distribution, also known as "volume effect", is only relevant in this study when pump and probe pulses are overlapped in time, and results in a higher yield of ions. A further discussion regarding the rationale for using TL pump and a chirped probe pulse and the volume effect will be given later.

For all experiments, part of the beam (after recombination) was directed to a 50 μm Type I β-BBO crystal generating the second harmonic generation (SHG) of the shaped laser pulses as an indicator of time zero and also for the purpose of monitoring laser stability.

Experimental samples of acetophenone ((Fluka >99.5%), β,β,β-d3-acetophenone (Aldrich>99%), 2-methyl acetophenone (Fluka >98.0%), 3-methyl acetophenone (Aldrich >98.0%), and 4-methyl acetophenone (Fluka >96.0%) were used without further purification.

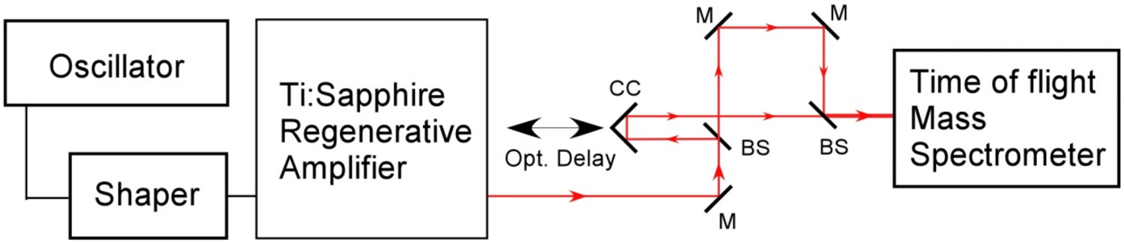

Figure 4.2 Schematic of the experimental setup. BS: 50/50 intensity beam splitter. M: silver coated reflective mirror. CC: Corner cube.

4.2 Results

4.2.1 Mass spectra of acetophenone

The mass spectra obtained for acetophenone when measured either by 70 eV electron ionization or 35fs transform limited (800nm) laser pulses are presented in Figure 4.3. The molecular ion is identified by its *m/z* 120. The major fragment ion species observed for both ionization methods are essentially the same. The mass spectrum of partially deuterated acetophenone (D_3) was also obtained by fs excitation pulses as a reference. The only differences observed between acetophenone and D_3-acetophenone in the bottom panel of Figure 4.3 are the molecular ion masses and the fragment ion with 43 and 46 *m/z*. This indicates that all other product ions lack the methyl group. If the methyl group remained attached, then the photofragments observed for partially deuterated acetophenone would have been shifted by three mass units corresponding to the three deuterium atoms in CD_3.

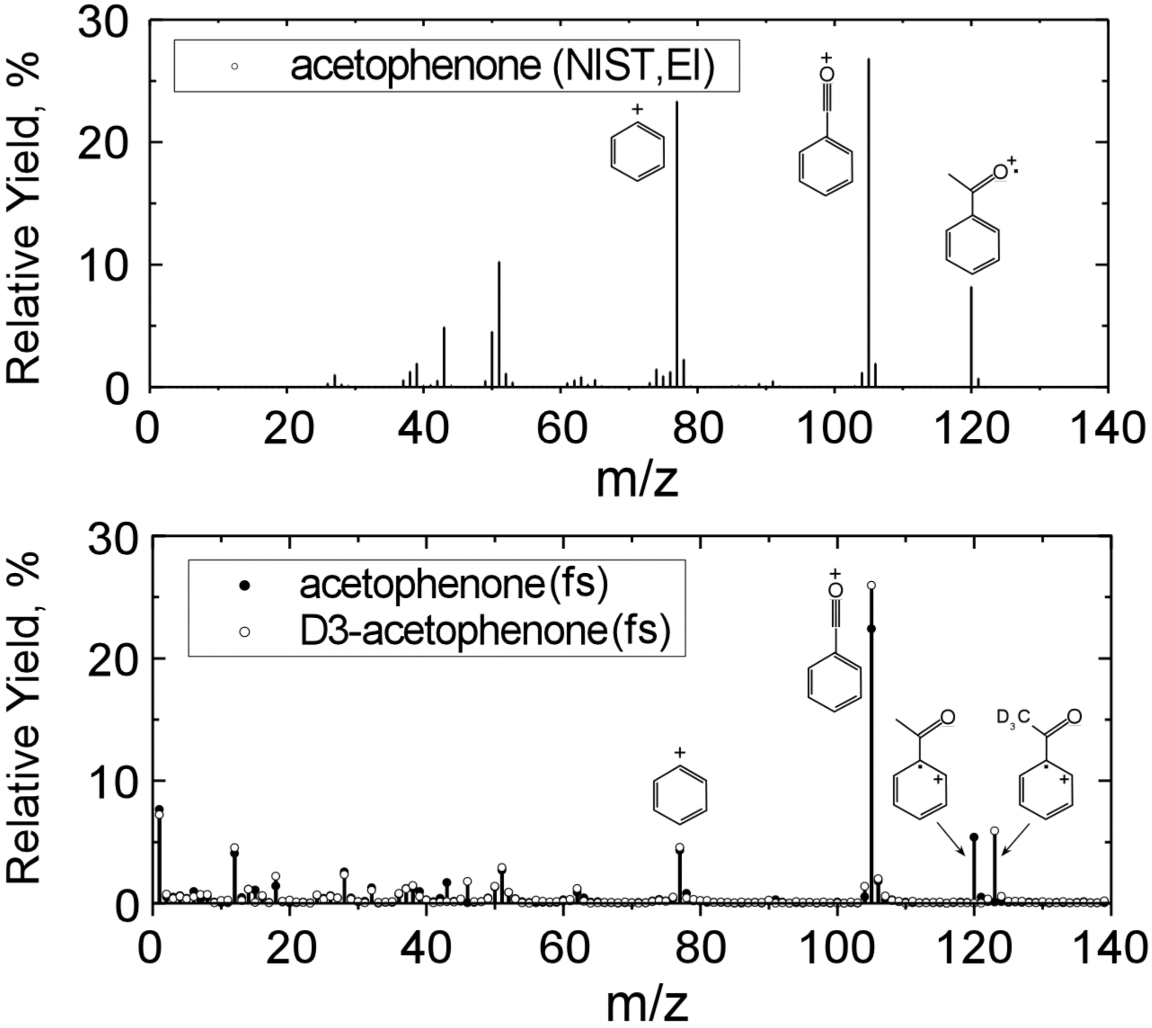

Figure 4.3 Top: Mass spectra of acetophenone obtained by 70 eV electron ionization. Bottom: Mass spectra of acetophenone and deuterated acetophenone obtained by fs laser ionization.

4.2.2 Mass Spectra of methyl-acetophenones

The mass spectra of three methyl-acetophenone isomers, with molecular ion at *m/z* 134, are presented in Figure 4.4. There is almost no difference in the fragmentation patterns of the three isomers when obtained by electron ionization. However, when fs pulses are used to induce the photoionization, the molecular ion abundance of 3-methyl acetophenone is significantly higher and its benzoyl ion abundance is significantly lower than those of the other two isomers. The reason of this difference will be discussed later.

4.2.3 Pump (TL)-Probe (TL) on acetophenone

Time-resolved photo-dissociation experiments of acetophenone were carried out using two 800nm transform-limited pulses (τ_{FWHM}=35 fs) for two different timescales, -5ps to 5ps, and -100ps to 100ps. The relative yields of several major fragments including molecular ion (*m/z* 120), benzoyl ion (*m/z* 105), phenyl ion (*m/z* 77) and methyl ion (*m/z* 15) were plotted with respect to the time delay between the pump and probe pulses, as shown in Figure 4.5. Given that laser pulse energies were always kept the same for the pump and the probe pulses, the relative yields of the fragments are symmetric about time zero. Therefore in Figure 4.5, only the results with positive time delays are shown.

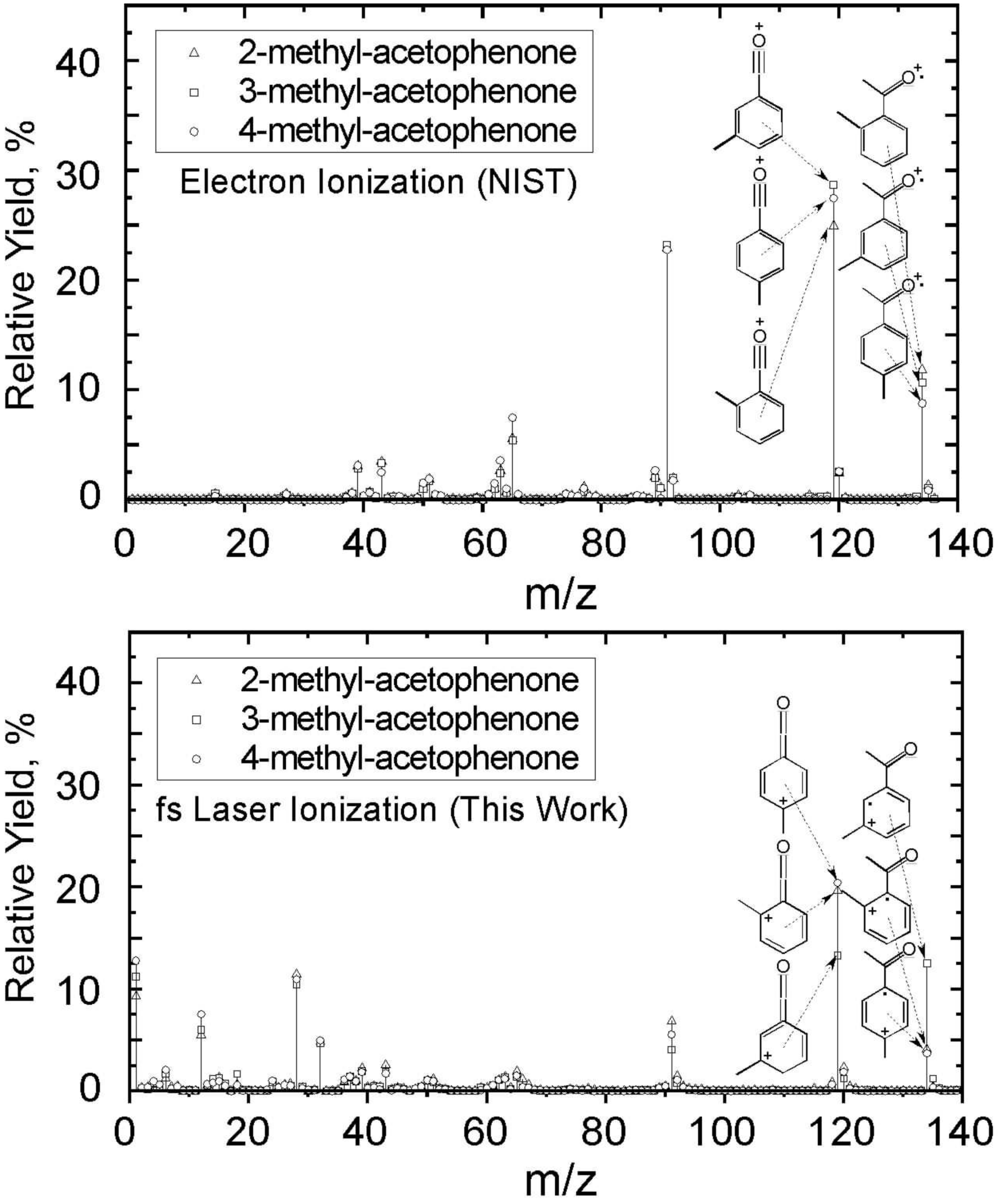

Figure 4.4 Mass spectra of methyl acetophenones obtained by electron ionization (top) and fs laser ionization (bottom).

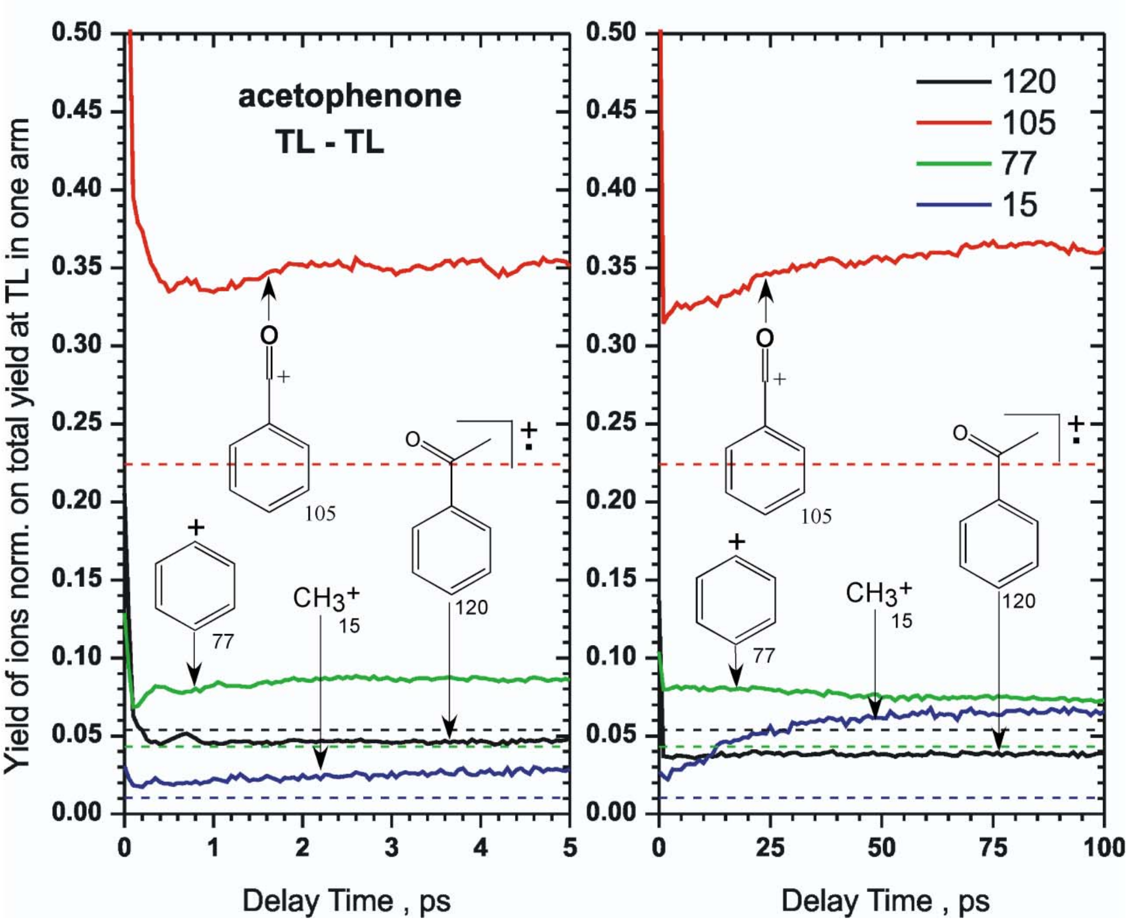

Figure 4.5 Yield of several major fragment ions from acetophenone plotted with respect to the time delay between (TL) pump and (TL) probe pulses. Dashed lines show yields of fragments when only one TL pulse was used. For interpretation of the references to color in this and all other figures, the reader is referred to the electronic version of this dissertation.

For all the fragment ions the maximum value was observed at time zero, and the maximum yield decayed following the cross correlation between pump and probe pulses <50fs. The relative yields of benzoyl ion (*m/z* 105) and methyl ion (*m/z* 15), having reached a minimum at early times, increase with time delay. An exponential rise with time constant of 20.0±1.6 ps and 18.5±0.7 ps was measured respectively. The relative yield of phenyl ion decreased with an exponential decay time constant of 19.6±1.8. The relative yield of the molecular ion remained almost unchanged after the first picosecond.

4.2.4 Pump (TL)-Probe (Chirped) on acetophenone

Measurements were also carried out for acetophenone using a TL pump pulse followed by a +2500fs^2 chirped probe pulse. The rationale behind these measurements was that we wanted to better understand the ~1ps modulation in the ion yields. By chirping the probe beam, it causes minimum ionization and more importantly, because of its lower intensity, it probes a smaller volume of molecules than the TL pump laser. Thus, the difference as a function of time is caused only by molecules that were first ionized by the pump laser. Given that the energy per pulse for both pump and probe is the same, the TL pulses have a 5.7 times higher peak intensity than the chirped pulses. When the TL pulses are used as the pump pulse, most of the molecules inside the reaction region are ionized. The chirped probe pulses now are able to interact with the molecular ions resulting in further fragmentation, which is the process of interest in this work. The relative yields of the major fragments as a function of the delay time between two pulses are shown in Figure 4.6. Clearly, the strategy to chirp the probe allowed us to better observe the picosecond modulation.

The results in Figure 4.6 show a fast feature observed around zero delay time with a longer decay time compared to the one observed for the TL-TL case. The increase in the relative yield of benzoyl ions (*m/z* 105) and the decrease in the relative yield of phenyl ions (*m/z* 77) with time delay were observed with time constants of 19.4±0.8 and 18.8±1.2 ps, respectively. An interesting observation from this experiment is the oscillations observed for the ion yield of molecular ions, benzoyl ions and phenyl ions within the first 3 ps, as can be seen in Figure 4.6(a).The period is determined to be 0.685±0.015 ps by fitting the data.

4.2.5 Pump (TL)-Probe (Chirped) on partially deuterated acetophenone and methyl-acetophenones

Pump probe measurements were also carried out for D_3-acetophenone and methyl-acetophenones using a TL pump pulse followed by a +2500 fs^2 chirped probe pulse. The yield of the benzoyl ion for which oscillations were observed is plotted with respect to the time delay between the pump (TL) and probe (chirped) pulses, as shown in Figure 4.7. The yield of benzoyl ion obtained from acetophenone molecules is also plotted as reference.

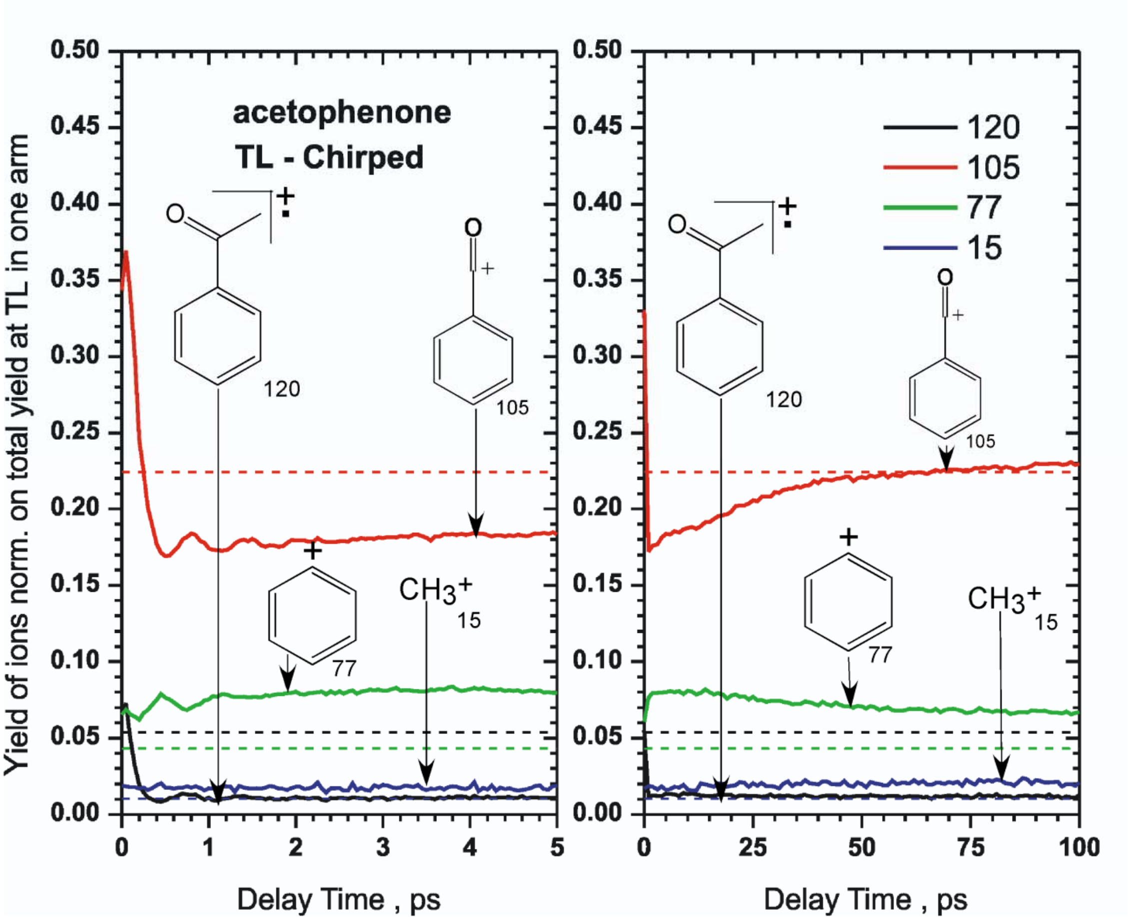

Figure 4.6 Yield of several major fragment ions from acetophenone plotted with respect to the time delay between (TL) pump and (Chirped) probe pulses. Dashed lines show yields of fragments when only one TL pulse was used. For interpretation of the references to color in this and all other figures, the reader is referred to the electronic version of this dissertation.

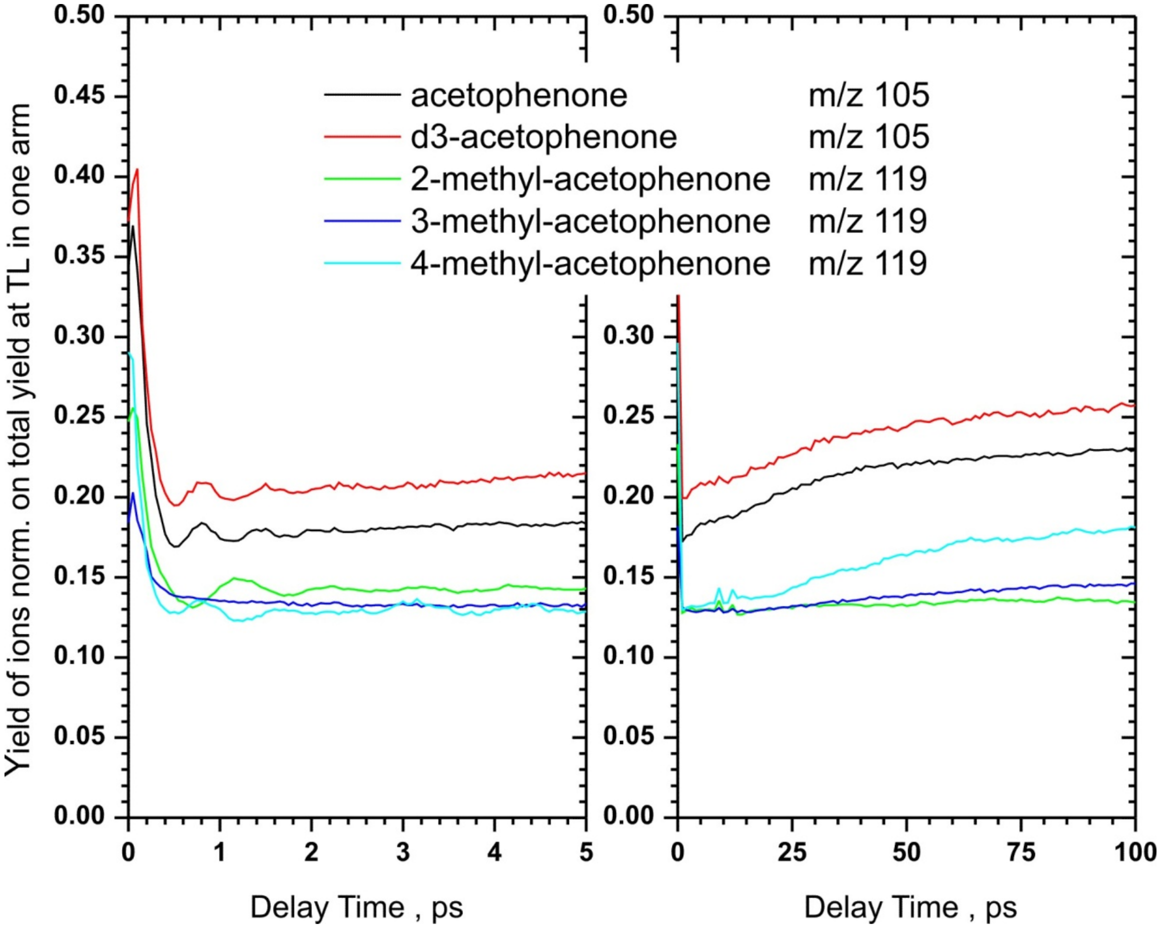

Figure 4.7 Yields of benzoyl ion from acetophenone, d3-acetophenone, and three methyl acetophenone isomers plotted with respect to the delay between TL pump pulse and Chirped probe pulse. For interpretation of the references to color in this and all other figures, the reader is referred to the electronic version of this dissertation.

As can be seen in the short time scale (Figure 4.7, left), the period of the oscillation does not change between acetophenone and deuterated acetophenone. For the methyl benzoyl ions generated from methyl acetophenones, a clear difference can be seen in the oscillations. The periods observed for ortho and para-methyl acetophenone are both 1.040±0.030 ps, approximately 53% longer period than observed for acetophenone molecules. On the other hand, no oscillations were observed for meta-methyl acetophenone.

4.3 Discussion

4.3.1 Photo-dissociation of acetophenone

In all the pump-probe experiments, a fast feature in the ion yields was observed when pump and probe pulses were overlapped in time. The temporal width of this feature was found to coincide with the cross correlation trace of the TL pump and chirped probe pulses. This feature serves as a convenient reference for determining the time when both pump and probe lasers are overlapped. In all the experiments, because the intensity of the pump TL pulses at the focus is 4×10^{15} W/cm^2, higher than the ionization threshold (I_{sat}) of acetophenone molecules (~10^{14} W/cm^2), most of the molecules are field ionized instantaneously. The appearance of the time zero feature is more likely due to the increase of the volume in which the laser intensity exceeds the ionization threshold I_{sat}.

The acetophenone radical cations can be formed by either taking a non-bonding electron from the carboxylic group oxygen (MI') or from the benzene ring (MI"), as illustrated in Figure 4.8. The most favored radical and charge sites in the molecular ion are assumed to arise from loss of the electron with lowest ionization energy in the molecule, which indicates the order of the electron loss should be according to the molecular orbitals $n>\pi>\sigma$. Photoelectron spectroscopy measurements corroborate the source of the first electron as coming from the oxygen non-bonding orbitals (Kobayash *et al.*, 1974). Thus MI' is the most probable structure of the molecular ion. When the probe pulse arrives, additional energy becomes available, MI' could undergo further fragmentation by α-cleavage (radical site initiated) or i-cleavage (charge site initiated). As can be seen from Figure 4.8, MI' can only undergo α-cleavage to form benzoyl cation ($C_6H_5CO^+$) and methyl radical ($CH_3\cdot$) or acylium cation (CH_3CO^+) and phenyl radical ($C_6H_5\cdot$). The bond dissociation energies are 0.82eV and 2.02eV respectively suggesting the first channel (benzoyl cation and CH_3 neutral radical) is dominant. The i-cleavage will form directly the phenyl cation or methyl cation, which is very unlikely to happen because of the much higher bond dissociation energies. Although less favorable, it is also possible to form MI" by removing an electron from the benzene ring. There is evidence that this process takes place within 200fs without absorbing additional photons (Baronavski *et al.*, 2001). As shown for MI", the only possible fragmentation channel is to form the benzoyl cation and methyl radical by α-cleavage. As stated before, MI" has higher energy and is more likely to undergo further fragmentation.

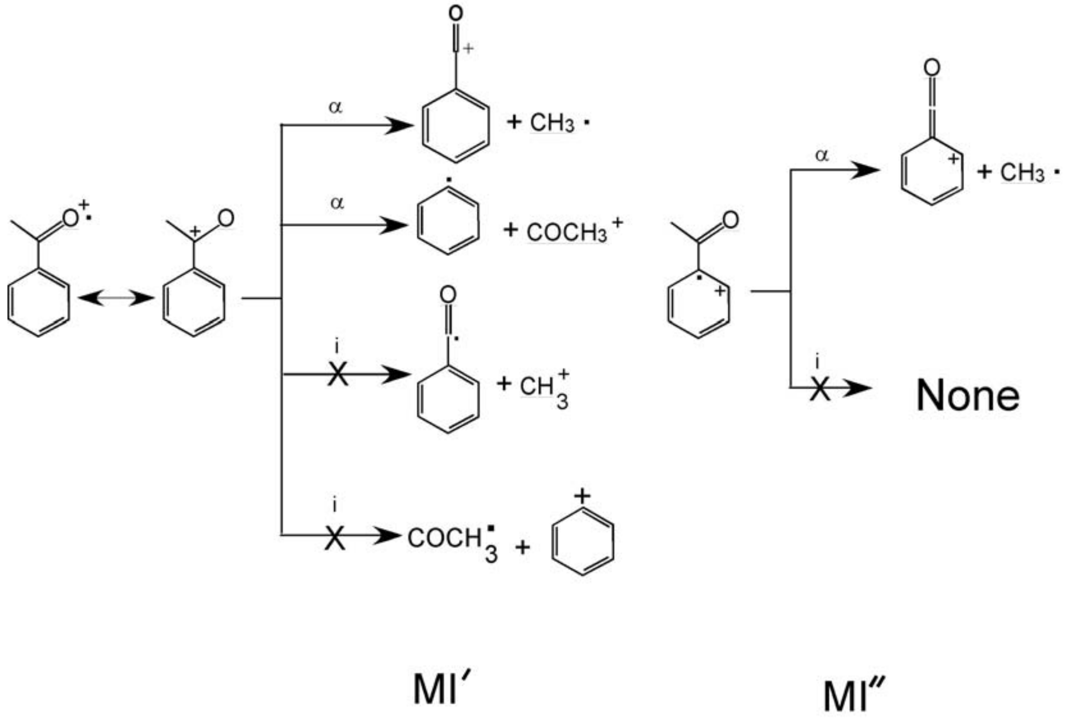

Figure 4.8 Structures of acetophenone molecular ions formed by losing an electron from the oxygen (MI’) or from the benzene ring (MI”), and their major fragmentation pathways.

The benzoyl ions have several resonance structures as shown in Figure 4.10. According to Bursey et al (1975), resonance structure 1 has the lowest energy. In the fragmentation of acetophenone, benzoyl ions are most abundant fragment observed. When these fragments absorb additional photons from the probe pulse they fragment into phenyl ions and CO, as shown in Figure 4.9. This is the main source of phenyl ions, and is supported by the data shown in Figure 4.5, in which the yield of benzoyl ions is found to mirror (opposite) the yield of phenyl ions. Note that the modulation in the yield of phenyl cations is out of phase from that of the benzoyl ions. On the other hand, benzoyl ions are likely to relax to resonant structure 1, which is more stable and less likely to absorb photons required for further fragmentation. As can be seen from Figure 4.6, the yield of benzoyl ion increases with a time constant of 20.0±1.6 ps. This suggests that the delay corresponds to the relaxation time of the benzoyl ions from resonance structures 2-4 to 1.

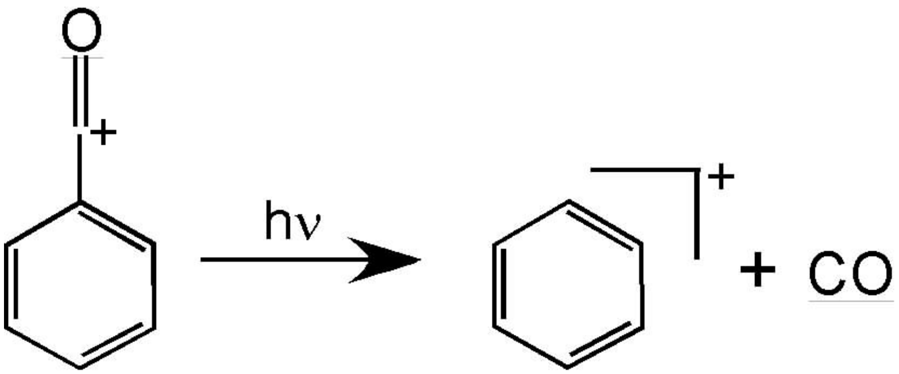

Figure 4.9 Fragmentation of the benzoyl cation.

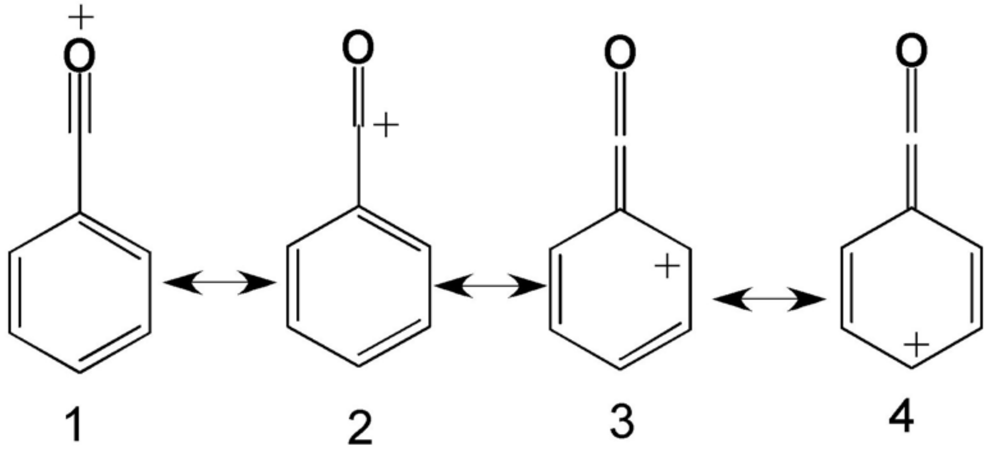

Figure 4.10 Resonance structures of benzoyl ion.

Another interesting result in this experiment is the observation of methyl cations. Normally, because of the higher ionization potential (IP=9.80eV) compared to the benzoyl cations (6.80eV), methyl cations are unlikely to be formed directly from the dissociation of the molecular ion. This is confirmed by the very low abundance of CH_3^+ (only 1%) obtained with a single TL pulse. However, in the data shown in Figure 4.5, the overall yield of methyl cation increases from 2% to 6% as the time delay increases from 0 to 100ps. There are two possible pathways forming methyl cations from acetophenone molecules, from Coulomb explosion through a doubly charged molecular ion, a process that is probably very fast, or from secondary ionization of methyl radicals. The slow ~20 ps rise rate abundance of CH_3^+ ions can only be explained by the secondary ionization of methyl radicals.

A closer look at the peak shapes of the fragment ions (figure not shown) reveals a small contribution from doublet structures for $COCH_3^+$ (*m/z* 43), $C_6H_5CO_2^+$ (*m/z* 52.5), $C_6H_5^+$ (*m/z* 77) and CH_3^+ (*m/z* 15). This type of peak shape is known to arise from coulomb explosion of multiply charged ions. Although coulomb explosion will not be discussed here because of its limited contribution, it would be interesting to study this process in detail in the future. The photo-dissociation pathways of acetophenone discussed above can be summarized by the ladder switching diagram shown in Figure 4.11.

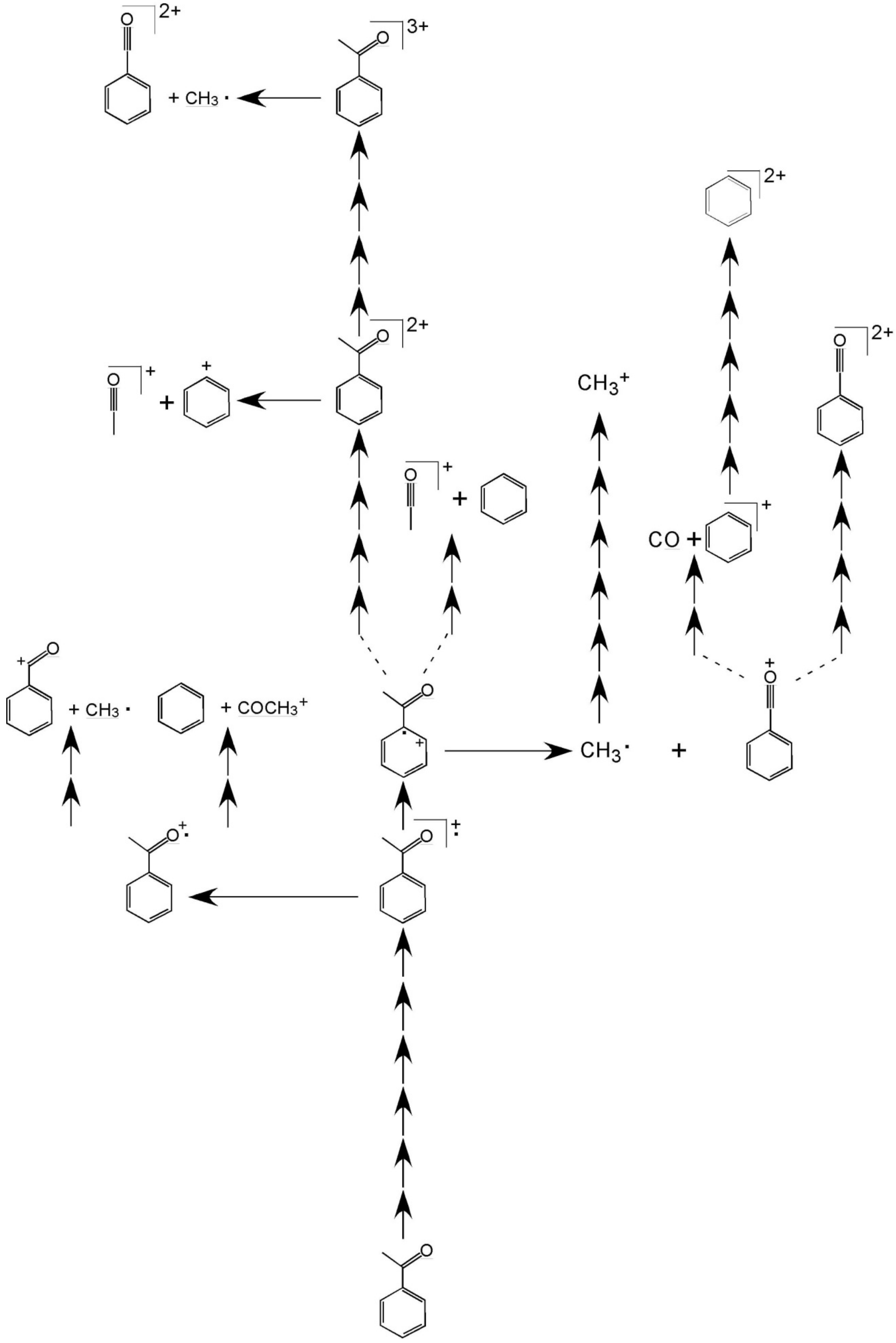
2+
3+
+ CH3 ·
2+
2+
+
+
+
CH3+
CO +
+
2+
+ CH3 ·
+ COCH3+
+
CH3·
+
+
+
+·

Figure 4.11 likely photodissociation pathways of acetophenone and its fragments upon fs-near IR excitation and field ionization. Letters and numbers under the some formulas indicated Coulomb doublet (d) or just a singlet (s) line shape and numbers are mass to charge ratios (m/z). Number of arrows in vertical transition shows number of photons required for excitation. The length of one the vertical arrows corresponds to a photon energy of 1.5 eV.

4.3.2 Photodissociation of methyl-acetophenones

As shown in Figure 4.4, the electron ionization mass spectra of three methyl acetophenone isomers are almost identical. However, for the mass spectra obtained by using femtosecond laser pulses, 3-methyl acetophenone showed significant less extend of fragmentation than the other two isomers. The photoelectron spectra for acetophenone and the three methyl acetophenone isomers are shown in Figure 4.12, measured by Kobayash et al (Kobayash *et al.*, 1974).

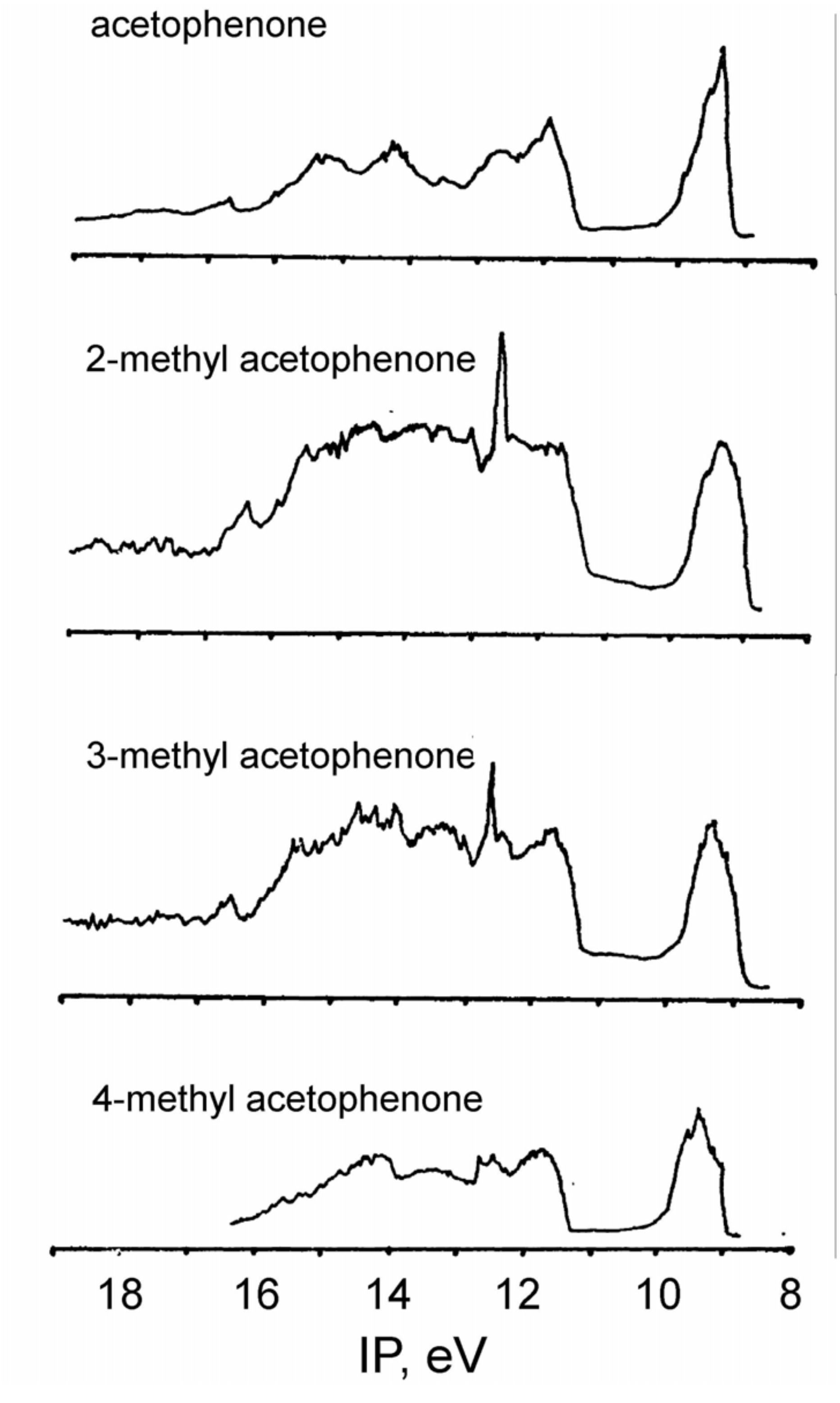

Figure 4.12 PES of acetophenone and three methyl acetophenone isomers.

As can be seen from Figure 4.12, the three methyl acetophenone photoelectron spectra are very similar, suggesting that the three isomers have very similar vertical ionization potentials. This indicates that the initial ionization, and the resulting electronic state is similar for all three molecules.

The difference in the fs laser ionization mass spectra can be explained by the absorption of the radical molecular cations at 800nm. As shown by Harada using the examples of 2,5-dimethyl-2,4-hexadiene and 2,3-dimethyl-1,3-butadiene, the overlap between the absorption spectrum of the radical molecular ions and the laser spectrum determines the extent of fragmentation of the molecular ion (Harada *et al.*, 2001). The molecular ions will undergo extensive fragmentation if they absorb efficiently at 800nm, as in the case of 2,3-dimethyl-1,3-butadiene, or will have limited fragmentation if they absorb inefficiently at 800nm, as in the case of 2,5-dimethyl-2,4-hexadiene. For three methyl acetophenone isomers, although their absorption spectra at 800nm are not available, the pump-probe results from this work provide convincing evidence showing that the molecular ions of 3-methyl acetophenone absorb less efficiently at 800nm than the molecular ions from the other two isomers.

In the TL-TL results, the case at time zero is equivalent to the case of using a single TL pulse. At a long delay such as 5 ps, the second TL pulse causes two processes. One is the ionization of the intact molecules left in the focus after first pulse, which will produce the same fragmentation pattern as the first TL pulse. In other words, this process won’t change the fragment ion relative abundances. The other process is the absorption of additional 800nm photons by the molecular ions formed by the first TL pulse. This process is influenced by the ion’s efficiency of absorbing 800nm photons resulting in further fragmentation, which will change the fragment ion relative abundance. In Table 2, the second column shows the ratio of the abundances between benzoyl ion and molecular ion at time zero and the third column shows the same ratio but at a time delay of 5 ps. The last column is the ratio calculated by column 3/column 2. If the molecular ion absorbs 800nm photons more efficiently, the second pulse causes more fragmentation of the molecular ions and the ratio is greater. As shown in Table 2, 2- and 4- methyl acetophenones have similar efficiencies for absorbing 800 nm photons, while 3-methyl acetophenone is significantly less efficient. This explains why more molecular ions and less benzoyl ions are observed in the mass spectrum of 3-methyl acetophenone obtained when using femtosecond laser pulses, comparing to the other two methyl acetophenone isomers.

	Benzoyl ion/MI		5ps/0ps
	t=0 ps	t=5 ps	
2-methyl acetophenone	4.11033	9.44775	2.29854
3-methyl acetophenone	1.13151	1.61528	1.42754
4-methyl acetophenone	5.14364	11.41365	2.21898

Table 2 Ratios showing the efficiency of absorption at 800 nm for three methyl acetophenone isomers.

4.3.4 Structural Dynamics

As mentioned earlier, one of the most interesting observations is the oscillations observed for a few ions. The observed benzoyl ion yield from deuterated acetophenone has the same oscillation period with that of acetophenone suggesting that the process associated with loss of the methyl group cannot be responsible for the oscillations.

For the methyl-substituted benzoyl ions generated from ortho and para-methyl acetophenones, the oscillation period was found to be longer than those for acetophenone (Figure 4.14). Unlike acetophenone, for methyl substituted acetophenone, photoionization occurs primarily from the π-system (Kobayash *et al.*, 1974). Additionally, the modulation of the ortho isomer was found to be out-of-phase with respect to acetophenone. The slow frequency of the oscillations and the fact that methyl acetophenones have slower oscillations than acetophenone might be an indication that the oscillations are possibly associated with an out of plane vibration, or a torsional motion.

The period of the oscillations in the yield of benzoyl ions from acetophenone was determined to be 0.685±0.015ps in this experiment. This is consistent with the microwave spectrum of acetophenone molecules (Onda et al., 1998) from which the torsional frequency for acetophenone was found to be 47.9 cm^{-1}, which corresponds to a period of 0.696ps. This motion is significantly slower than other intramolecular vibrations in acetophenone molecules.

The methyl group in the ortho and para positions causes the period of the torsional motion to increase by ~50% comparing to acetophenone. This can be explained using the mechanism proposed by Fateley (Fateley, 1973), who measured torsional frequencies for phenol molecules with different ring substitution at ortho, meta or para positions. In phenol molecules, OH is an electron donor. When the substituent X is an electron donor too, the electron donation from the OH group on to the C-O bond decreases. This decreases the double-bond character of the C-O bond and lowers the barrier for the torsional motion resulting in higher torsional frequency. The same rationale can be applied to substituted acetophenone. In this case, the carbonyl group is electron withdrawing. As shown in Figure 4.13. when X is an electron donor, the benzene π electrons should delocalize more onto the C-CO bond which should increase the double-bond character of the bond. This increases the barrier and will result in slower torsional motion. Based on this explanation, because CH_3 is a stronger electron-donor than H, methyl-acetophenones should have higher torsional barrier than acetophenone and slower torsional motion, which is confirmed by the experimental data.

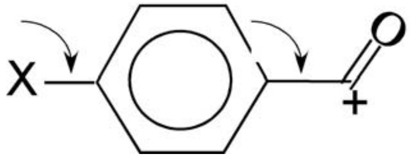

Figure 4.13 The effect of substitution on torsional barrier between the phenyl ring and carbonyl group.

In Figure 4.13, the carbonyl group is in a bent configuration, which is probably not the equilibrium configuration. However, according to Park et al. (Park *et al.*, 2006), the carbonyl group was found to have an angle of 130.6°, after the ultrashort excitation pulse and measured by time-resolved electron diffraction. This bent configuration allows the torsional motion, and as indicated by the TL-Chirp pump probe data (Figure 4.6), the benzoyl ions with higher energy and probably non-equilibrium configuration relax to the most stable form over 50 ps.

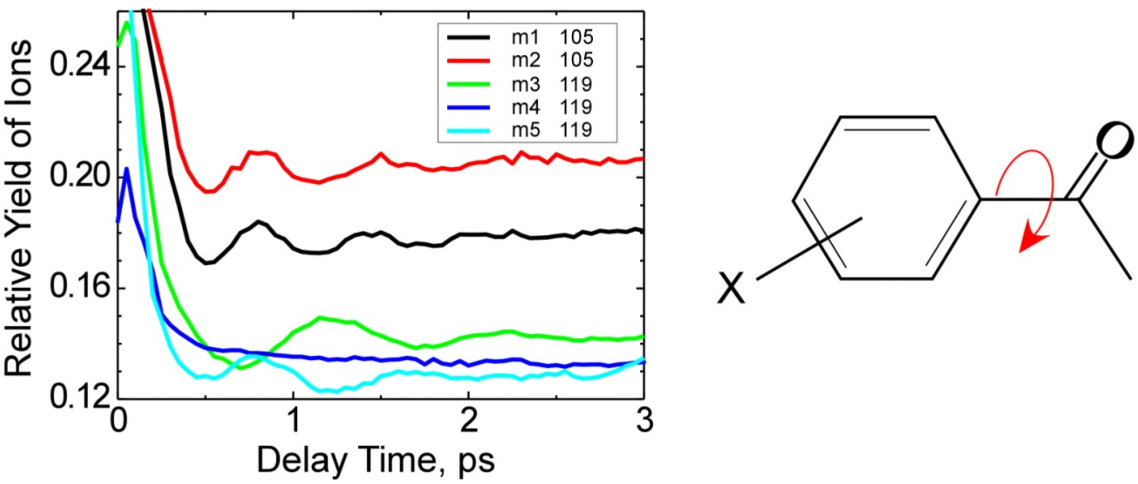

Figure 4.14 Zoom in of the oscillations shown in Figure 4.7. A schematic of the torsional vibration of the phenyl ring is shown on the right. Molecules are m1: acetophenone; m2: d3-acetophenone; m3: 2-methyl-acetophenone; m4: 3-methyl-acetophenone; m5: 4-methyl-acetophenone. For interpretation of the references to color in this and all other figures, the reader is referred to the electronic version of this dissertation.

Careful examination of the resonance structures of the molecular ions expected from methyl acetophenones provides information that can be used to explain why methyl acetophenone does not show the oscillations (See Figure 4.15). The resonance structures for ortho and para isomers lack a conjugate double bond between the carbonyl carbon and phenyl ring, therefore the carbonyl group is able to rotate out of plane. For the meta isomer, however, all the resonance structures have the conjugate double bond structure, therefore the carbonyl in the meta-methyl acetophenone ions cannot rotate out of plane. The extended π system between the carbonyl group and the phenyl ring better stabilizes the radical cation of the meta isomer. In the case of electron ionization, the radical ion is formed by removing an electron from oxygen. This leads to no difference between the yields among all isomers.

It has been found that cyclic aromatic hydrocarbon ions lack electronic transitions at 800 nm (Harada et al., 2001). Therefore when the carbonyl group rotates out of the plane with respect to the phenyl group, the unpaired electron is confined within the phenyl ring and is not likely to absorb additional 800nm photons. This results in less fragmentation and more intact molecular or benzoyl ions. When the phenyl ring is in the same plane with the carbonyl group, the unpaired electron can be delocalized within the entire π system. The increased polarizability increases the probability of absorbing 800nm photons, resulting in the loss of the carbonyl group and a lower molecular and benzoyl ion yields and greater phenyl ion yield. This is why the modulation of benzoyl and phenyl ion yields is out of phase.

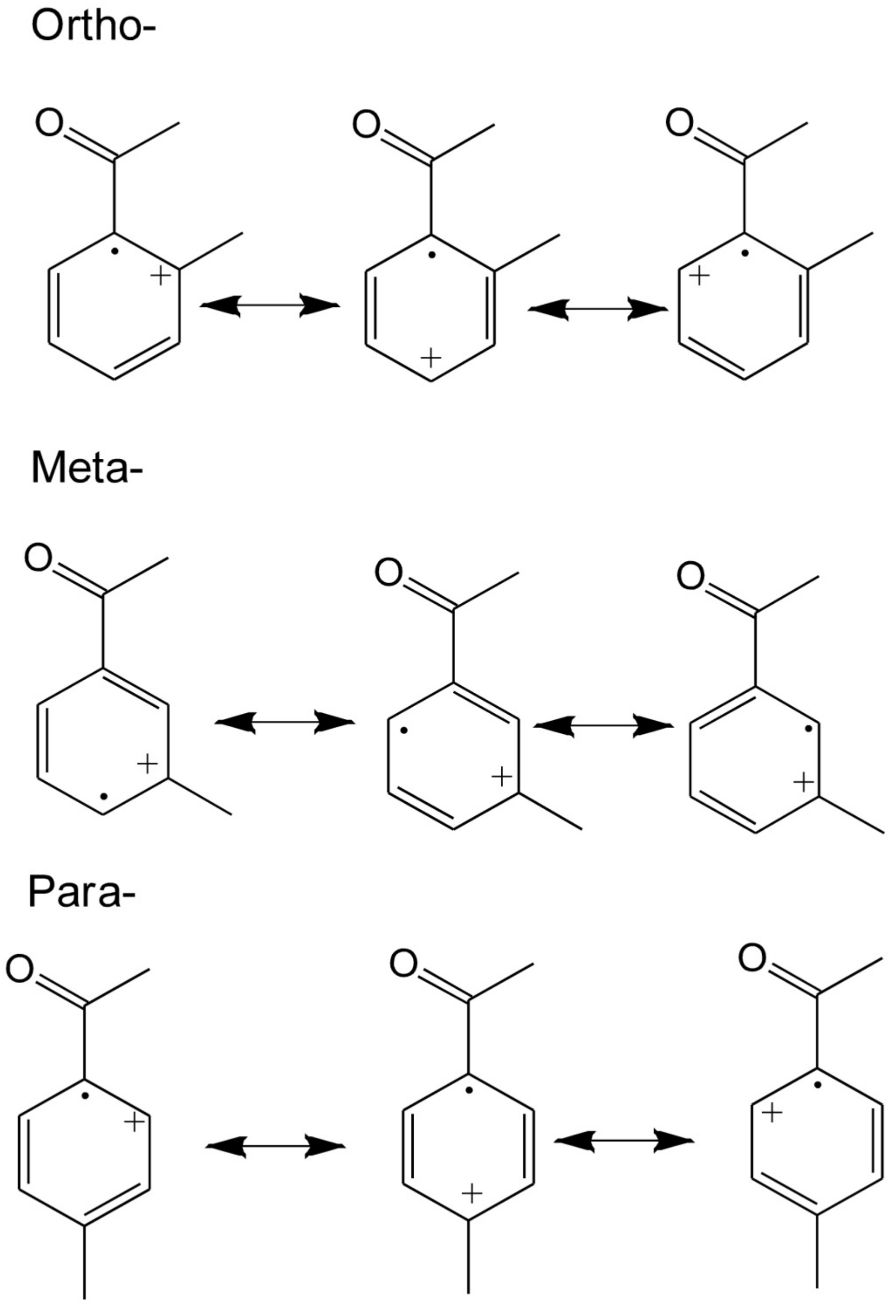

Figure 4.15 Resonance Structures of the ortho, meta and para isomers of acetophenone upon intial field ionization.

4.4 Conclusion

In this work, the time resolved photo-dissociation of acetophenone is investigated using a pump-probe scheme. From the change of ion abundances with respect to the time delay between two pulses, a number of ladder climbing and ladder switching pathways and their time constants are discussed. It is likely that these processes explain why pulse duration plays a critical role in determining product ion distributions in laser control experiments involving shaped non-resonant laser pulses (Lozovoy, V. V. *et al.*, 2008). An interesting oscillation was observed for the yield of benzoyl ions. Following analysis of the time dependent data from deuterated acetophenone and methyl-substituted acetophenone isomers, we believe it is likely that the oscillations are caused by the torsional motion of the carbonyl group, indicating conformational control of the chemical reactions can be achieved by controlling the delay between two pulses.

Chapter 5 Conclusion

When intense ($10^{15} – 10^{17}$ W/cm^2) near-IR pulses interact with polyatomic molecules, a number of different processes take place resulting in molecular fragments (neutral and ions), photoelectrons and photons with frequencies that span from the terahertz regime down to the x-ray regime. This dissertation focuses on determining to what extent these processes can be controlled by altering the phase and amplitude characteristics of the laser field and the rate at which the electronic (<50 fs), vibrational (10-1000 fs), and rotational (1-100 ps) coherence dephase. Photo-fragmentation of 16 different molecules including isomers was studied comprehensively when we change the pulse characteristics systematically. Order of magnitude laser control over the relative yields of different fragment ions was observed for most of the molecules studied and interestingly, a single linear chirp scan was sufficient to cause these large changes. This observation implies that fragmentation caused by intense IR pulses depends on the time duration of the pulses and is independent from the particular time-frequency structure of the shaped laser pulses. Coherence thus does not play a role in the observed changes in yield as a function of pulse shaping.

In order to begin to understand how pulse duration influences the yield of different fragment ions, time-resolved dynamics that ensue following the interaction of the molecules with a strong 10^{15} W/cm^2 non-resonant near-infrared laser field was explored. The data reveal that most of the fragmentation processes occur well after ionization. The molecular dynamics are followed in the 10^{-14}- 10^{-10} s time scale. Studies carried out on acetophenone derivatives showed the vibrational motion of the benzoyl product ions, which is found to regulate further ionization and fragmentation through electronic coordination. The resulting experimental data, together with electronic calculations and the electron-ionization mass spectra of these compounds allow us to propose ladder switching processes taking place in this family of compounds which regulate the different fragment ions observed.

Bibliography

Bibliography I

Abbott, J. E., Peng, X. Z., & Kong, W. (2002). Symmetry properties of electronically excited states of nitroaromatic compounds. *Journal of Chemical Physics, 117*(19), 8670-8675.

Assion, A., Baumart, T., Bergt, M., Brixner, T., Kiefer, B., Sayfried, V., et al. (1998). Control of Chemical Reactions by Feedback-Optimized Phase-Shaped Femtosecond Pulses. *Science, 282*, 919-922.

Baer, T., Morrow, J. C., Shao, J. D., & Olesik, S. (1988). Gas-Phase Heats of Formation of C7h7+ Isomers - Meta-Tolyl, Para-Tolyl, and Benzyl Ions. *Journal of the American Chemical Society, 110*(17), 5633-5638.

Baronavski, A. P., & Owrutsky, J. C. (2001). Ketone excited state lifetimes measured by deep UV ultrafast photoionization spectroscopy. *Chemical Physics Letters, 333*(1-2), 36-40.

Bergt, M., Brixner, T., Dietl, C., Kiefer, B., & Gerber, G. (2002). Time-resolved organometallic photochemistry - Femtosecond fragmentation and adaptive control of CpFe(CO)(2)X (X = Cl, Br, I). *Journal of Organometallic Chemistry, 661*(1-2), 199-209.

Bergt, M., Brixner, T., Kiefer, B., Strehle, M., & Gerber, G. (1999). Controlling the femtochemistry of Fe(CO)(5). *Journal of Physical Chemistry A, 103*(49), 10381-10387.

Beynon, J. H., Bertrand, M., & Cooks, R. G. (1973). Metastable Loss of No from Aromatic Nitro-Compounds. *Journal of the American Chemical Society, 95*(6), 1739-1745.

Brif, C., Chakrabarti, R., & Rabitz, H. Control of quantum phenomena: past, present and future. *New Journal Of Physics, 12*.

Brill, T. B., James, K. J., Chawla, R., Nicol, G., Shukla, A., & Futrell, I. H. (1999). Influence of the substituent on the major decomposition channels of the NO2 group in para-substituted nitrobenzenes: a tandem mass spectrometric study. *Journal of Physical Organic Chemistry, 12*(11), 819-826.

Brixner, T., Damrauer, N. H., Krampert, G., Niklaus, P., & Gerber, G. (2003). Femtosecond learning control of quantum dynamics in gases and liquids: technology and applications. *Journal of Modern Optics, 50*(3-4), 539-560.

Brixner, T., Kiefer, B., & Gerber, G. (2001). Problem complexity in femtosecond quantum control. *Chemical Physics, 267*(1-3), 241-246.

Brown, P. (1970). Kinetic Studies in Mass Spectrometry.9. Competing M-No2! And M-No! Reactions in Substituted Nitrobenzenes - Approximate Activation Energies from Ionization and Appearance Potentials. *Organic Mass Spectrometry, 4*, 533-544.

Brumer, P., & Shapiro, M. (1986). Control of Unimolecular Reactions Using Coherent-Light.

Chemical Physics Letters, 126(6), 541-546.

Bursey, M. M., Kao, J. L., & Pedersen, L. (1975). Lowest Electronic States of Benzoyl Ion - Molecular-Orbital Study with Configuration Interaction. *Organic Mass Spectrometry, 10*(1), 38-42.

Bursey, M. M., & McLaffer.Fw. (1966). Rearrangements and Flat-Topped Metastable Ions in Mass Spectra of Substituted Nitrobenzenes. *Journal of the American Chemical Society, 88*(21), 5023-5025.

Cardoza, D., Baertschy, M., & Weinacht, T. (2005a). Interpreting closed-loop learning control of molecular fragmentation in terms of wave-packet dynamics and enhanced molecular ionization. *Journal of Chemical Physics, 123*(7), Art. No. 074315.

Cardoza, D., Baertschy, M., & Weinacht, T. (2005b). Understanding learning control of molecular fragmentation. *Chemical Physics Letters, 411*(4-6), 311-315.

Cardoza, D., Langhojer, F., Trallero-Herrero, C., Monti, O. L. A., & Weinacht, T. (2004). Changing pulse-shape basis for molecular learning control. *Physical Review A, 70*(5), Art. No. 053406.

Cardoza, D., Pearson, B. J., Baertschy, M., & Weinacht, T. (2006). Charge-transfer as a mechanism for controlling molecular fragmentation. *Journal of Photochemistry and Photobiology a-Chemistry, 180*(3), 277-281.

Cardoza, D., Trallero-Herrero, C., Langhojer, F., Rabitz, H., & Weinacht, T. (2005c). Transformations to diagonal bases in closed-loop quantum learning control experiments. *Journal of Chemical Physics, 122*(12), Art. No. 124306.

Cassady, C. J., & McElvany, S. W. (1993). Collision-Induced Dissociation and Photodissociation of Nitroaromatic Molecular-Ions - a Unique Isomerization for P-Nitrotoluene and P-Ethylnitrobenzene Ions. *Organic Mass Spectrometry, 28*(12), 1650-1657.

Cerullo, G., Bardeen, C. J., Wang, Q., & Shank, C. V. (1996). High-power femtosecond chirped pulse excitation of molecules in solution. *Chemical Physics Letters, 262*(3-4), 362-368.

Choe, J. C., & Kim, M. S. (1991). Photodissociation Kinetics of the Para-Nitrotoluene Molecular Ion on a Nanosecond Time Scale. *Journal of Physical Chemistry, 95*(1), 50-56.

Coello, Y., Lozovoy, V. V., Gunaratne, T. C., Xu, B. W., Borukhovich, I., Tseng, C. H., et al. (2008). Interference without an interferometer: a different approach to measuring, compressing, and shaping ultrashort laser pulses. *Journal Of The Optical Society Of America B-Optical Physics, 25*(6), A140-A150.

Comstock, M., Lozovoy, V. V., Pastirk, I., & Dantus, M. (2004). Multiphoton intrapulse interference 6; binary phase shaping. *Optics Express, 12*(6), 1061-1066.

Cooper, L., Shpinkova, L. G., Rennie, E. E., Holland, D. M. P., & Shaw, D. A. (2001). Time-of-flight mass spectrometry study of the fragmentation of valence shell ionised nitrobenzene. *International Journal of Mass Spectrometry, 207*(3), 223-239.

Damrauer, N. H., Dietl, C., Krampert, G., Lee, S. H., Jung, K. H., & Gerber, G. (2002). Control of bond-selective photochemistry in CH2BrCl using adaptive femtosecond pulse shaping. *European Physical Journal D, 20*(1), 71-76.

Dantus, M., & Lozovoy, V. V. (2004). Experimental coherent laser control of physicochemical processes. *Chemical Reviews, 104*(4), 1813-1859.

Dantus, M., Lozovoy, V. V., & Pastirk, I. (2007). MIIPS characterize and corrects femtosecond pulses. *Laser Focus World*(May), 101-104.

Dantus, M., Rosker, M. J., & Zewail, A. H. (1987). Real-Time Femtosecond Probing Of Transition-States In Chemical-Reactions. *Journal Of Chemical Physics, 87*(4), 2395-2397.

Dantus, M., Rosker, M. J., & Zewail, A. H. (1988). Femtosecond Real-Time Probing of Reactions.2. The Dissociation Reaction of Icn. *Journal of Chemical Physics, 89*(10), 6128-6140.

Dela Cruz, J., M., Lozovoy, V., V., & Dantus, M. (2007). Isomeric identification by laser control mass spectrometry. *Journal of Mass Spectrometry, 42*(2), 178-186.

Dela Cruz, J. M., Lozovoy, V. V., & Dantus, M. (2005). Quantitative mass spectrometric identification of isomers applying coherent laser control. *Journal of Physical Chemistry A, 109*(38), 8447-8450.

Dela Cruz, J. M., Pastirk, I., Lozovoy, V. V., Walowicz, K. A., & Dantus, M. (2004). Multiphoton intrapulse interference 3: Probing microscopic chemical environments. *Journal of Physical Chemistry A, 108*(1), 53-58.

Fateley, W. (1973). Barriers and conformations. *Pure and applied chemistry, 36*(1-2), 109.

Fork, R. L., Greene, B. I., & Shank, C. V. (1981). Generation Of Optical Pulses Shorter Than 0.1 Psec By Colliding Pulse Mode-Locking. *Applied Physics Letters, 38*(9), 671-672.

Fraser, G. W. (2002). The ion detection efficiency of microchannel plates (MCPs). *International Journal of Mass Spectrometry, 215*(1-3), 13-30.

Fuss, W., Schmid, W. E., & Trushin, S. A. (2000). Time-resolved dissociative intense-laser field ionization for probing dynamics: Femtosecond photochemical ring opening of 1,3-cyclohexadiene. *Journal of Chemical Physics, 112*(19), 8347-8362.

Galloway, D. B., Bartz, J. A., Huey, L. G., & Crim, F. F. (1993). Pathways and Kinetic-Energy Disposal in the Photodissociation of Nitrobenzene. *Journal of Chemical Physics, 98*(3), 2107-2114.

Galloway, D. B., Glenewinkelmeyer, T., Bartz, J. A., Huey, L. G., & Crim, F. F. (1994). The Kinetic and Internal Energy of No from the Photodissociation of Nitrobenzene. *Journal of*

Chemical Physics, 100(3), 1946-1952.

Graham, P., Menkir, G., & Levis, R. J. (2003). An investigation of the effects of experimental parameters on the closed-loop control of photoionization/dissociation processes in acetophenone. *Spectrochimica Acta Part B-Atomic Spectroscopy, 58*(6), 1097-1108.

Greenfield, M., McGrane, S. D., & Moore, D. S. (2009). Control of cis-Stilbene Photochemistry Using Shaped Ultraviolet Pulses. *Journal of Physical Chemistry A, 113*(11), 2333-2339.

Gross, M. L., Chess, E. K., Lyon, P. A., Crow, F. W., Evans, S., & Tudge, H. (1982). Triple Analyzer Mass-Spectrometry For High-Resolution Ms/Ms Studies. *International Journal Of Mass Spectrometry And Ion Processes, 42*(4), 243-254.

Gruebele, M., & Bigwood, R. (1998). Molecular vibrational energy flow: beyond the Golden Rule. *International Reviews in Physical Chemistry, 17*(2), 91-145.

Hankin, S. M., Villeneuve, D. M., Corkum, P. B., & Rayner, D. M. (2000). Nonlinear ionization of organic molecules in high intensity laser fields. *Physical Review Letters, 84*(22), 5082-5085.

Hankin, S. M., Villeneuve, D. M., Corkum, P. B., & Rayner, D. M. (2001). Intense-field laser ionization rates in atoms and molecules. *Physical Review A, 64*(1), Art. No. 013405.

Harada, H., Shimizu, S., Yatsuhashi, T., Sakabe, S., Izawa, Y., & Nakashima, N. (2001). A key factor in parent and fragment ion formation on irradiation with an intense femtosecond laser pulse. *Chemical Physics Letters, 342*(5-6), 563-570.

Harris, F. M., Mukhtar, E. S., Griffiths, I. W., & Beynon, J. H. (1981). Design of a High-Resolution Mass-Spectrometer for Studying the Photo-Dissociation of Organic Ions in the Gas-Phase. *Proceedings of the Royal Society of London Series a-Mathematical Physical and Engineering Sciences, 374*(1759), 461-473.

Hwang, W. G., Kim, M. S., & Choe, J. C. (1996). Photodissociation dynamics of nitrobenzene molecular ion on a nanosecond time scale. *Journal of Physical Chemistry, 100*(22), 9227-9234.

Iaconis, C., & Walmsley, I. A. (1998). Spectral phase interferometry for direct electric-field reconstruction of ultrashort optical pulses. *Optics Letters, 23*(10), 792-794.

Itakura, R., Yamanouchi, K., Tanabe, T., Okamoto, T., & Kannari, F. (2003). Dissociative ionization of ethanol in chirped intense laser fields. *Journal of Chemical Physics, 119*(8), 4179-4186.

Judson, R. S., & Rabitz, H. (1992). Teaching Lasers to Control Molecules. *Physical Review Letters, 68*(10), 1500-1503.

Kobayash, T., & Nagakura, S. (1974). Photoelectron-Spectra Of Substituted Benzenes. *Bulletin Of The Chemical Society Of Japan, 47*(10), 2563-2572.

Kosmidis, C., Ledingham, K. W. D., Clark, A., Marshall, A., Jennings, R., Sander, J., et al.

(1994a). On the Dissociation Pathways of Nitrobenzene. *International Journal of Mass Spectrometry and Ion Processes, 135*(2-3), 229-242.

Kosmidis, C., Ledingham, K. W. D., Kilic, H. S., McCanny, T., Singhal, R. P., Langley, A. J., et al. (1997). On the fragmentation of nitrobenzene and nitrotoluenes induced by a femtosecond laser at 375 nm. *Journal of Physical Chemistry A, 101*(12), 2264-2270.

Kosmidis, C., Marshall, A., Clark, A., Deas, R. M., Ledingham, K. W. D., & Singhal, R. P. (1994b). Multiphoton Ionization and Dissociation of Nitrotoluene Isomers by Uv Laser-Light. *Rapid Communications in Mass Spectrometry, 8*(8), 607-614.

Kotur, M., Weinacht, T., Pearson, B. J., & Matsika, S. (2009). Closed-loop learning control of isomerization using shaped ultrafast laser pulses in the deep ultraviolet. *Journal of Chemical Physics, 130*(13).

Krems, M., Zirbel, J., Thomason, M., & DuBois, R. D. (2005). Channel electron multiplier and channelplate efficiencies for detecting positive ions. *Review of Scientific Instruments, 76*(9).

Lablanquie, P., Ohashi, K., & Nishi, N. (1993). Laser Photodissociation of C7h7+ Created through Multiphoton Ionization of Para-Chlorotoluene. *Journal of Chemical Physics, 98*(1), 399-408.

Langhojer, F., Cardoza, D., Baertschy, M., & Weinacht, T. (2005). Gaining mechanistic insight from closed loop learning control: The importance of basis in searching the phase space. *Journal of Chemical Physics, 122*(1), Art. No. 014102.

Ledingham, K. W. D., Kilic, H. S., Kosmidis, C., Deas, R. M., Marshall, A., McCanny, T., et al. (1995). A comparison of femtosecond and nanosecond multiphoton ionization and dissociation for some nitro-molecules. *Rapid Communications in Mass Spectrometry, 9*(15), 1522-1527.

Letokhov, V. S., & Makarov, A. A. (1978). Excitation Of Multilevel Molecular Systems By Laser Ir Field - Frequency - Dynamic Effects. *Applied Physics, 16*(1), 47-57.

Levis, R. J., Menkir, G. M., & Rabitz, H. (2001). Selective bond dissociation and rearrangement with optimally tailored, strong-field laser pulses. *Science, 292*(5517), 709-713.

Levis, R. J., & Rabitz, H. A. (2002). Closing the loop on bond selective chemistry using tailored strong field laser pulses. *Journal of Physical Chemistry A, 106*(27), 6427-6444.

Lozovoy, V., V., & Dantus, M. (2006a). Laser control of physicochemical processes; experiments and applications. *Annu. Rep. Prog. Chem., Sect. C, 102*, 227-258.

Lozovoy, V. V., & Dantus, M. (2005a). Coherent control in femtochemistry. *Chemphyschem, 6*(10), 1970-2000.

Lozovoy, V. V., & Dantus, M. (2006b). Laser control of physicochemical processes; experiments and applications. *Annu. Rep. Prog. Chem., Sect. C, 102*, 227-258.

Lozovoy, V. V., Gunaratne, T. C., Shane, J. C., & Dantus, M. (2006c). Control of molecular fragmentation using binary phase shaped femtosecond laser pulses. *ChemPhysChem*, in press.

Lozovoy, V. V., Pastirk, I., & Dantus, M. (2004). Multiphoton intrapulse interference. IV. Ultrashort laser pulse spectral phase characterization and compensation. *Optics Letters, 29*(7), 775-777.

Lozovoy, V. V., Pastirk, I., Walowicz, K. A., & Dantus, M. (2003). Multiphoton intrapulse interference. II. Control of two- and three-photon laser induced fluorescence with shaped pulses. *Journal of Chemical Physics, 118*(7), 3187-3196.

Lozovoy, V. V., Shane, J. C., Xu, B. W., & Dantus, M. (2005b). Spectral phase optimization of femtosecond laser pulses for narrow-band, low-background nonlinear spectroscopy. *Optics Express, 13*(26), 10882-10887.

Lozovoy, V. V., Xu, B. W., Shane, J. C., & Dantus, M. (2006d). Selective nonlinear optical excitation with pulses shaped by pseudorandom Galois fields. *Physical Review A, 74*(4), Art. No. 041805.

Lozovoy, V. V., Zhu, X., Gunaratne, T. C., Harris, D. A., Shane, J. C., & Dantus, M. (2008). Control of molecular fragmentation using shaped femtosecond pulses. *Journal of Physical Chemistry A, 112*(17), 3789-3812.

Marshall, A., Clark, A., Jennings, R., Ledingham, K. W. D., & Singhal, R. P. (1992). Wavelength-Dependent Laser-Induced Fragmentation of Nitrobenzene. *International Journal of Mass Spectrometry and Ion Processes, 112*(2-3), 273-283.

Mathur, D., & Rajgara, F. A. (2004). Dissociative ionization of methane by chirped pulses of intense laser light. *Journal of Chemical Physics, 120*(12), 5616-5623.

Meshulach, D., & Silberberg, Y. (1998). Coherent quantum control of two-photon transitions by a femtosecond laser pulse. *Nature, 396*(6708), 239-242.

Moini, M., & Eyler, J. R. (1987). Infrared Multiphoton Dissociation of the Nitrobenzene Cation. *International Journal of Mass Spectrometry and Ion Processes, 76*(1), 47-54.

Muller, A. M., Uiterwaal, C., Witzel, B., Wanner, J., & Kompa, K. L. (2000). Photoionization and photofragmentation of gaseous toluene using 80-fs, 800-nm laser pulses. *Journal of Chemical Physics, 112*(21), 9289-9300.

Nishimura, T., Das, P. R., & Meisels, G. G. (1986). On the Dissociation Dynamics of Energy-Selected Nitrobenzene Ion. *Journal of Chemical Physics, 84*(11), 6190-6199.

NIST. (2005). Release.

Onda, M., Kohama, Y., Suga, K., & Yamaguchi, I. (1998). Microwave spectrum and molecular planarity of acetophenone. *Journal of Molecular Structure, 442*(1-3), 19-22.

Osterheld, T. H., Baer, T., & Brauman, J. I. (1993). Infrared Multiple-Photon Dissociation of the Nitrobenzene Radical-Cation - a Paradigm for Competitive Reactions. *Journal of the American Chemical Society, 115*(14), 6284-6289.

Panczel, M., & Baer, T. (1984). A Photoelectron Photoion Coincidence (Pepico) Study of Fragmentation Rates and Kinetic-Energy Release Distributions in Nitrobenzene. *International Journal of Mass Spectrometry and Ion Processes, 58*(JUN), 43-61.

Park, S. T., Feenstra, J. S., & Zewail, A. H. (2006). Ultrafast electron diffraction: Excited state structures and chemistries of aromatic carbonyls. *Journal Of Chemical Physics, 124*(17).

Pastirk, I., Brown, E. J., Zhang, Q. G., & Dantus, M. (1998). Quantum control of the yield of a chemical reaction. *Journal of Chemical Physics, 108*(11), 4375-4378.

Pastirk, I., Kangas, M., & Dantus, M. (2005). Multidimensional analytical method based on binary phase shaping of femtosecond pulses. *Journal of Physical Chemistry A, 109*(11), 2413-2416.

Pastirk, I., Lozovoy, V., V., & Dantus, M. (2006a). Femtosecond pulse shaping adds a new dimension to mass spectrometry. *Appl. Optics*, submitted.

Pastirk, I., Resan, B., Fry, A., MacKay, J., & Dantus, M. (2006b). No loss spectral phase correction and arbitrary phase shaping of regeneratively amplified femtosecond pulses using MIIPS. *Optics Express, 14*(20), 9537-9543.

Pastirk, I., Zhu, X., Lozovoy, V. V., & Dantus, M. (2007). Femntosecond pulse shaping adds a new dimension to mass spectrometry. *Applied Optics, 46*(19), 4041-4045.

Pearson, B. J., & Weinacht, T. C. (2007). Shaped ultrafast laser pulses in the deep ultraviolet. *Optics Express, 15*(7), 4385-4388.

Pitts, T. A., Luk, T. S., Gruetzner, J. K., Nelson, T. R., McPherson, A., Cameron, S. M., et al. (2004). Propagation of self-focusing laser pulses in atmosphere: experiment versus numerical simulation. *Journal of the Optical Society of America B-Optical Physics, 21*(11), 2008-2016.

Posthumus, J. H. (2004). The dynamics of small molecules in intense laser fields. *Reports on Progress in Physics, 67*(5), 623-665.

Robson, L., Ledingham, K. W. D., McKenna, P., McCanny, T., Shimizu, S., Yang, J. M., et al. (2005). Volumetric intensity dependence on the formation of molecular and atomic ions within a high intensity laser focus. *Journal of the American Society for Mass Spectrometry, 16*(1), 82-89.

Ronn, A. M. (1979). Laser Chemistry. *Scientific American, 240*(5), 114-&.

Rose, T. S., Rosker, M. J., & Zewail, A. H. (1988). Femtosecond Real-Time Observation Of Wave Packet Oscillations (Resonance) In Dissociation Reactions. *Journal Of Chemical Physics, 88*(10), 6672-6673.

Rosker, M. J., Dantus, M., & Zewail, A. H. (1988). Femtosecond Real-Time Probing of Reactions.1. The Technique. *Journal of Chemical Physics, 89*(10), 6113-6127.

Shane, J. C., Lozovoy, V. V., & Dantus, M. (2006). Search space mapping: Getting a picture of coherent control. *J. Phys. Chem. A, 110*(40), 11388-11391.

Sheng, L. S., Wu, G. H., Gao, H., & Zhang, Y. W. (1997). Photoionization studies on p-nitrotoluene with synchrotron radiation. *Chemical Journal of Chinese Universities-Chinese, 18*(12), 2041-2043.

Spence, D. E., Kean, P. N., & Sibbett, W. (1991). 60-Fsec Pulse Generation From A Self-Mode-Locked Ti-Sapphire Laser. *Optics Letters, 16*(1), 42-44.

Sussman, B. J., Lausten, R., & Stolow, A. (2008). Focusing of light following a 4-f pulse shaper: Considerations for quantum control. *Physical Review A, 77*(4).

Szaflarski, D. M., & Elsayed, M. A. (1988). Kinetic-Energy and Formation Mechanisms of I+ and Ch3+ from 266-Nm Picosecond Versus Nanosecond Laser Multiphoton Absorption. *Journal of Physical Chemistry, 92*(8), 2234-2239.

Tang, X. P., Becker, A., Liu, W., Sharifi, S. M., Kosareva, O. G., Kandidov, V. P., et al. (2005). Self-action effects in ionization and fragmentation of toluene by femtosecond laser pulses. *Applied Physics B-Lasers and Optics, 80*(4-5), 547-557.

Tannor, D. J., Kosloff, R., & Rice, S. A. (1986). Coherent Pulse Sequence Induced Control of Selectivity of Reactions - Exact Quantum-Mechanical Calculations. *Journal of Chemical Physics, 85*(10), 5805-5820.

Tannor, D. J., & Rice, S. A. (1985). Control of Selectivity of Chemical-Reaction Via Control of Wave Packet Evolution. *Journal of Chemical Physics, 83*(10), 5013-5018.

Tasker, A. D., Robson, L., Ledingham, K. W. D., McCanny, T., Hankin, S. M., McKenna, P., et al. (2002). A high mass resolution study of the interaction of aromatic and nitro-aromatic molecules with intense laser fields. *Journal of Physical Chemistry A, 106*(16), 4005-4013.

Tonnies, K., Schmid, R. P., Weickhardt, C., Reif, J., & Grotemeyer, J. (2001). Multiphoton ionization of nitrotoluenes by means of ultrashort laser pulses. *International Journal of Mass Spectrometry, 206*(3), 245-250.

Trebino, R., & Kane, D. J. (1993). Using Phase Retrieval To Measure The Intensity And Phase Of Ultrashort Pulses - Frequency-Resolved Optical Gating. *Journal Of The Optical Society Of America A-Optics Image Science And Vision, 10*(5), 1101-1111.

Uiterwaal, C., Gebhardt, C. R., Schroder, H., & Kompa, K. L. (2004). Predicting intense-field photoionization of atoms and molecules from their linear photoabsorption spectra in the ionization continuum. *European Physical Journal D, 30*(3), 379-392.

Walowicz, K. A., Pastirk, I., Lozovoy, V. V., & Dantus, M. (2002). Multiphoton intrapulse interference. 1. Control of multiphoton processes in condensed phases. *Journal of Physical Chemistry A, 106*(41), 9369-9373.

Wang, P. Q., Sayler, A. M., Carnes, K. D., Esry, B. D., & Ben-Itzhak, I. (2005). Disentangling the volume effect through intensity-difference spectra: application to laser-induced dissociation of H-2(+). *Optics Letters, 30*(6), 664-666.

Warren, W. S., & Zewail, A. H. (1981). Optical Analogs Of Nmr Phase Coherent Multiple Pulse Spectroscopy. *Journal Of Chemical Physics, 75*(12), 5956-5958.

Warren, W. S., & Zewail, A. H. (1983a). Multiple Phase-Coherent Laser-Pulses In Optical Spectroscopy.1. The Technique And Experimental Applications. *Journal Of Chemical Physics, 78*(5), 2279-2297.

Warren, W. S., & Zewail, A. H. (1983b). Multiple Phase-Coherent Laser-Pulses In Optical Spectroscopy.2. Applications To Multilevel Systems. *Journal Of Chemical Physics, 78*(5), 2298-2311.

Warren, W. S., & Zewail, A. H. (1983c). Optical Multiple Pulse Sequences For Multiphoton Selective Excitation And Enhancement Of Forbidden Transitions. *Journal Of Chemical Physics, 78*(6), 3583-3592.

Watson, J. T. (1997). *Introduction to mass spectrometry* (3rd ed.). Philadelphia: Lippincott-Raven.

Weickhardt, C., & Tonnies, K. (2002). Short pulse laser mass spectrometry of nitrotoluenes: ionization and fragmentation behavior. *Rapid Communications in Mass Spectrometry, 16*(5), 442-446.

Weiner, A. M., & Heritage, J. P. (1987). Picosecond And Femtosecond Fourier Pulse Shape Synthesis. *Revue De Physique Appliquee, 22*(12), 1619-1628.

Weiner, A. M., Heritage, J. P., & Kirschner, E. M. (1988). High-Resolution Femtosecond Pulse Shaping. *Journal Of The Optical Society Of America B-Optical Physics, 5*(8), 1563-1572.

Weiner, A. M., Leaird, D. E., Patel, J. S., & Wullert, J. R. (1990). Programmable Femtosecond Pulse Shaping By Use Of A Multielement Liquid-Crystal Phase Modulator. *Optics Letters, 15*(6), 326-328.

Weinkauf, R., Aicher, P., Wesley, G., Grotemeyer, J., & Schlag, E. W. (1994). Femtosecond Versus Nanosecond Multiphoton Ionization and Dissociation of Large Molecules. *Journal of Physical Chemistry, 98*(34), 8381-8391.

Wells, E., Betsch, K. J., Conover, C. W. S., DeWitt, M. J., Pinkham, D., & Jones, R. R. (2005). Closed-loop control of intense-laser fragmentation of S-8. *Physical Review A, 72*(6), Art. No. 063406.

Wohlleben, W., Buckup, T., Herek, J. L., & Motzkus, M. (2005). Coherent control for spectroscopy and manipulation of biological dynamics. *Chemphyschem, 6*(5), 850-857.

Xu, B. W., Gunn, J. M., Dela Cruz, J. M., Lozovoy, V. V., & Dantus, M. (2006). Quantitative investigation of the multiphoton intrapulse interference phase scan method for simultaneous phase measurement and compensation of femtosecond laser pulses. *Journal of the Optical Society of America B-Optical Physics, 23*(4), 750-759.

Yang, J. J., Gobeli, D. A., & Elsayed, M. A. (1985). Change in the Mechanism of Laser Multiphoton Ionization Dissociation in Benzaldehyde by Changing the Laser-Pulse Width. *Journal of Physical Chemistry, 89*(15), 3426-3429.

Yazawa, H., Tanabe, T., Okamoto, T., Yamanaka, M., Kannari, F., Itakura, R., et al. (2006). Open-loop and closed-loop control of dissociative ionization of ethanol in intense laser fields. *Journal of Chemical Physics, 124*(20), Art. No. 204314.

Zewail, A. H. (1980). Laser Selective Chemistry - Is It Possible. *Physics Today, 33*(11), 27-33.

Zhang, L., Frasinski, L. J., & Codling, K. (1994). The Effect of Truncating a Gaussian-Beam on the Yields of Multiply-Charged Ions. *Journal of Physics B-Atomic Molecular and Optical Physics, 27*(15), 3427-3434.

Zhu, X., Gunaratne, T. C., Lozovoy, V. V., & Dantus, M. (2009). Comment on "Closing the Loop on Bond Selective Chemistry Using Tailored Strong Field Laser Pulses". *Journal Of Physical Chemistry A, 113*(17), 5264-5266.